Transtensional Rifting in the Late Proto-Gulf of California Near Bahía Kino, Sonora, México

Scott Edmund Kelsey Bennett

A thesis submitted to the faculty of the University of North Carolina at Chapel Hill in partial fulfillment of the requirements for the degree of Master of Science in the Department of Geological Sciences.

Chapel Hill
2009

Approved by:

Michael Oskin

Allen Glazner

Kevin Stewart

ABSTRACT

SCOTT EDMUND KELSEY BENNETT: Transtensional Rifting in the Late Proto-Gulf of California Near Bahía Kino, Sonora, México
(Under the direction of Michael Oskin)

The Gulf of California provides an active rift example to test the role of rift obliquity in continental rupture. Continental rifts require focused strain to rupture and form an ocean basin. Strike-slip faults are ubiquitous in oblique rifts and focused transtensional strain adjacent to these faults may be a catalyst for rupture. To test this hypothesis, I completed structural mapping, fault-kinematic analysis, geochronology, basin analysis, and paleomagnetism of pre- and syn-rift rocks exposed in coastal Sonora, México. Sedimentary basins record ~16 km of west-northwest-directed transtension across the Kino-Chueca Shear Zone. Onset of transtension in the study area is estimated to be ca. 7 Ma and lasted for approximately 1 million years. This represents a significant portion (~28%) of plate boundary deformation over this time interval. Dextral shear was progressively localized within this zone of extensional deformation, and together shear and extension acted to focus lithospheric-scale strain into a narrower zone.

ACKNOWLEDGMENTS

Funding from the National Science Foundation (Tectonics and MARGINS), a Geological Society of America's Graduate Research Grant, and the University of North Carolina, Chapel Hill Geological Sciences Department Martin Fund made this research possible. Michael Tappa, Monica Iglecia, Dhelia Tucker, Karen Bossenbroek, and Jordan Ford all provided great company, safety, and support while conducting fieldwork in Sonora and Baja California. Joe Kirschvink and the Caltech Paleomagnetics Laboratory assisted with paleomagnetic analysis. Tadeo Pfister, Tom Donovan, and the Prescott College Kino Bay Center for Cultural and Ecological Studies staff provided comfortable accommodations while mapping in Sonora. I thank Ernesto Molina and the native Comcáac tribe who granted access to their lands.

I owe much gratitude to my parents, Edmund and Susan Bennett, for their support throughout my college career. I thank my mother for her patience and convincing me that college was a good idea. I thank my father for our many trips together where we have enjoyed countless beautiful western landscapes and for introducing me to geology and the outdoors. I cannot quantify my appreciation for the encouragement and companionship from my fiancée, Monica. Her help in and out of the field, made our time in North Carolina quite unforgettable.

TABLE OF CONTENTS

LIST OF TABLES

Table

LIST OF FIGURES

Plate

Figure

INTRODUCTION AND MOTIVATION

Continental rifting and formation of ocean basins has been a fundamental component of plate tectonics for the majority of Earth history. Because continental crust is typically thick (30 - 60 km) and tends to stretch rather than break, (McKenzie, 1978; Lavier and Manatschal, 2006) strain localization must somehow occur in order to rupture a continent and form a new ocean basin. Generally, continental rifting has been classified into three modes: narrow-rift, wide-rift, and core-complex (Buck, 1991). The mode of a rift is dependent upon whether deformation remains fixed and upon the effectiveness of lower crustal flow. 'Narrow rift' mode occurs where extension is focused in both the crust and mantle lithosphere and is favored in thick, cold, and relatively strong lithosphere. 'Wide rift' mode exhibits distributed stretching over typically thinner, warmer, and thus somewhat weaker lithosphere. 'Core-complex' mode is a bi-modal mode of strain with focused upper crustal extension and widely distributed lower crustal thinning. This mode occurs in hot, weak, low-viscosity lithosphere. Continental rifts likely evolve from one mode to another during their extensional history. Ultimately, formation of a narrow rift and continental rupture require strain to be localized across the lithospheric column (Buck, 1991; Lavier and Manatschal, 2006).

Multiple parameters have been called upon to control the mode of rifting. Numerical models show that initial thermal state and crustal thickness (Buck, 1991), presence of lower crustal flow (Buck, 1991; Hopper and Buck, 1996; Buck et al., 1999; Al-Zoubi and ten Brink, 2002), buoyancy contrasts (Lavier et al., 1999; Buck, 1991; Forsyth, 1992; Buck et al., 1999), strain rate (England, 1983; Kusznir and Park, 1987; Bassi, 1995; Huismans and Beaumont, 2003), and intensity of rift magmatism (Buck et al., 1999; Kusznir and Park, 1987; Hopper and Buck, 1996) can each be a controlling factor in the rift style and may

influence the rupture potential of a rift. Many of these parameters are intricately linked to one another; for example, a low strain rate that produces slow exhumation allows for conductive cooling of the lithosphere, which permits it to maintain strength. These linked processes create both negative and positive feedbacks on the ability for lithospheric-scale strain to become localized and allow a rift to proceed to rupture.

LOCALIZED EXTENSIONAL STRAIN

A narrow rift forms either under favorable initial conditions or by positive feedbacks on the ability of a wide rift to evolve into a narrow rift. Initial conditions favorable for formation of a narrow rift are initially cold and thick lithosphere. Rifting in such strong lithosphere tends to remain focused into a zone of necking (Artemjev and Artyushkov, 1971; Buck, 1991; Hopper and Buck, 1996), where one or more of the parameters introduced above work to overcome thermal diffusion and sufficiently concentrate lithospheric strain. If these initial conditions are not met, typically a wide rift will initially form. A transition must occur, where a necking instability develops, allowing a wide rift to evolve into a narrow rift that proceeds to continental rupture. For example, formation of a trans-lithospheric fault, in the form of a detachment fault or ductile shear zone (e.g. Louden and Chian, 1999), where strain can localize, may lead to rupture (Lavier and Manatschal, 2006).

Strain rate and magnitude both control the ability of the crust to conductively cool. Fast strain rates and large strains promote shear heating of the lithosphere (Kaus and Podladchikov, 2006). Shear heating and the advection of heat due to uplift of warm material towards the surface will increase the geothermal gradient in extensional regions. In response, the rate of cooling will also increase. However, the resultant temperature of the lithosphere will increase in the presence of shear heating and it will locally weaken the lithosphere

because of the insufficient time for it to cool and strengthen. This ‘strain softening’ leads to a concentration of deformation in a narrow zone, which in turn allows an increased strain rate (England, 1983). This positive feedback between increased strain rate and lithospheric weakening allows for large amounts of localized thinning and a high potential for crustal rupture (Kusznir and Park, 1987; Huismans and Beaumont, 2003). Results from Buck (1991, his Fig. 11) suggested that as strain rate is increased, rift style may switch from wide rift to narrow rift for 40 km-thick crust and from core-complex to narrow rift for 60 km-thick crust. Buck (1991) also argued that as the crust is thinned for a constant heat flow, rift style generally evolves from core complex to narrow rift, with wide rift as an occasional intermediate step. Therefore, by moderating the ability of the crust to conductively cool, strain rate may control the style of rifting. In short, extended regions with lower strain rates will form wide rifts, and areas with higher strain rates will form narrow rifts with higher rupture potential.

The presence of magmatism in the form of diking also controls the rupture potential of a rift (Buck et al., 1999). In a magmatic rift, diking adds heat that can weaken the lithosphere. Dikes also reduce the tectonic force required for crustal extension. When the fluid pressure of magma beneath a rift exceeds the resisting forces that act to keep cracks closed, diking can occur. Therefore, where magmatic diking is present, it assists extension insomuch that less extensional force is required to stretch the lithosphere. Consequently, extension in the presence of magmatic diking has a higher potential for focused deformation, lithospheric necking, and eventual lithospheric rupture. Ultimately, a rift that proceeds to rupture requires magmatic intrusion via diking of mafic magma. Thus, magmatism may not only control rift style, but helps to define when a rift has ruptured.

In contrast to these localizing parameters, other parameters create negative feedbacks on the ability of a wide rift to transition into a narrow rift and further promote the distribution of strain and rift widening. In extended regions, lateral variations in lithospheric thickness develop as a result of extensional faulting. These thickness variations cause differential vertical body forces, where greater vertical stresses are predicted for thicker areas and smaller stresses are predicted for areas thinned via extension (Buck, 1991). These stress differences produce horizontal stress gradients. For a rift axis flanked by thicker rift margins, these stress gradients will be towards areas of relatively thinner lithosphere, and act to constrict regions of active extension. Thinner regions are thus inhibited from further extension, and extensional strain is distributed elsewhere, which promotes rift widening. In the absence of lateral crustal density heterogeneities, these differential stresses also cause lateral pressure variations whose gradients may drive lower crustal flow of weaker or relatively warmer crust (Buck, 1991). Typically, lower crust will flow from areas of relatively thick crust into areas of thinned crust, preventing further localized extension in thinned areas, and effectively widening the rift (Buck, 1991; Buck et al., 1999; Bialas et al., 2007). Evidence for the inflow of ductile lower crust has been observed along multiple rifted passive margins such as the Exmouth Plateau of northwest Australia (Driscoll and Karner, 1998) and both the Iberia-Newfoundland and Galicia-Newfoundland margins of the northern Atlantic (Louden and Chian, 1999), in regions of highly-extended continental crust and core-complex formation of the Basin and Range of western North America (Block and Royden, 1990), and has been proposed for the early stages of rupture in the northern Gulf of California (González-Fernández et al., 2005).

Flexural forces within a rift also act to promote wide rifts. Crustal thinning occurs as extensional faults slip, with thinnest crust found adjacent to the fault trace. The resulting

differential buoyancy forces cause isostatic rebound of thinned areas. Empirical evidence for isostatic rebound of thinned continental crust substantiates this process (Coleman and Walker, 1994). Forsyth (1992) argued that this uplift creates flexural forces on the normal fault surface, such that continued slip on the normal fault is inhibited. When the initiation of a new normal fault better optimizes the use of regional stresses than continued slip on an existing fault, extensional strain migrates elsewhere, forming a wider rift.

A factor not considered by current models is the three-dimensional rift geometry. In particular, current two-dimensional models fail to evaluate the role of rift obliquity. (e.g. Buck, 1991; Lavier et al., 1999; Lavier and Manatschal, 2006). Rift obliquity is a common feature of some active rifts such as the Gulf of California (Umhoefer and Stone, 1996) and the Gulf of Aden (Withjack and Jamison, 1986) and of ancient rifts as seen in the Triassic Harford basin of eastern North America (deBoer and Clifton, 1988). A fundamental distinction between oblique rifts and orthogonal rifts is the occurrence of significant shear accommodated along steep strike-slip faults. Orthogonal continental extension tends to be distributed because of crustal thickness variations (Buck, 1991) and flexural forces on normal faults (Forsyth, 1992). Because a strike-slip fault does not by itself build topography, buoyancy forces do not hinder its total displacement and strain rate. Where extension is hosted within a strike-slip-dominated setting, very large extensional strains may result (e.g. Walker Lane, Unruh et al., 2003) and higher extensional strain rates are locally observed (e.g. Dead Sea rift, Al-Zoubi and ten Brink, 2002). Elevated strain and strain rates that occur in transtensional regions may ultimately influence the rupture potential of a rift.

THE GULF OF CALIFORNIA

The Gulf of California is a youthful marine basin well suited to study the processes of continental rupture. The Gulf of California is located between the Baja California peninsula and mainland Mexico, two landmasses of continental crust (Gastil et al., 1975, Gastil and Krummenacher, 1977a,b) that have been rifted apart (Fig. 1). Furthermore, this rift possesses temporal and along strike variations of rift maturity (Atwater, 1989), volcanic activity (Hausback, 1984), and extensional style (Lizarralde et al., 2007) that allow for comparative studies.

The Gulf of California rift, in the largest sense, is an active releasing bend along the Pacific-North America (PAC-NAM) plate boundary, immediately south of the restraining bend of the San Andreas fault system of southern California (Fig. 1). This releasing bend geometry causes a low angle of obliquity (0 - 30°) between the trend of the rift and the PAC-NAM relative displacement direction. For this magnitude of rift obliquity, analytical and experimental models predict combinations of NW-trending dextral strike-slip, NE-trending sinistral strike-slip, north-trending dip-slip, and variously oriented oblique-slip structures (Withjack and Jamison, 1986). Field studies in the Gulf of California (e.g. Fenby and Gastil, 1991; Lonsdale, 1989) have identified significant rift structures in the Gulf of California that corroborate these model predictions (Fig. 1). Together, these structures accommodate oblique PAC-NAM relative motion.

Proto-Gulf of California Tectonic Evolution

Prior to ~16 Ma, the southwestern edge of the North American plate along northwestern Mexico was a subduction boundary (Fig. 2A; Atwater, 1970). By ~12.5 Ma, the Rivera Triple Junction jumped southeastward, setting the stage for transfer of the Baja

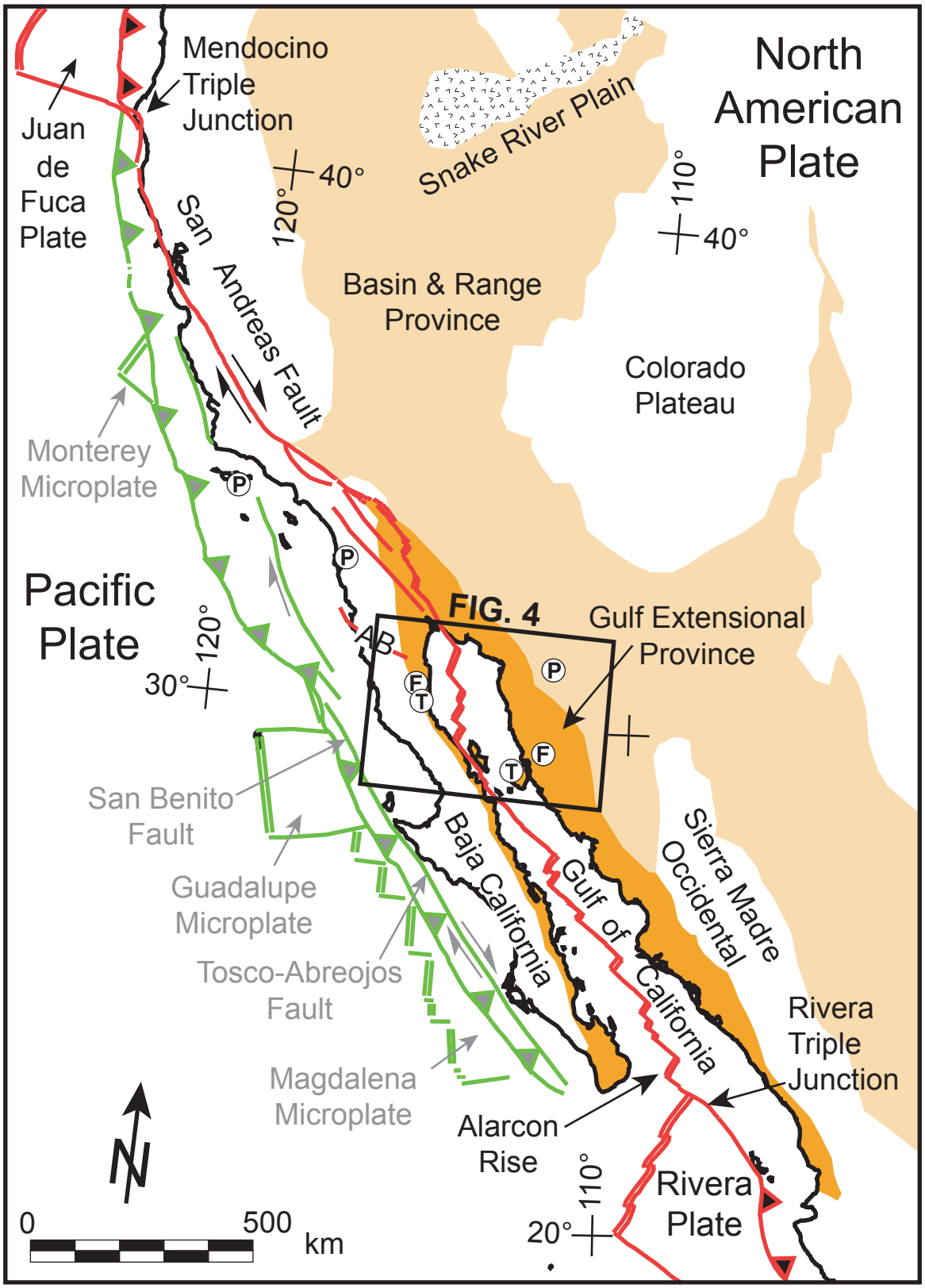

Figure 1. Regional tectonic map of Western North America showing the diffuse boundary between the Pacific-North American lithospheric plates (after Oskin and Stock, 2003a). Active faults and spreading centers in red; inactive in green. AB - Agua Blanca fault; Tie Points: P - Poway conglomerate (Abbott and Smith, 1989); F - fusulinid-rich clast conglomerate (Bryant, 1986; Gastil and Krummenacher, 1977b); T - Tuff sequence (Oskin et al., 2001; Oskin and Stock, 2003a)

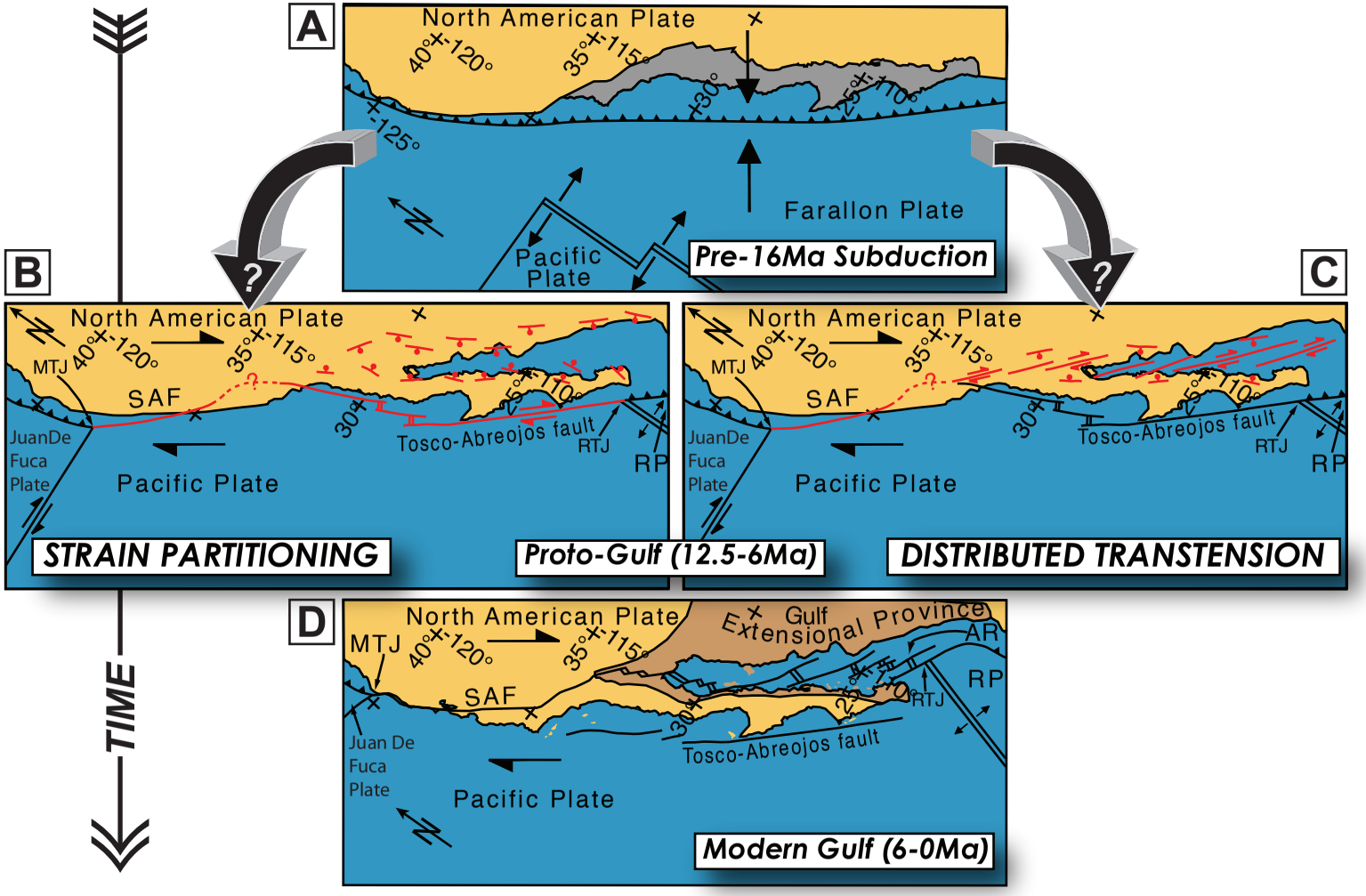

Figure 2. The creation and evolution of the PAC-NAM lithospheric boundary from ~16 Ma to present. Two end-member hypotheses attempt to explain the transition from Farallon subduction (A) to modern-Gulf transtension (D). Of these, the 'Strain Partitioning' end-member proposes regional scale strain partitioning between the dextral Tosco-Abreojos fault and extension within the Gulf Extensional Province (B) (Atwater, 1970; Stock & Hodges, 1989). In contrast, the 'Distributed Transtension' end-member supports unimodal dextral transtension within the GEP with insignificant slip on the Tosco-Abreojos fault, much similar to the modern plate boundary (C) (Gans, 1997; Fletcher et al., 2007). Red faults in proto-Gulf diagrams indicate major active structures along the Pacific-North America plate boundary for each model. AR-Alarcon Rise, RTJ-Rivera Triple Junction, RP-Rivera Plate, MTJ-Mendocino Triple Junction, SAF-San Andreas fault.

California peninsula from the North American plate to the Pacific plate, and initiating the Gulf of California rift. Traditionally, the history of the Gulf of California rift has been divided into two stages: an early proto-Gulf stage spanning from ~12.5 - 6 Ma, and a later modern-Gulf stage spanning from ~6 Ma to present.

Throughout the earlier proto-Gulf period, strain was distributed in an uncertain way between the dextral San Benito and Tosco-Abreojos faults located west of the Baja California peninsula and the Gulf Extensional Province (GEP) of interior Mexico (Fig. 1, 2B,C; Spencer and Normark, 1979; Stock and Hodges, 1989). The uncertainty surrounding proto-Gulf strain distribution hinders understanding of continental rupture processes from tectonic reconstructions of the Gulf of California. Observations of cumulative modern-Gulf (post-6 Ma) offsets of geologic features in the Gulf of California (Oskin et al., 2001; Oskin and Stock, 2003a) corroborate expected PAC-NAM relative motions determined from the global plate circuit (Atwater and Stock, 1998). However, similar observations during proto-Gulf time do not account for ~300 km of dextral PAC-NAM motion (Fig. 3; Stock, 2007; Stock and Hodges, 1989; Stock and Molnar, 1988). Candidate locations for this missing proto-Gulf slip include west of the Baja California peninsula (e.g. the San Benito and Tosco-Abreojos faults) and the region between the Sonora coastline and the western edge of the Sierra Madre Occidental of central Mexico (Fig. 1). Attempts to account for this proto-Gulf shear has led to two disparate end-member models: (1) partitioned deformation with significant dextral strike-slip west of Baja California along the San Benito and Tosco-Abreojos fault systems and WSW-extension within the GEP (Fig. 2B, Stock & Hodges, 1989), and (2) distributed shear and extension within the GEP, broadly similar to but less localized than the modern plate boundary (Fig. 2C, Gans, 1997; Fletcher et al., 2007). These

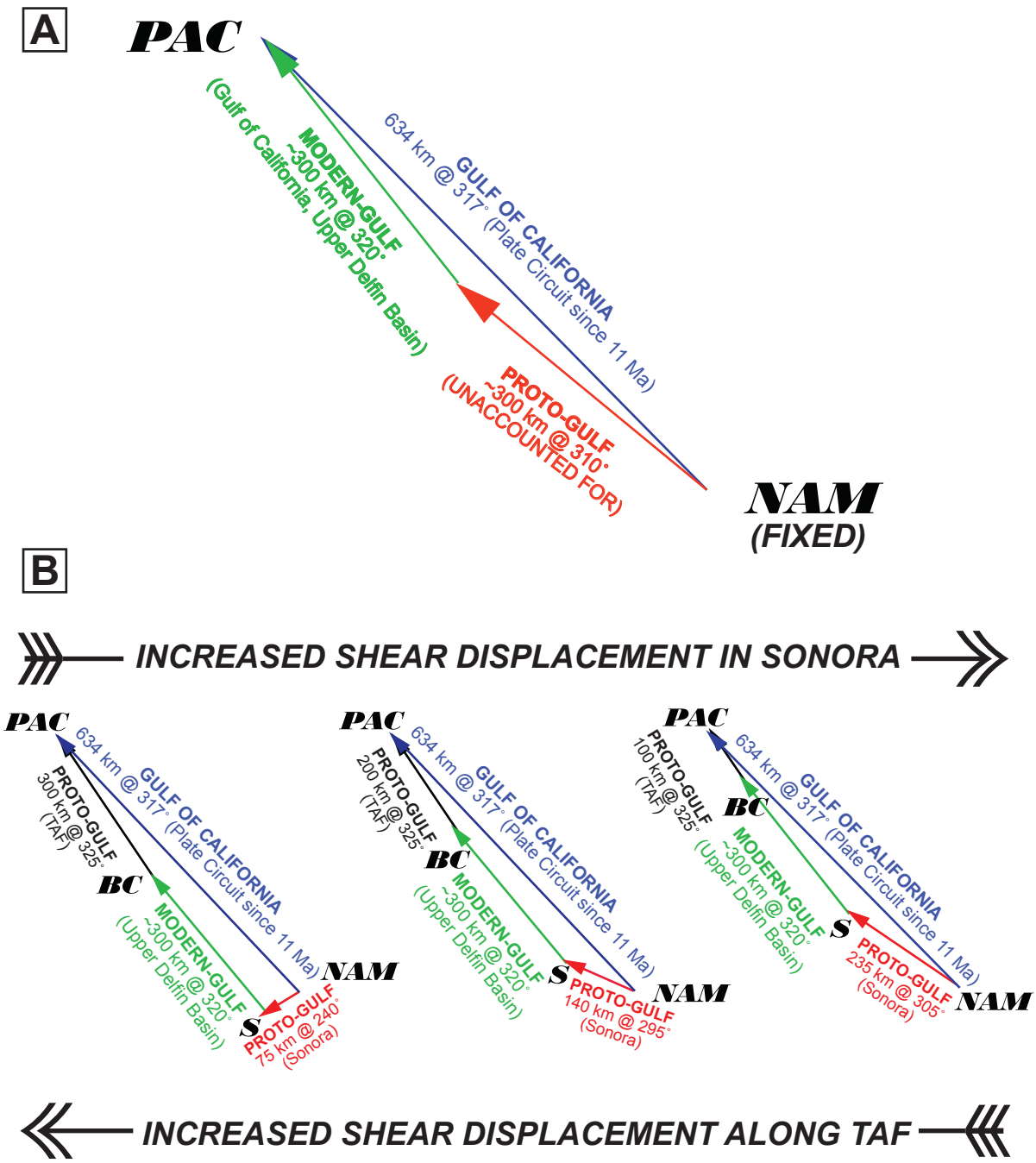

Figure 3. (A) Global plate circuit reconstructions (Atwater and Stock, 1998; Royer et al., 2006) have accurately determined that the PAC-NAM relative plate motion caused the Pacific plate to be displaced 634 km along azimuth 317˚ since 11 Ma (blue arrow; figure modified from Stock, 2007). (B) Modern-Gulf displacement across the Upper Delfin basin (green arrow; Oskin et al., 2001) is constrained to 300 km along azimuth 320˚. The remaining proto-Gulf displacement is unaccounted for and can be decomposed further into displacement distributed in an unknown way between the Tosco-Abreojos fault west of Baja California (black arrow) and the coastal Sonora region within the Gulf Extensional Province (red arrow). These three plate vector diagrams demonstrate that proto-Gulf shear in coastal Sonora is approximately inversely proportional to proto-Gulf shear along the Tosco-Abreojos fault. Greater amounts of proto-Gulf shear in coastal Sonora requires less shear along the Tosco-Abreojos fault. Scenarios of 100-300 km of displacement along the Tosco-Abreojos fault are allowable with variable amounts of proto-Gulf displacement in Sonora. See Figure 1 for geologic and geographic context of faults and regions described here. TAF - Tosco-Abreojos fault, PAC - Pacific plate, NAM - North America plate, BC - Baja California vector, S - Sonora vector

two end-member models will be referred to as ‘strain partitioning’ and ‘distributed transtension’ respectively.

One alternative to these end-member models would be a hybrid ‘progressive localization’ model. In this model, the proto-Gulf period commences (ca. 12.5 Ma) with deformation partitioned into a shear component west of the Baja California peninsula and an extensional component within the GEP, following the ‘strain partitioning’ model. With time, proto-Gulf strain incrementally transitions towards a more distributed pattern of non-localized transtension within the GEP as the shear component west of Baja California gradually becomes less significant, following the ‘distributed transtension’ model. By the end of the proto-Gulf period (~6 Ma), shear deformation progressively becomes more localized along focused dextral shear zones within the GEP that remain embedded within a broader extensional region.

Observations from both sides of the northern Gulf of California lend support to the notion that coastal Sonora may have hosted a component of proto-Gulf shear. Gans (1997) provided the first alternative to the ‘strain partitioning’ model, with observations that large-magnitude extensions in Sonora may entirely pre-date 12 Ma and are not rift related. Based upon observations of distributed dextral faulting that post-dates this extension, he further suggested that the Gulf of California opened via northwest-directed transtension throughout both proto-Gulf and modern-Gulf time. Observations of 12 - 9 Ma dextral motion in coastal Sonora near Guaymas have been reported as evidence for a gradual proto-Gulf organization of the rift system within the GEP (Herman and Gans, 2006; Gans et al., 2006). Fletcher et al., (2007) examined offset submarine fan deposits that are truncated by the Tosco-Abreojos fault west of Baja California, and determined that total post-13 Ma offset along the Tosco-Abreojos fault was <150 km, much less than earlier predictions of as much as 300 km. These

data led to the prediction that the ~150 km of missing strike-slip faulting is required to be within the GEP (Fig. 1). Using relative plate motion vector constraints from northeastern Baja California, Nagy and Stock (2000) suggested that transform faults west of Baja California may have accommodated smaller amounts of slip during proto-Gulf time as the plate boundary gradually migrated eastward into the GEP. Altogether, these observations begin to suggest that the extreme end-member version of the 'strain partitioning' model of Stock and Hodges (1989) may not accurately represent the distribution of proto-Gulf strain and deformation. Alternatively, these data suggest that either the 'distributed transtension' or 'progressive localization' model may more accurately reflect the composition of proto-Gulf tectonics.

Rift Localization and the Modern-Gulf of California

In contrast to the proto-Gulf period, there is general consensus about the evolution of the modern-Gulf of California. Shortly after 6.1 Ma, transfer of the Baja California peninsula to the Pacific plate was largely complete with the plate boundary focused into the modern-day Gulf of California (Oskin et al., 2001; Oskin and Stock, 2003a). Additionally, the 6.5 - 6.3 Ma marine incursion into the northern Gulf of California is coincident with this onset of focused PAC-NAM plate motion, which likely helped to create a continuous axis of crustal thinning that facilitated the incursion of marine waters (Oskin and Stock, 2003c). Following ~6 Ma, the active rift axis was focused in extensional basins found today in the eastern marine basins of the Gulf of California. The rift axis migrated westward ca. 3.3 - 2.0 Ma, abandoning this N-S string of eastern extensional basins, and has since been focused along the western edge of the Gulf of California (Aragón-Arreola and Martín-Barajas, 2007). During modern-Gulf time, the PAC-NAM plate boundary was, and remains, a largely

focused oblique plate boundary of short extensional basins connecting right-stepping dextral fault systems (Fig. 2D).

TESTING THE RIFT OBLIQUITY HYPOTHESIS

Because the oblique Gulf of California rift is dominated by major dextral strike-slip faults, it is important to examine the role of these structures in strain localization. If localized extension was favored in areas of strike-slip faulting, then the onset of dextral shear in the Gulf of California may have set the stage for subsequent continental rupture ca. 6 Ma. I hypothesize that the well-documented rupture of the Gulf of California at ca. 6 Ma was coincident with or closely preceded by earliest dextral faulting within the Gulf Extensional Province. These dextral faults acted to enhance extensional strain rates, concentrate lithospheric strain, and focus a broad extensional plate boundary into a narrow zone of focused rifting. Ultimately, this focused lithospheric strain was the catalyst for formation of trans-lithospheric faults and rupture of continental lithosphere in the Gulf of California.

To test the role of obliquity and its ability to facilitate focused rifting, timing constraints for the onset of transtensional tectonics must be obtained. Determining this timing will aid in testing whether earliest dextral shear within the GEP coincided with either (1) continental rupture at the beginning of the modern-Gulf stage (strain partitioning), or (2) prior to rupture during the proto-Gulf stage (distributed transtension). If the onset of transtension coincided closely with the onset of continental rupture in the Gulf of California, this lends support to the hypothesis that the obliquity of a rift and the resultant enhanced strain rate plays a key role in the rupture potential of a continent.

To evaluate the magnitude of proto-Gulf dextral shear in coastal Sonora and therefore test the role of obliquity in continental rifting, a study area was selected along the eastern

margin of the Gulf of California (Fig. 4, Plate 1). Here, dextral faults (e.g. Sacrificio fault) are recognized onshore (Gastil and Krummenacher, 1977a,b; Oskin and Stock, 2003a) that may be directly linked to the transform faults offshore (e.g. De Mar fault, Fig. 4; Aragón-Arreola and Martín-Barajas, 2007) that accommodated oblique Gulf opening. In addition to its proximity to the modern rift axis, the study area is also host to both pre-rift and syn-rift volcanic and sedimentary rocks (Gastil and Krummenacher, 1977a; Oskin and Stock, 2003a,b) that could likely record a continuous and detailed rift history.

This study utilizes detailed structural field mapping, fault kinematic analysis, paleomagnetic analysis, stratigraphic analysis, and geochronology in an investigation of these deformed pre-rift and syn-rift rocks to construct a detailed geologic history for coastal Sonora from Miocene time to the present. Based upon detailed structural field mapping, I construct a stratigraphic and structural context for pre-rift and syn-rift volcanic and sedimentary deposits. Fault kinematic analysis provides a quantitative representation of paleo-stress fields. Paleomagnetic analysis of pre-rift and syn-rift isotopically-dated volcanic rocks quantifies the amount of vertical-axis rotation that is associated with dextral shear and provides timing constraints for these rotations. Stratigraphic analysis of sedimentary rocks builds a framework for depositional environments and their tectonic significance. Geochronology of these pre-rift and syn-rift volcanic rocks provide chronologic constraints for earliest basin formation related to rift-related tectonics. Altogether, this study aims to better understand the role of obliquity in continental rifting, while testing the hypothesis that the rupture of the Gulf of California at ca. 6 Ma was coincident with or closely preceded by earliest dextral faulting within the Gulf Extensional Province.

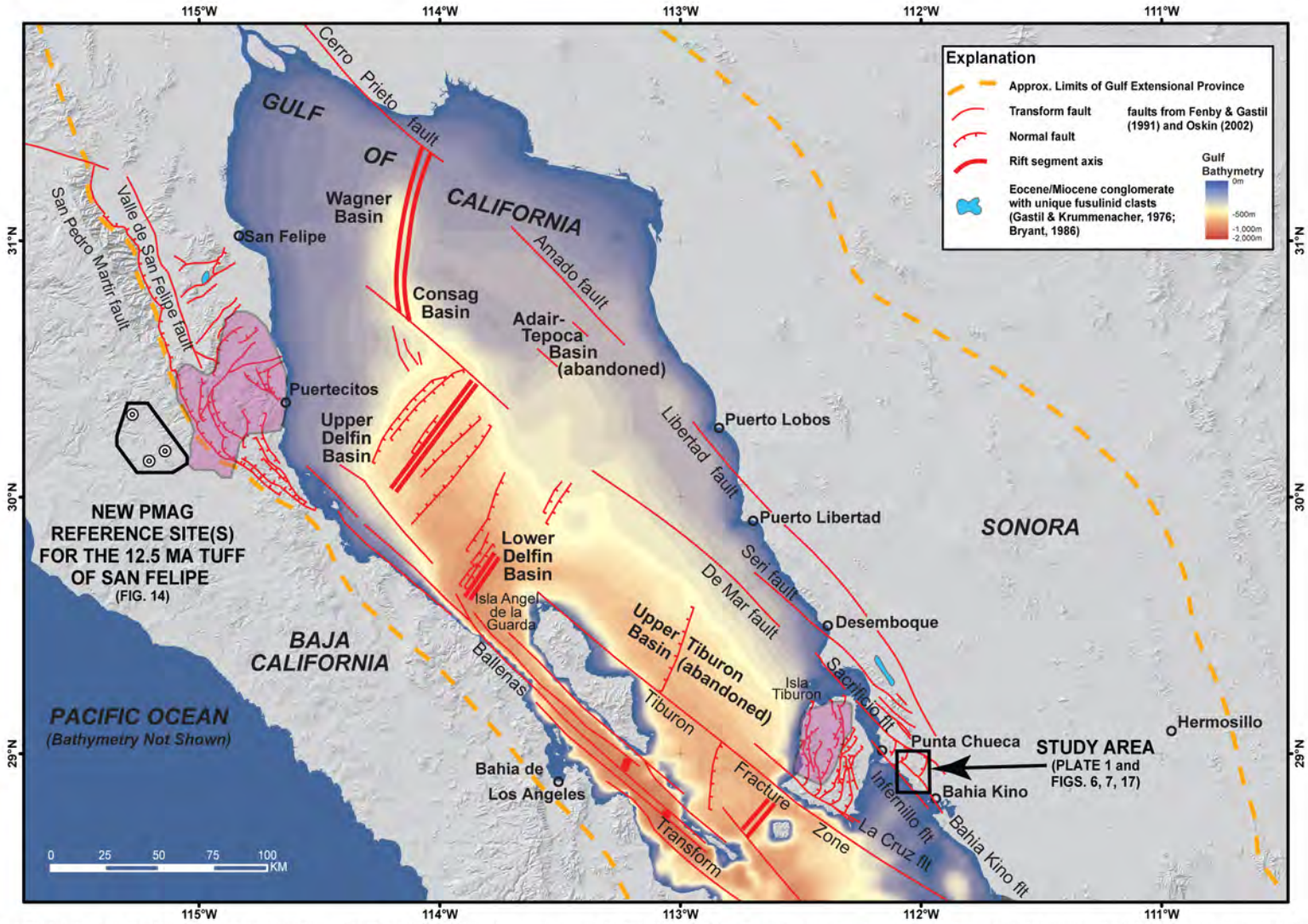

Figure 4. Hillshade and bathymetry of the northern Gulf of California, showing area of detailed 1:10,000-scale geologic mapping in coastal Sonora (black rectangle), and smaller-scale geologic mapping in central Baja California (black polygon; Figure 14) where a new paleomagnetic reference site for the Tuff of San Felipe in central Baja California was drilled (white dots). Structures related to oblique rifting (red) are shown. Correlation of late Miocene (6.4 - 6.1 Ma) volcanic deposits across the Upper Delfin Basin (purple polygons; Oskin et al., 2001) constrain the opening of the northern Gulf to post- ~6 Ma.

PREVIOUS WORK

Pacific-North America Plate Boundary

Wegener (1924) applied continental drift concepts to explain the Gulf of California when he suggested that the Baja California peninsula had been dragged to the south, away from mainland Mexico. He also correctly suggested a northward sliding of the peninsula, or lag relative to the Mexican mainland, which was presumably sliding southward at a faster rate. The PAC-NAM plate boundary in the Gulf of California was first accurately recognized as a transtensional pull-apart feature by Hamilton (1961) who suggested that the Baja California peninsula had been translated ~150 miles towards the northwest with ~100 miles of separation (extension) along faults related to the San Andreas fault system. Larson et al. (1968) confirmed this idea with magnetic anomaly transects at the mouth of the Gulf demonstrating that the southernmost tip of the peninsula was torn from the mainland of Mexico by 4 Ma. Spencer and Normark (1979) discovered the Tosco-Abreojos fault zone west of Baja California, and attributed it as a major component of the PAC-NAM plate boundary from 12 - 4 Ma. Stock and Hodges (1989) first proposed the 'strain partitioning' model with examination of the timing and direction of extensional structures during proto-Gulf time, along with direction and amount of PAC-NAM plate motion throughout Miocene time. Oskin et al. (2001) reinforced this concept with correlation of 12.5 - 6.1 Ma volcanic stratigraphy located within the GEP that are offset by the same amount across the GEP. In contrast, Gans (1997) proposed the unimodal 'distributed transtension' concept through observations of 27 - 12 Ma extensional structures in the GEP that are cut by proto-Gulf dextral faults.

Coastal Sonora

McGee and Johnson (1896) accurately summarized the geology of the coastal Sonoran region when they wrote, "…the intermontane expanses are simply planed rock strata with a scant veneer of torrent-spread alluvium." They also reported evidence for a recent high sea level stand to explain marine shells found in the southeastern corner of the study area, where closed depressions slightly below sea level are common. Of course, not all marine shells in the region are evidence for recent high sea level stands. Throughout the study area, sun-bleached marine shells can be found intercalated in modern drainages and on bedrock hillslopes multiple kilometers inland at elevations exceeding 100 m. These marine shells are likely the littered remains of meals eaten historically by members of the native Comcáac tribe who have inhabited the coastal Sonora region for centuries, rather than evidence of a recent sea level high.

After visiting the Bahía Kunkaak area, Beal (1948) published a 1:1,000,000 reconnaissance geologic map of the Gulf of California and the Baja California peninsula that illustrated some major rift-related structures west of Isla Tiburón. However, no structures near the study area are depicted and the entire study area is mapped as crystalline or metamorphic basement. During a 1940 Scripps Cruise into the Gulf of California, Anderson (1950) made fundamental observations about the nonconformable contact and age relationships between Late Cretaceous basement rocks and the overlying Tertiary rocks near Guaymas. These relationships hold true in the study area and throughout much of the northern Gulf of California region. Gastil and Krummenacher produced a 1:150,000-scale regional geologic map (1977a) and reconnaissance report with geochronologic results (1977b) of the deformed rocks in the study area. Oskin (2002) improved on the resolution of the study area with a 1:50,000-scale map (his Plate 1) based on interpretations of Landsat

imagery and reconnaissance mapping of Late Miocene ignimbrite deposits. Regional geochronologic, geochemical, and isotopic studies of the coastal Sonora batholith (Ramos-Velázquez et al., 2008; Valencia-Moreno et al., 2001; Valencia-Moreno et al., 2003) dated and documented a variety of igneous rocks in coastal Sonora. Paleomagnetic studies by Oskin et al. (2001) and Herman and Gans (2006) identified clockwise vertical-axis rotation of rocks exposed along the Sonoran coastline that could have occurred during the proto-Gulf time period.

GEOLOGIC MAPPING IN COASTAL SONORA

Detailed geologic mapping (Plate 1) was conducted on a variety of base maps at a variety of scales (Plate 1 inset). Mapping in coastal Sonora during Winter 2006/2007 was completed on the 'Bahía Kino', 'Bahía Kunkaak', and 'Punta Chueca' 1:50,000-scale 1/3-degree (longitude) by 1/4-degree (latitude) Instituto Nacional de Estadística y Geografía (INEGI) topographic base maps enlarged to 1:12,000-scale. Mapping in Sonora during Winter 2007/2008 was completed on 1:10,000-scale, Quickbird satellite imagery with topographic contours derived from the 90-m Shuttle Radar Topography Mission (SRTM) digital elevation model (DEM). Quickbird imagery included three multispectral bands at 2.4 m resolution and one panchromatic band at 0.6 m resolution. The multispectral bands were pan-sharpened to generate a 0.6 m resolution false-color base map. This integrated imagery dataset enhanced the different wavelengths of light reflected from rocks of variable iron composition and assisted with locating structures and geologic contacts between lithologic units (Hook et al., 1998). The imagery dataset was exploited both in the field while mapping on paper maps, and in the office when completing areas not mapped on foot. Mapping in central Baja California in May 2008 was conducted on the 'El Metate' and 'Matomi'

1:50,000-scale INEGI topographic base maps at both 1:50,000-scale and on enlarged 1:20,000-scale base maps.

STRATIGRAPHY AND GEOCHRONOLOGY

Stratigraphic and Geographic Context

A regional stratigraphic framework for the northern Gulf of California (Oskin and Stock, 2003b) divides the stratigraphy into four groups overlying basement rocks. For the sake of continuity and clarity, this study adopts and applies this framework to the local stratigraphy mapped in coastal Sonora (Fig. 5).

Within the study area, basement rocks and stratigraphic groups one and two consist of lithologic units present prior to rifting in the Gulf of California. Basement rocks include both the Late-Cretaceous coastal Sonora batholith (Ramos-Velázquez et al., 2008) and their Paleozoic metamorphic host rocks (Gastil and Krummenacher, 1977a,b). Group one includes Oligo-Miocene fluvial sedimentary rocks that lay nonconformably on basement. Group two consists mostly of andesitic and basaltic flows and pyroclastic deposits emplaced in association with a subduction-related arc (Hausback, 1984, Oskin and Stock, 2003b). Group two also includes the 12.5 Ma Tuff of San Felipe, a regional ignimbrite than spans both margins of the Gulf of California rift (Stock et al., 1999; Oskin et al, 2001). Group three consists of interfingering basalt and rhyolite flows, non-marine sedimentary deposits, and pyroclastic rocks, culminating with the 6.4 Ma Tuffs of Mesa Cuadrada, and were deposited broadly during proto-Gulf time. Group four consists of additional non-marine sedimentary deposits, occasional interbedded pyroclastic ash deposits, all of which were deposited during latest proto-Gulf time. Alluvial and coastal deposits are late Quaternary in age. Published

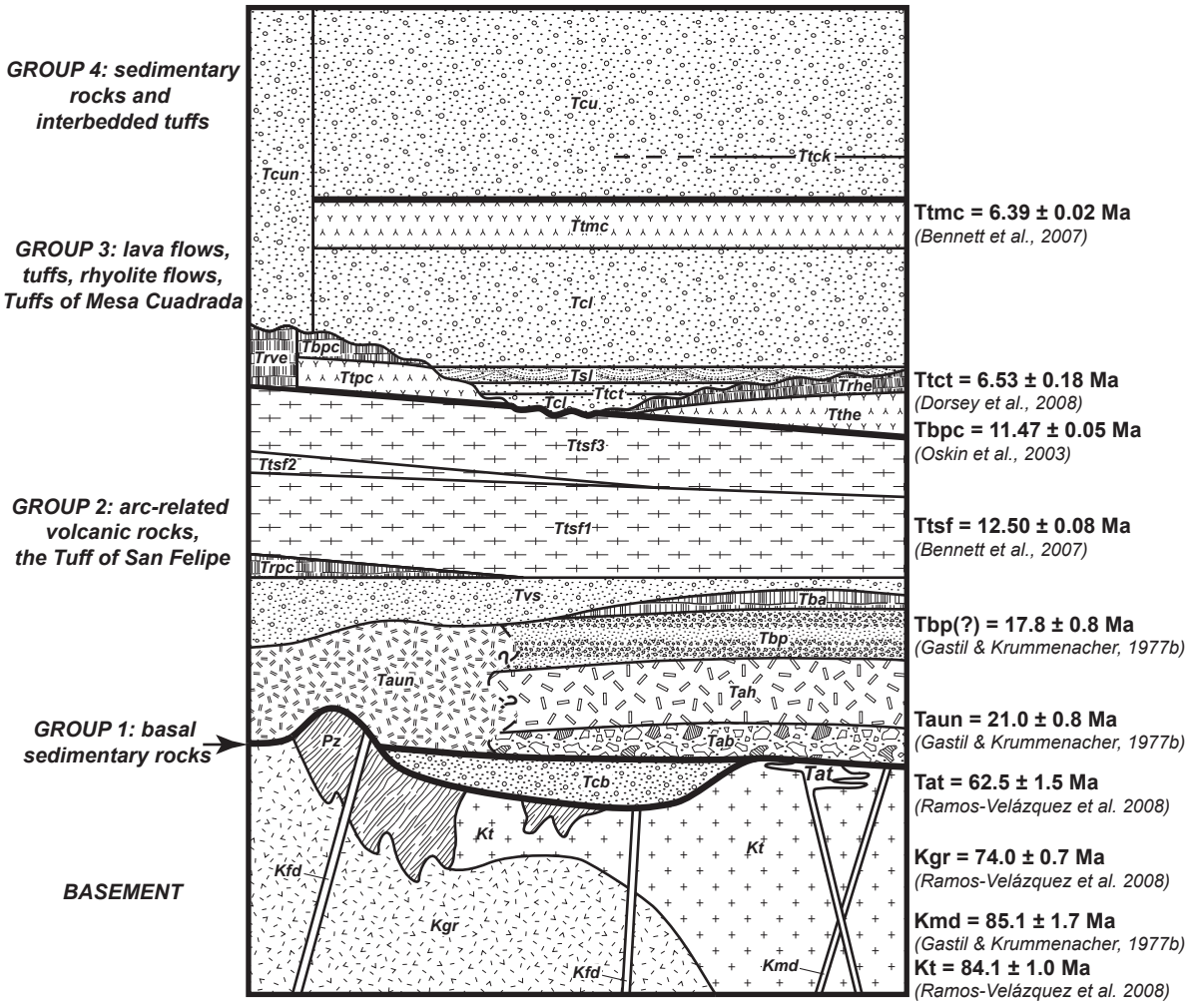

Figure 5. Generalized stratigraphic and chronologic relationships of mapped pre-Quaternary geologic units from the coastal Sonora study area. Bold black lines separate the four chronologic groups, following Oskin and Stock (2003b). See text and geologic map (Plate 1) for detailed unit names, unit descriptions, and published geochronology. Published isotopic ages (Table 1) from individual units within the study area are shown.

Table 1. Summary of published geochronologic results from lithologic units within the coastal Sonora study area.

Lithologic Group	Published Lithologic Name	Map Symbol of This Study	Fault Block of This Study	Published Rock Type	Sample #	X Location, Latitude or Easting (m)	Y Location, Latitude or Northing (m)	Published Age (Ma)	Isotopic Technique	Mineral	Reference
Basement											
	Kino Granodiorite	Kt	Cerro Kino	granodiorite	KI-03-07	399405	3194133	84.1 ± 1.0	U/Pb	zircon	Ramos-Velázquez et al. (2008)
	Older porphyritic dike rocks	Kmd	Cerro Kino	hornblende andesite	S1G-5	112°01'50"	28°52'20"	85.1 ± 1.7	K-Ar	hornblende	Gastil & Krummenacher (1977b)
	Rancho Nuevo Granite	Kgr	Granito	granite	KI-03-03	402750	3198692	74.0 ± 0.7	U/Pb	zircon	Ramos-Velázquez et al. (2008)
	Tordillo Andesite	Tat	Eco	andesite	KI-04-08	400894	3202605	62.5 ± 1.5	K-Ar	whole rock	Ramos-Velázquez et al. (2008)
Group 2											
	Tertiary volcanic rocks	Tbp(?)	Cerro Kino	dacite	S3G-764	112°00'05"	28°52'35"	17.8 ± 0.8 20.8 ± 5.7	K-Ar K-Ar	hornblende biotite	Gastil & Krummenacher (1977b) Gastil & Krummenacher (1977b)
	Tertiary volcanic rocks	Taun	Cerro Tordillo	andesite	S2K-31	112°02'45"	28°59'20"	21.0 ± 0.8	K-Ar	hornblende	Gastil & Krummenacher (1977b)
	Tuff of San Felipe	Ttsf	Punta Chueca	ash-flow tuff	PC-98-18	394475	3208720	12.50 ± 0.08	Ar-Ar	anorthoclase	Bennett et al. (2007)
Group 3											
	Basalt of Punta Chueca	Tbpc	Punta Chueca	basalt	PC-00-06	394680	3208770	11.47 ± 0.05	Ar-Ar	volcanic matrix	Oskin et al. (2003)
	Tuff of Cerro Tordillo	Ttct	Punta Chueca	air-fall tuff	BK-08-32	394740	3206320	6.53 ± 0.18	U/Pb	zircon	Dorsey et al. (2008)
	Tuffs of Mesa Cuadrada	Ttmc	Punta Chueca	ash-flow tuff	BK-02-08	394790	3206850	6.39 ± 0.02	Ar-Ar	sanidine	Bennett et al. (2007)

geochronologic results from samples collected within the study area are summarized in Table 1 and labeled in Figure 5.

The study area is divided into fault blocks that are defined by rift-related structures that will be discussed later. These structures created and later deformed tectonic basins (Fig. 6). These fault blocks and tectonic basins are frequently referred to for both geologic and geographic context.

Basement

Pre-Eocene Basement Rocks

Pre-Eocene basement rocks consist of probable Paleozoic-age metamorphic rocks (Gastil, 1993) that are intruded by Late Cretaceous tonalite, granite, both mafic and felsic dikes, and Early Paleocene shallow intrusions (Plate 1; Ramos-Velázquez et al., 2008).

Paleozoic-age map units group meta-sedimentary (*Pzms*), meta-carbonate (*Pzcb*) and meta-igneous (*Pzig*) rocks. *Pzms* consists of gray to black quartzite and slate. *Pzig* consists of meta-basalt or meta-gabbro with multiple crosscutting felsic dikes. *Pzcb* consists of meta-limestones and meta-carbonate-cemented sandstones that form 0.5 - 5 cm-thick alternating bands of gray, white, and orangish-red.

Basement rocks in much of the southern, central, and western portions of the study area are comprised of a tonalite (*Kt*) containing plagioclase (long axis up to 0.5 cm) ≈ hornblende (long axis up to 1.0 cm) ≈ quartz (locally up to 1.0 cm in diameter) > biotite. Ramos-Velázquez et al. (2008) reported an U/Pb zircon age of 84.1 ± 1.0 Ma for their 'Kino Granodiorite' where *Kt* is exposed in the Cerro Kino block. Here, multiple sub-vertical hornblende-rich mafic dikes (*Kmd*), up to 35 m-thick, intrude the tonalite, and have coarser

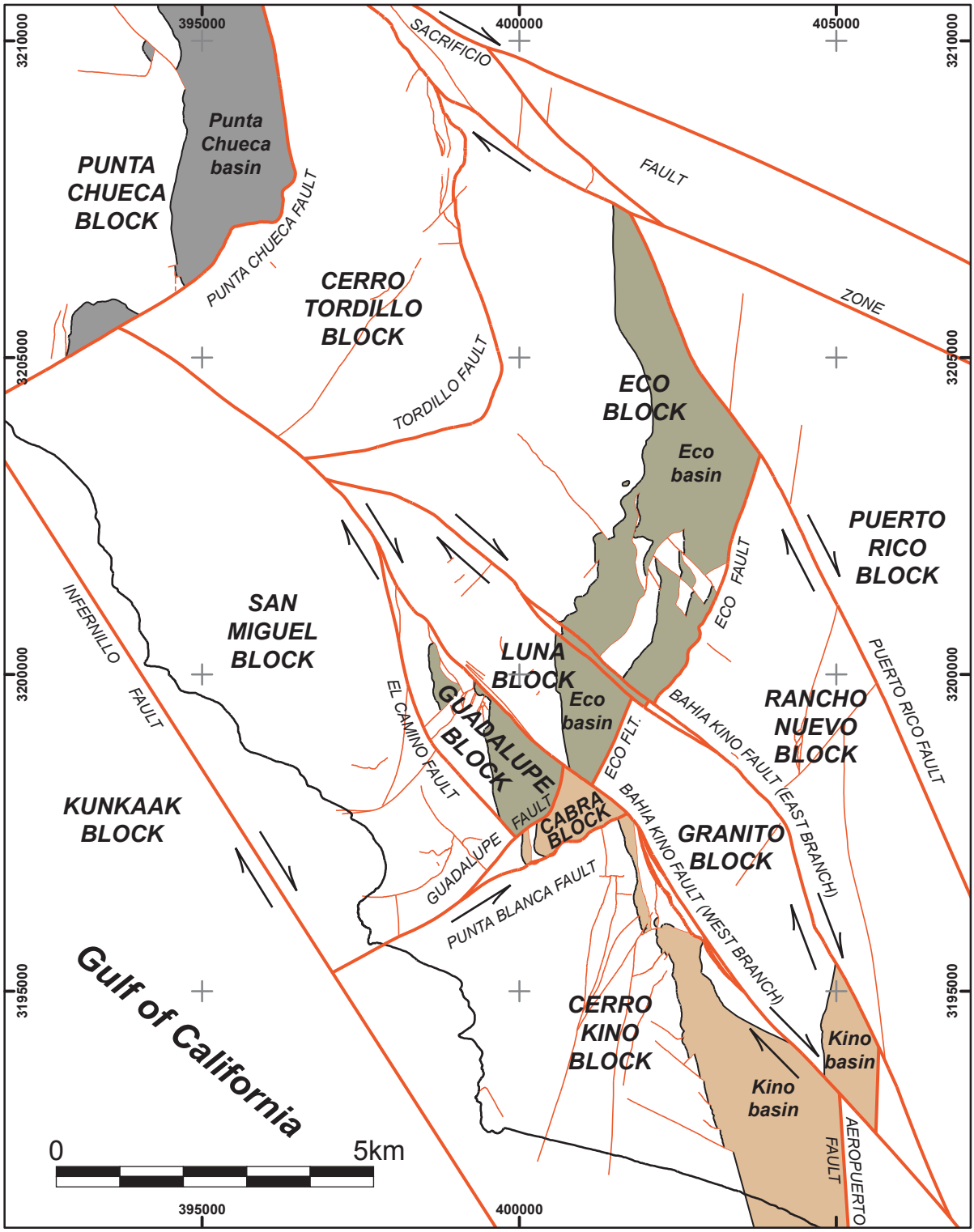

Figure 6. Simplified geologic map showing major faults (thick red lines) that bound fault blocks. Three distinct sedimentary basins (Punta Chueca, Eco, and Kino) formed in the hanging wall of N- to N-striking normal fault systems. Minor faults (thin red lines) also deform these sedimentary basins. Base of sedimentary basins (thin black lines). See Plate 1 for detailed geology.

porphyritic to pegmatitic edges and finer phaneritic to porphyritic cores. Gastil & Krummenacher (1977b) reported a K-Ar age of 85.1 ± 1.7 Ma from these mafic dikes.

Basement rocks in much of the eastern and northern portions of the study area are comprised of a granite (*Kgr*) with abundant alkali-feldspar megacrysts up to 2 cm in length > quartz >> plagioclase-feldspar ≈ biotite ≈ amphibole. Multiple intrusive contacts demonstrate that *Kgr* is younger than *Kt* and all Paleozoic units (e.g. baked contacts, *Kgr* dikes cutting all other basement rocks). Locally, modern-Gulf faults have preferentially localized along these intrusive contacts as pre-existing planes of weakness (e.g. Eco and Puerto Rico blocks, Plate 1). Ramos-Velázquez et al. (2008) reported a U/Pb zircon age of 74.0 ± 0.7 Ma for their 'Rancho Nuevo Granite" in the Granito block where *Kgr* is observed. Ramos-Velázquez et al. (2008) also reported an U/Pb zircon age of 90.1 ± 1.1 Ma for their 'Kino Granodiorite' in the Puerto Rico block where the alkali-feldspar megacryst granite (*Kgr*) is mapped. This age is at least 6.0 Myr older than all other dated 'Kino Granodiorite' samples in coastal Sonora and does not appear to be a granodiorite. This sample may have been collected from an older episode of granitic pluton emplacement that may pre-date both *Kgr* and *Kt*, not yet differentiated by existing mapping.

Felsic dikes (*Kfd*) appear to cut all basement rocks. *Kfd* is mapped where these dikes are thick (up to 15 m-thick) and are useful for bedrock offsets across brittle faults.

The hypabyssal Tordillo Andesite (*Tat*) is locally observed below Oligocene and younger volcanic and sedimentary units. *Tat* is observed intruding only into basement rocks; its contact with Oligocene and younger rocks is an erosional nonconformity. *Tat* is a phaneritic andesite, too mafic to be considered *Kt* and too coarsely crystalline to be part of the overlying extrusive Miocene rocks. *Tat* consists of hornblende (up to 1.5 cm in length) >> plagioclase-feldspar > biotite > quartz. Ramos-Velázquez et al., (2008) also observed

outcrops of *Tat* in the Eco block where they reported a 62.5 ± 1.5 Ma K-Ar whole rock age. These *Tat* outcrops in the Eco block were not observed during this study and the limits of this unit in the Eco block are not delineated on the geologic map (Plate 1) nor on maps by Ramos-Velázquez et al., (2008). A candidate for the *Tat* feeder dike is observed within the San Miguel block, though petrographic examination is needed to verify the correlation.

The upper contact of all basement rocks is a nonconformity buried by both sedimentary and volcanic units typically deposited on an erosional surface lacking significant relief. At this nonconformity, paleosols were locally observed to have developed, with alteration penetrating up to 3 m into basement rocks.

Group 1

Tertiary Basal Sedimentary Rocks (*Tcb*)

Locally, coarse-grained conglomerate (*Tcb*) nonconformably overlies basement rocks. These basal deposits have purplish-gray to maroon matrix, are typically moderately- to well-stratified, and range from fine-grained sandstone to pebbly sandstones to cobble conglomerates with clast compositions dominated by andesite and less common clasts of all basement units. Together these deposits suggest a fluvial environment near a volcanic source. Uncommon pyroclastic breccias are also present in *Tcb*. Deposits of *Tcb* are up to 300 m thick with individual beds measuring up to 2 m-thick.

An Oligocene to Early Miocene age is assigned to *Tcb*, which is underlain by Cretaceous tonalite and overlain by Early Miocene volcanic rocks. This preferred age is based on three assumptions: (1) the time needed to exhume the underlying crystalline basement, (2) the dips of *Tcb* and the overlying Early Miocene volcanic rocks are indistinguishable, suggesting little time elapsed between deposition of both units, and (3)

clast composition appears similar to the overlying andesitic rocks, suggesting nearby arc-related andesite flows older than, but related to, the overlying volcanic section where eroded and transported into the study area.

Group 2

Miocene Arc-related Volcanic Rocks

Arc-related volcanic rocks ranging from 200 - 700 m-thick overlie basement rocks in nonconformable contact or conformably overlie group one rocks. These group two volcanic deposits are likely related to arc volcanic activity associated with the Early- to Middle-Miocene Comondú arc and subduction of progressively younger oceanic Farallon lithosphere (Gastil et al., 1979; Hausback, 1984).

In the southern part of the study area, this volcanic section is a thick sequence of andesitic flows and pyroclastic breccias (*Tab*), multiple flows consisting of a distinctive hornblende-rich porphyritic andesite (*Tah*), pyroclastic breccias (*Tbp*), and a basaltic-andesite flow (*Tba*), that are typically ~700 meters in combined thickness. *Tab* is a moderately resistant unit that varies along strike from a maroon mono-lithologic andesitic pyroclastic breccia with rare blocks of *Kt*, to a porphyritic andesite flow with centimeter-scale hornblende and plagioclase phenocrysts. *Tah* is a very resistant ridge- and cliff-forming unit that consists of multiple stacked andesitic flows that locally exhibits a 1 - 3 cm-spaced foliation. Each flow is a purplish-gray massive porphyritic andesite flow with centimeter-scale hornblende (locally twinned) >> sub-centimeter plagioclase and olivine phenocrysts, and few xenolith boulders of *Kt* up to 60 cm in diameter. *Tbp* is a resistant unit that consists of multiple poly-lithologic pyroclastic breccia and tuff breccia layers containing 30-80% sub-angular lithic fragments of dacite, andesite, rhyolite, and rare tonalite (*Kt*) up to 1 m in

diameter, 10-30% andesitic pumice up to 0.5 cm in diameter, and 40-60% tan and pink nonwelded ash matrix. Individual pyroclastic beds range from 0.5 to 2 m-thick, locally with an epiclastic layer up to 2 m-thick at the base of *Tbp*. Locally, a 2 m-thick light gray to purplish-gray basalt flow (*Tbbp*) is locally mapped within *Tbp* in the southernmost corner of the San Miguel block. *Tba* is a moderately-resistant basaltic andesite flow consisting of (1) a 1-2 m-thick basal breccia of dark gray and pink scoria fragments with olivine and hornblende phenocrysts, (2) a 5 m-thick main body of dark purplish-gray poorly-foliated basaltic andesite with <10% phenocrysts of olivine (1-3 mm) and oxidized hornblende (1-5 mm), and (3) a 1-3 m-thick upper breccia similar to the basal breccia. The basal contact of *Tba* is sharp but undulatory on the underlying pyroclastic deposits (*Tbp*).

In the central and northern part of the study area, the group two volcanic section is mapped as undifferentiated andesite (*Taun*). *Taun* is generally thinner than the group two section to the south, ranging from 200 - 600 m-thick. It consists of aphanitic andesite or hornblende-rich porphyritic andesite with local and discontinuous 3 m-thick red pyroclastic beds mapped as internal marker beds. *Taun* to the north and the andesitic sequence in the south are likely coeval volcanic deposits formed from distinctive volcanic centers. *Taun* in the northern study area may correlate to *Tah* in the south, based on their similar abundance of hornblende phenocrysts observed in hand sample. Other units would presumably pinch out along strike. However, subsequent rift-related faulting complicates this correlation across the El Camino fault and further petrographic studies are required to verify the correlation. In the overlying sedimentary rocks, clasts from the southern and northern volcanic sections are usually indistinguishable, so any clast from the andesitic-rich group two section will be referred to as *Ta2*.

Gastil and Krummenacher (1977b) reported K-Ar ages for two samples from this volcanic section within the study area: a 21.0 ± 0.8 Ma hornblende age on an andesite within the Cerro Tordillo block where *Taun* is observed, and both a 17.8 ± 0.8 Ma hornblende age and a 20.8 ± 5.7 Ma biotite age from a "dacite" within the Cerro Kino block where the thick southern volcanic sequence is observed. Because no quartz phenocrysts were observed from any unit within this volcanic sequence, this latter age is likely either a dacitic lapilli or block from within *Tbp* or a misidentified andesite flow.

Overlying both the southern volcanic sequence and the undifferentiated section in the north is a map unit dominated by both epiclastic and pyroclastic deposits (*Tvs*). *Tvs* varies from thick (220 m) resistant cliff-forming deposits that thicken to the south in the southern study area, to thick (120 m) and recessive deposits in the northern study area, to thin (0 - 30 m) and recessive in the eastern study area. The best exposures of *Tvs* are in the Cerro Kino block, which consists of (1) a basal unit of moderately- to well-sorted fine- to medium-grained orange volcaniclastic sandstone beds up to 10 cm-thick, (2) reversely-sorted orange and pink volcaniclastic debris-flow deposits with lower portions of each deposit typically consisting of 90% ash matrix, 0% pumice, and 10% lithic fragments of andesite, basaltic-andesite, and tonalite, and upper portions typically consisting of 50% ash matrix, 5% pumice up to 10 cm in length, and 45% lithic fragments of andesite, basaltic-andesite, and tonalite up to 20 cm in length, (3) multiple welded ash-flow lapilli tuffs typically consisting of 70% ash and plagioclase phenocryst matrix, 5% flattened and devitrified pumice with plagioclase and hornblende phenocrysts, and 25% lithic fragments of andesite, basaltic-andesite, and tonalite up to 10 cm in diameter, (4) multiple 2 - 3 m-thick pisolitic tuffs comprised of spherical accretionary lapilli up to 5 cm-diameter, (5) a welded ash-flow lapilli tuff as (3) above, and (6) ~10 m of 10 - 50 cm-thick fluvial volcaniclastic beds of medium-grained sandstone and

coarse-gravel conglomerate. In the Cerro Tordillo block *Tvs* consists of (1) fluvial pebbly sandstone with subrounded to rounded clasts of underlying andesitic units, (2) poorly-stratified burgundy-red clast-supported pebble-cobble conglomerate with angular to subrounded clasts of rhyolite, andesite, and rare crystalline basement up to 30 cm in diameter, (3) poorly-stratified clast-supported sandy cobble-boulder conglomerate and cross-bedded pebbly sandstone with subrounded clasts of andesite up to 30 cm in diameter.

Rhyolite of Punta Chueca (*Trpc*)

The Rhyolite of Punta Chueca (*Trpc*) locally underlies *Ttsf* in the southwestern corner of the Punta Chueca block. Within these limited outcrops, *Trpc* is 10 to 30 m thick and exhibits a 1 - 5 cm-spaced flow foliation.

Tuff of San Felipe (*Ttsf*)

Deposits of the Tuff of San Felipe (*Ttsf*), a regionally extensive Miocene ignimbrite deposit that blanketed >4,000km^2 of present-day northeastern Baja California and western Sonora (Oskin and Stock, 2003a), can be found throughout the study area and act as an excellent marker for structural studies. In coastal Sonora *Ttsf* lies disconformably on older group two rocks and generally thickens to the northwest, from 135 m thick in the Cerro Kino block (Oskin, 2002), to ~200 m thick in the Eco block, to ~340 m thick in the northern Cerro Tordillo block, to >500 m thick in the Punta Chueca block. After stretched pumice-fiamme lineations measured in tilted deposits of *Ttsf* (flattening axes ratio up to 20:1) are restored about a strike-line axis, pumice-fiamme long axes suggest an approximate E-W flow direction for the *Ttsf* eruption in the northern study area (Fig. 7). These data combined with the observed thickening trends for *Ttsf* are consistent with *Ttsf* the vent location proposed by

Oskin (2002) and Oskin and Stock (2003a) to lie just west of the northwestern edge of the study area, near Punta Chueca.

Ttsf consists of up to three cooling units, each varying in thickness across the study area. The first cooling unit (*Ttsf1*) consists of (1) a basal nonwelded yellow airfall tuff with few volcanic lithics up to 1.0 cm in diameter, and is observed to be 0.5 to 7 m-thick (typically <1 m-thick), overlain by (2) black glassy vitrophyre 0.5 to 8 m thick (anomalously ~20 - 30 m thick in the Granito block), with occasional sub-centimeter oxidized spherulites. The vitrophyre grades upward into (3) a densely welded spherulite-rich zone of pumice-poor brick-red tuff up to 5 m thick. Some large spherulites have been dissolved away leaving voids (geodes) up to 10-cm diameter containing concentrations of euhedral quartz and/or chalcedony on internal walls. The spherulitic zone grades upward into (4) a variably thick densely welded zone of pumice-fiamme-rich burgundy lapilli tuff with a distinctive eutaxitic foliation of pumice-fiamme. Large pumice are flattened to 0.1 - 2 cm thick and stretched up to 1 m in length measured in the lineation direction. *Ttsf* commonly displays a platy or fissile weathering pattern, where large resistant pumice-fiamme protrude from the recessive vapor-phase altered welded ash matrix. Pumice concentration increases higher in the unit, as does the degree of vapor-phase alteration. Segregation pipes oriented orthogonal to eutaxitic foliation are observed in the upper few meters. Local internal rheomorphic flow deformation is observed as strong folding and/or brecciation of foliated pumice-fiamme, commonly overturned and/or oriented perpendicular to the strike of the unit. Locally, *Ttsf1* contains <5 m of distinctively foliated fiamme-rich tuff immediately above the basal vitrophyre, below the spherulitic-rich zone. Within fiamme-rich portions of *Ttsf1*, rare to uncommon pods of distinctive cognate black rhyolite lava inclusions that contain alkali-feldspar, plagioclase, and fayalite phenocrysts (Oskin and Stock, 2003a) are observed.

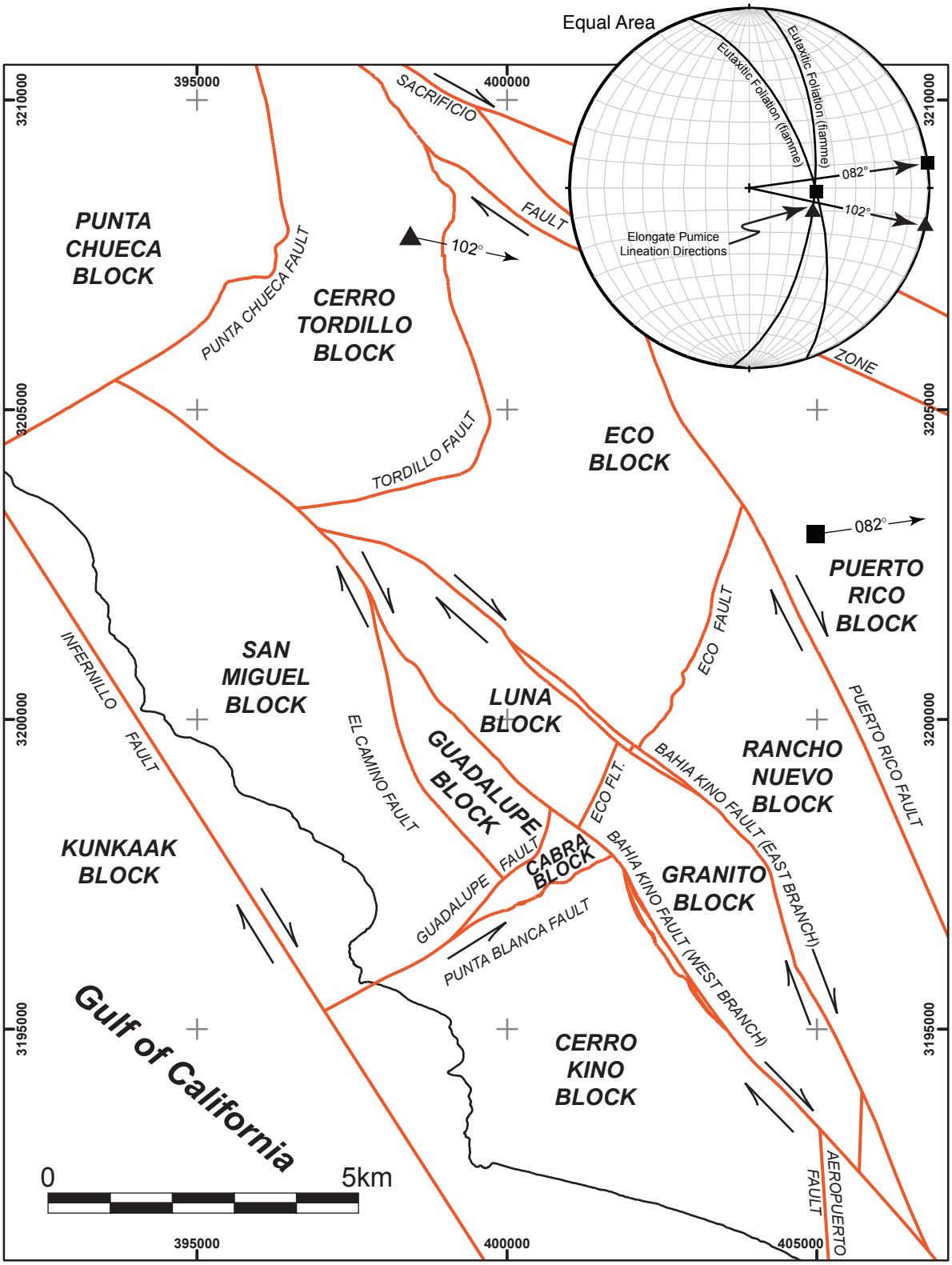

Figure 7. Stereonet shows trend and plunge of titled (right center of net) and corrected (right edge of net, black arrows on map) stretched pumice lineations measured in the Tuff of San Felipe (Ttsf) ignimbrite deposit. After corrections for the structural tilting of these lines, these two lineations suggest an easterly flow direction and a vent location for the Tuff of San Felipe west of the northern study area. This location agrees with previous work (Oskin, 2002) that suggested a vent location between the town of Punta Chueca and the northwestern edge of the study area. If dextral offset is assumed for the Puerto Rico fault system, restoration of this slip, not yet quantified, would likely strengthen the precision of these data.

The second cooling unit (*Ttsf2*) consists of (1) a basal black vitrophyre up to 5 m thick with tabular segregation pipes up to 5 cm thick oriented approximately paleo-vertical (i.e. orthogonal to eutaxitic foliation), overlain by (2) a yellow poorly welded ash-flow lapilli tuff 8-15 m thick with similar segregation pipes as its underlying vitrophyre. *Ttsf2* is observed only in the central and northern study area, appears to thicken from southeast (Cerro Tordillo block) to northwest (Punta Chueca block), similar to the thickening trend of the general *Ttsf* unit, and is best exposed in the southeast corner of the Cerro Tordillo block.

The third cooling unit (*Ttsf3*) consists of (1) a ~1 m-thick basal surge deposit of trough cross-bedded dunes and antidunes of orangish-yellow ash, overlain by (2) a black glassy vitrophyre 0.1 to 1.0 m thick, overlain by (3) a densely welded spherulitic-rich zone of pumice-poor brick-red tuff up to 2 m thick with spherulite geodes up to 5-cm diameter containing concentrations of euhedral quartz or chalcedony on internal walls, which grades upward into (4) a densely welded zone similar to upper *Ttsf1*. *Ttsf3* is best exposed in the southeast corner of the Cerro Tordillo block.

Where all three cooling units are observed, the densely welded *Ttsf1* and *Ttsf3* units are both thicker than *Ttsf2*. The *Ttsf2* cooling unit is of limited regional extent. Where *Ttsf2* is not present, only the *Ttsf1* unit is mapped. However, in the Cerro Kino block subtle and discontinuous evidence exists for two cooling units (Oskin, 2002) that likely represent both of the densely welded cooling units of *Ttsf1* and *Ttsf3*, which are basically indistinguishable without *Ttsf2* to separate them. Subtle evidence for a similar tuff stratigraphy (*Ttsf3* on *Ttsf1*) may also exist in the Eco block. Both the *Ttsf1* and *Ttsf3* cooling units represent large-volume eruptions that likely occurred within hours to days of each other and are representative of the regionally extensive outcrops of *Ttsf* observed across both margins of the northern Gulf of California. A similar tuff stratigraphy of two cooling units within *Ttsf*

may also exist at the new paleomagnetic reference site in central Baja California discussed in detail later. When referring to *Ttsf* as a chrono-lithologic unit, the more general acronym, *Ttsf*, will be used and *Ttsf* may include from one to three cooling units.

Deposits of the Tuff of San Felipe across the northern Gulf of California consistently have an unusual shallow up (~5°) to the southwest direction of paleomagnetic remanence (Stock et al., 1999; Oskin and Stock, 2003a; this study). Even taking into account magnetic secular variation, this remanence direction lies far from the expected Miocene magnetic field at this latitude, and likely cooled during a magnetic field excursion or reversal during reversed polarity subchron C5Ar.2r (Stock et al., 1999). This unique magnetic signature only strengthens the utility of the Tuff of San Felipe as a regional tectonic marker.

Geochronologic ages for *Ttsf* from northeastern Baja California (Gastil et al., 1979; Stock, 1989; Lewis, 1996; Nagy et al., 1999; Stock et al., 1999) and central and coastal Sonora (Paz-Moreno, 1992; McDowell et al., 1997; Page et al., 2003; Vidal Solano et al., 2005; Vidal-Solano et al., 2007; Bennett et al., 2007) display a significant range of calculated ages (9.1 – 16.7 Ma), for the most part, using the K-Ar technique on either single crystal or whole-rock measurements. Stock et al. (1999) point out evidence that some of these discrepant ages are locally constrained by other isotopically-dated units, and suggest that a 12.6 Ma age corroborates best with its stratigraphic position. A more detailed examination of high-precision $^{40}Ar/^{39}Ar$ ages on single sanidine crystals separated from trachyte inclusions within *Ttsf* from Baja California (Stock et al., 2008) demonstrate that a minor xenocrystic contamination may slightly influence calculated ages for *Ttsf*. Stock et al. (2008) suggest that an age of 12.35 Ma may be the most accurate. Nevertheless, Bennett et al. (2007) reported an $^{40}Ar/^{39}Ar$ age of 12.50 ± 0.08 Ma on multiple anorthoclases from *Ttsf* in the study area (Fig.

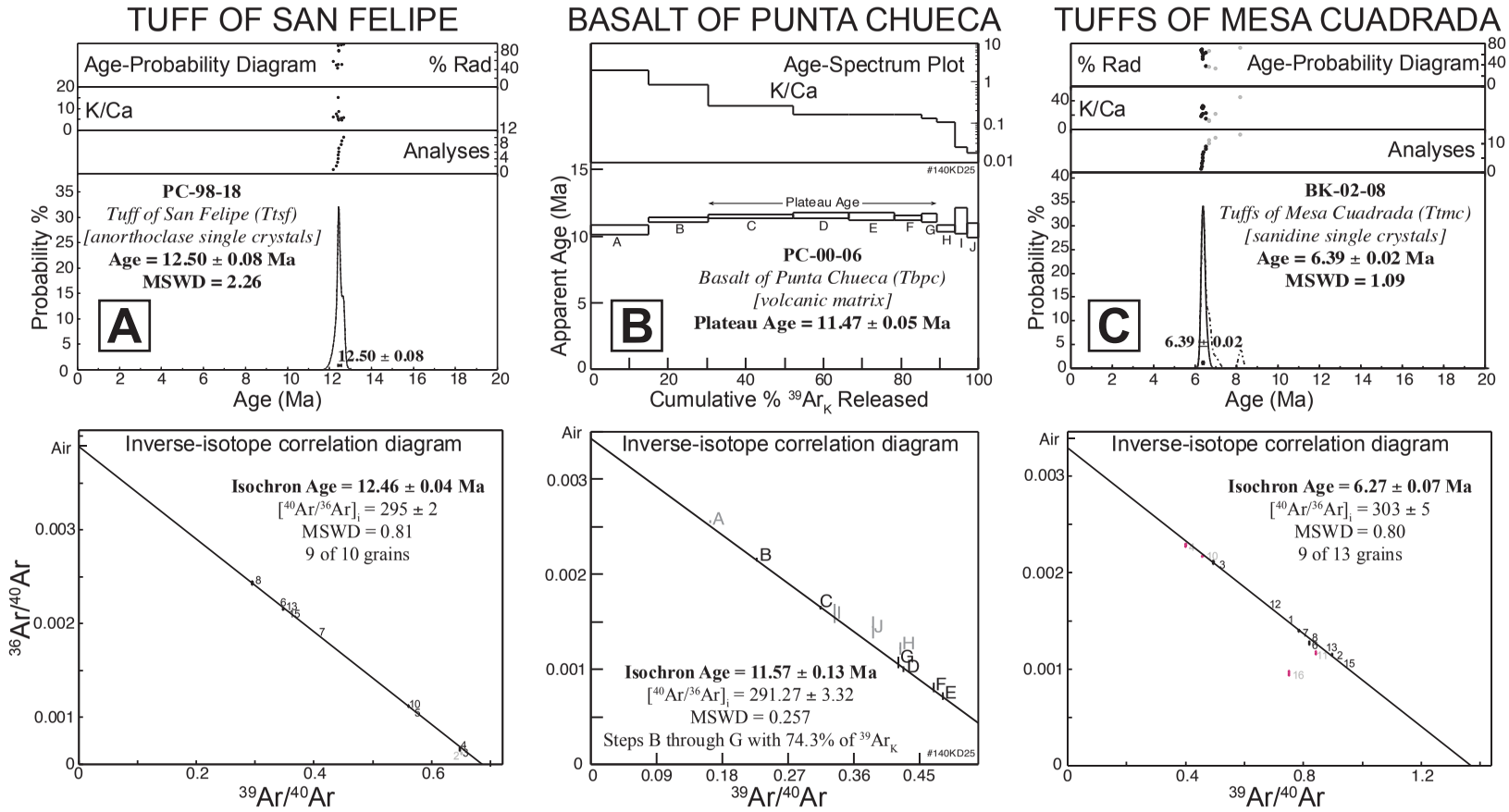

Figure 8. $^{40}Ar/^{39}Ar$ geochronological ages calculated for group two and group three rocks from coastal Sonora. (A) Age-probability diagram and inverse-isotope correlation diagram for sample from the Tuff of San Felipe (Ttsf) (Bennett et al., 2007); (B) Age spectrum plot and inverse-isotope correlation diagram for sample from Punta Chueca Basalt (Tbpc) (Oskin et al., 2003); (C) Age-probability diagram and inverse-isotope correlation diagram for sample from the Tuffs of Mesa Cuadrada (Ttmc) (Bennett et al., 2007). $^{40}Ar/^{39}Ar$ age for Ttsf corroborates well with Ttsf ages reported from northeastern Baja California (Stock et al., 1999). $^{40}Ar/^{39}Ar$ age for the Basalt of Punta Chueca is a constraint for the minimum age for the underlying Tuff of Punta Chueca (undated). $^{40}Ar/^{39}Ar$ age for the Tuffs of Mesa Cuadrada corroborates well with ages reported from northeastern Baja California (Stock, 1989; Lewis, 1996; Nagy et al., 1999) and Isla Tiburon (Gastil and Krummenacher, 1977; Oskin, 2002)
[Samples A, B, and C collected by Michael Oskin in 1998, 2000, and 2002 respectively. Analyses conducted by collaborator, Alex Iriondo, from UNAM-Juriquilla]

8A), consistent with an $^{40}Ar/^{39}Ar$ age of 12.43 ± 0.14 Ma from the Santa Rosa Basin of northeastern Baja California (Stock et al., 1999). The age from Bennett et al. (2007) is also consistent with $^{40}Ar/^{39}Ar$ ages of 12.44 ± 0.05 Ma and 12.56 ± 0.08 Ma from central Sonora (Vidal Solano et al., 2005) on ignimbrite deposits that Stock et al. (2006) correlate to *Ttsf* using paleomagnetic methods. Additionally, *Ttsf* may also correlate to thick ignimbrite deposits of approximately the same age (11.9 – 12.5 Ma) (Paz-Moreno, 1992; McDowell et al., 1997; Page et al., 2003; Vidal-Solano et al., 2007) or that have similar unique paleomagnetic signature (Hernández-Ménez et al., 2008) that are located ~100 km north, east, and south of Hermosillo in central Sonora.

Group 3

Tuff of Punta Chueca (*Ttpc*)

The Tuff of Punta Chueca (*Ttpc*) is a recessive, nonwelded, pumice-rich ash-flow tuff, which locally overlies *Ttsf* in the northern study area. *Ttpc* consists of two distinct units: (1) a lower nonwelded lithic-poor, 20 m-thick pyroclastic flow deposit with 1 - 3% centimeter-scale volcanic lithics, 3 - 10% pumice up to 20 cm, and locally displays a black basal vitrophyre 1 - 3 m thick, and (2) an upper nonwelded lithic-rich, 70 m-thick pyroclastic flow deposit with up to 10% volcanic lithics up to 2 cm and 3 - 10% pumice up to 5 cm, and sedimentary structures (e.g. trough cross-bedding) that indicate the upper 1 - 2 meters are fluvially reworked. Outcrops of *Ttpc* are limited due to the limited depositional extent of this unit and/or erosion of *Ttpc* prior to deposition of overlying conglomeratic units. The age of *Ttpc* is constrained by the underlying 12.5 Ma Tuff of San Felipe and the overlying 11.5 Ma Basalt of Punta Chueca.

Basalt of Punta Chueca (*Tbpc*)

An aphanitic, locally vesicular basalt flow (*Tbpc*), ~5 - 10 m thick, overlies the Tuff of Punta Chueca. Outcrops of *Tbpc* typically consist of resistant, yet unstable, ridgelines of unorganized piles of large *Tbpc* boulders, limiting exposures for obtaining reliable structural information. Vague 1 - 15 cm-spaced foliations are measured within this unit within the limited extent of intact outcrops. Where the basal contact of *Tbpc* is exposed, the lower 1 m is brecciated and in sharp planar contact with the underlying *Ttpc*. Oskin et al. (2003) dated volcanic matrix from *Tbpc* in the study area with $^{40}Ar/^{39}Ar$ isotopic methods, yielding a plateau age of 11.47 ± 0.05 Ma (Fig. 8B).

Tuff of Hast Eucla (*Tthe*)

The Tuff of Hast Eucla (*Tthe*) is a poorly welded airfall tuff that is locally exposed only within the Cerro Kino block. *Tthe* is light lime green on fresh surfaces, but weathers to orangish-yellow and contains common to abundant andesitic lithic fragments up to 0.5 cm in diameter. *Tthe* overlies *Ttsf* and is typically 1 - 4 m thick, but thickens within the Kino Syncline, possibly due to axial compression and bulk thickening from folding.

Rhyolite of Hast Eucla (*Trhe*)

The Rhyolite of Hast Eucla (*Trhe*) locally overlies both *Ttsf* and *Tthe* in the Cerro Kino block, and overlies only *Ttsf* in the Granito block. This unit is up to 90 m thick in the Cerro Kino block and up to 60 m thick in the Granito block and commonly exhibits a 1 - 5 cm-spaced flow foliation. These inclined foliation values were measured, but ignored during cross-section reconstructions, because these foliations are not a reliable paleo-horizontal datum.

Rhyolite of Valle del Eco (*Trve*)

The Rhyolite of Valle del Eco (*Trve*) locally overlies *Ttsf* in the eastern portion of the Eco block. Within these limited outcrops, *Trpc* is ~15 m thick and exhibits a 1 - 8 cm-spaced flow foliation.

The packages of (1) Tuff of Hast Eucla and the Rhyolite of Hast Eucla in the southern study area, (2) the Rhyolite of Valle del Eco in the central study area, and (3) the Tuff of Punta Chueca and the Basalt of Punta Chueca in the northern study area, are not observed in contact with the other. Additionally, each of these packages overlie the Tuff of San Felipe, and underlie all basin conglomerates. Due to these contact relationships the age of these packages relative to each other is unknown.

Late Miocene Lower Conglomerates (*Tcl*)

Three distinct sedimentary basins have been identified that formed in the hanging walls of the Punta Chueca, Eco, and Aeropuerto faults in the northern, eastern, and southern study area respectively (Fig. 6). All sedimentary rocks near the base of these basins (*Tcl*) are non-marine deposits, despite proximity of the study area to the Gulf of California. Surface exposures of *Tcl* are limited to the Punta Chueca basin, where they are ~225 m thick, and a small exposure in the Eco basin, where *Tcl* is <10 m thick. *Tcl* may be present, but unexposed, within the Kino basin. Two tuff deposits are interbedded within *Tcl*: the Tuff of Cerro Tordillo and the Tuffs of Mesa Cuadrada.

Deposits of *Tcl* consist of gray, tan, and orange poorly- to well-stratified, poorly- to well-sorted, fine-grained sandstone with centimeter-scale beds, pebbly sandstone, and sandy- to cobble-conglomerate, with individual stratified beds up to 2 m thick. Within *Tcl*, a 15 m-thick package (*Tsl*) of fine- to medium-grained light pink to buff sandstone with abundant

cross-beds up to 5 cm thick is observed. Clast composition of *Tcl* consists of *Kt*, *Taun*, *Ttsf*, and *Tbpc*, which provides some relative age relationships for *Tcl*; *Tcl* is younger than the underlying *Tbpc* and older than overlying Tuffs of Mesa Cuadrada. The lower contact of *Tcl* is exposed as an angular unconformity in the Punta Chueca block on the underlying *Ttsf3*, and in the Eco block on *Trve*.

Tuff of Cerro Tordillo (*Ttct*)

The Tuff of Cerro Tordillo (*Ttct*) is a Late Miocene bedded airfall deposit exposed only in the Punta Chueca block 80 m above the base of *Tcl*. *Ttct* is a 2 m-thick gray to yellow tuff with centimeter-scale sorted beds. Dorsey et al. (2008) obtained a SHRIMP $^{206}Pb/^{238}U$ weighted mean age of 6.53 ± 0.18 Ma (n=14; MSWD=1.3) on zircons separated from *Ttct* (Fig. 9A).

Tuffs of Mesa Cuadrada (*Ttmc*)

The Tuffs of Mesa Cuadrada (*Ttmc*) is another regionally extensive Miocene ignimbrite deposit that blanketed >2,100 km^2 of present-day northeastern Baja California (Stock, 1989; Lewis, 1996; Nagy et al., 1999), Isla Tiburón (Oskin and Stock, 2003a,b), and coastal Sonora (Oskin and Martín-Barajas, 2003). Only the *Tmr3* cooling unit of the Tuffs of Mesa Cuadrada of Oskin and Stock (2003a) is present within the study area.

Deposits of *Ttmc*, up to 30 m thick, are found near the base of the Punta Chueca and Eco basins, and *Ttmc* may be present, but unexposed, within the Kino basin. *Ttmc* in coastal Sonora is a poorly welded to nonwelded salmon-colored ash-flow tuff with 5 - 10% phenocrysts of alkali-feldspar ≈ quartz >> hornblende ≈ zircon ≈ sphene ≈ pyroxene, 5% poorly welded to nonwelded pumice with similar phenocrysts as matrix, 5 - 10% very

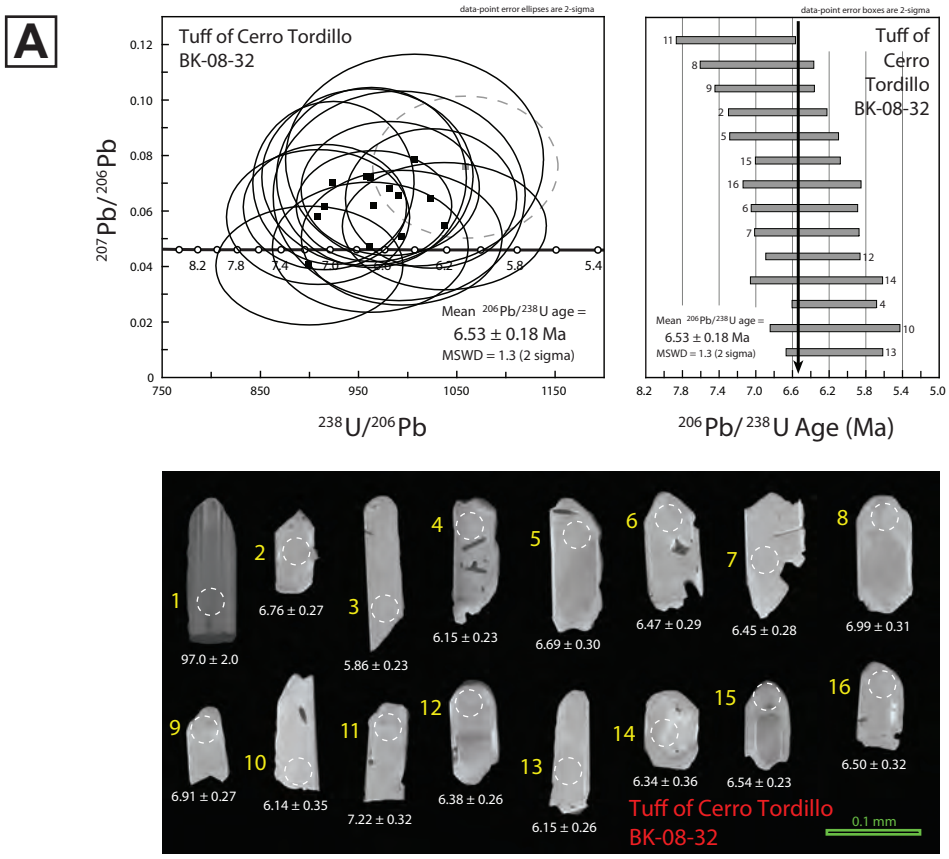

Figure 9. $^{206}Pb/^{238}U$ geochronology for tuffs interbedded within syn-tectonic basin sediments. (A) Tera-Wasserburg concordia diagram, age spectrum diagram, and optical cathodoluminescence image of analyzed zircon grains from the Tuff of Cerro Tordillo (Dorsey et al., 2008).

[Samples collected during 2008 field season of this study. Analyses conducted by collaborator, Alex Iriondo, from UNAM-Juriquilla.]

Figure 9B continues on next page.

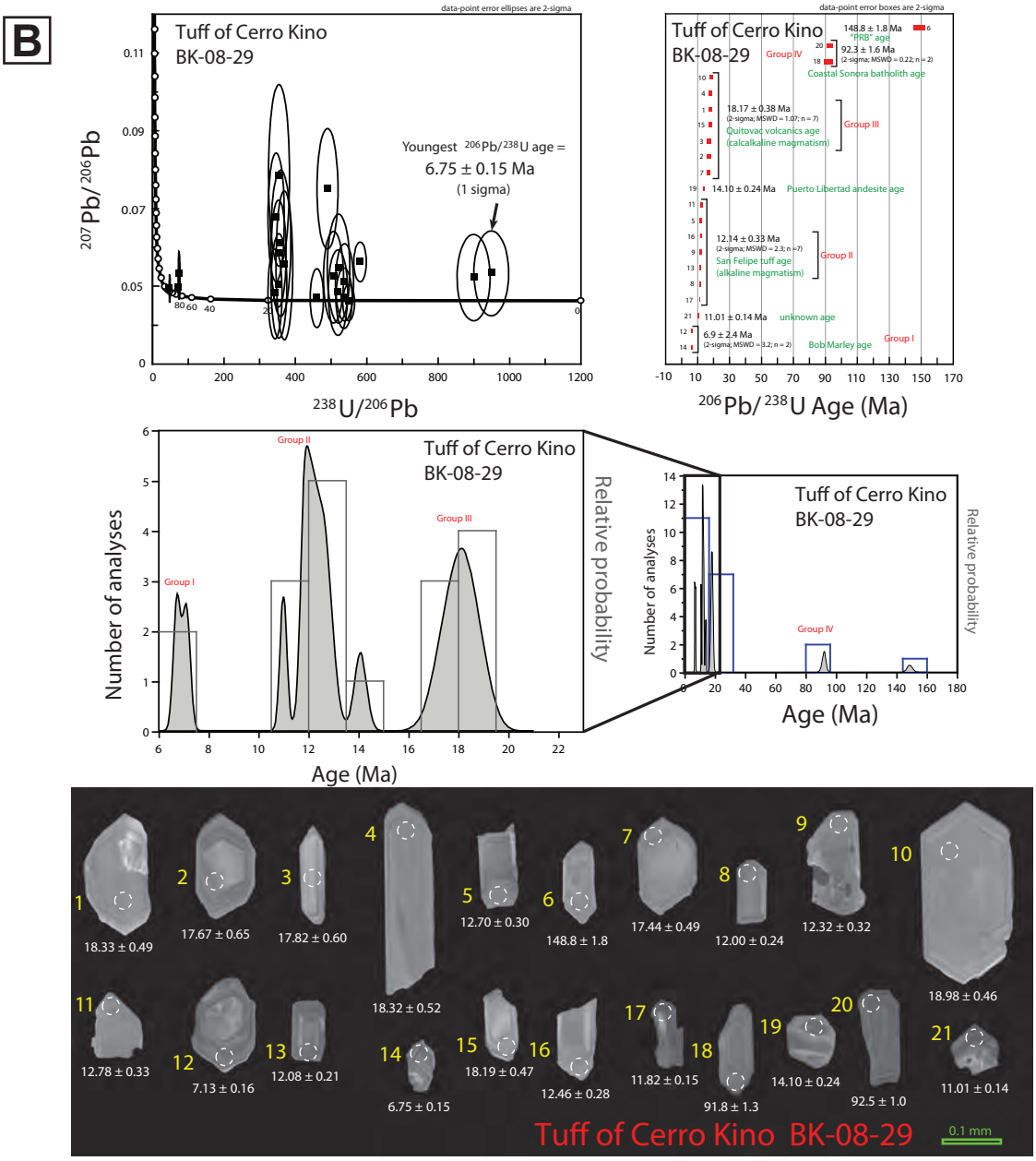

Figure 9. (cont.) $^{206}Pb/^{238}U$ geochronology for tuffs interbedded within syn-tectonic basin sediments.(B) Tera-Wasserburg concordia diagram, age spectrum diagram, relative probability age diagram with blow-up of Miocene time, and optical cathodo-luminescence image of analyzed zircon grains from the Tuff of Cerro Kino (unpublished, Alex Iriondo). The concordant $^{206}Pb/^{238}U$ age for the Tuff of Cerro Tordillo helps constrain timing for earliest Gulf-related extension and basin formation. The wide distribution of ages obtained from Tuff of Cerro Kino zircons, the youngest zircon is 6.75 ± 0.15 Ma, does not corroborate with its stratigraphic position; the Tuff of Cerro Kino is interbedded within sediments that bear 6.4 Ma Tuffs of Mesa Cuadrada clasts. An $^{40}Ar/^{39}Ar$ age on sanidines from the Tuff of Cerro Kino is in progress to hopefully determine its age.

[Samples collected during 2008 field season of this study. Analyses conducted by collaborator, Alex Iriondo, from UNAM-Juriquilla.]

angular lithic fragments of dark brown to purple aphanitic andesite and rhyolite typically 0.5 - 2 cm in diameter. Accidental lithic fragments of *Taun* and *Ttsf* are common within the lowest 1 - 2 m of this deposit. Both the matrix and pumice weather to light orange. Welding in *Ttmc* increases up section. Tabular, lithic-rich segregation pipes 8 - 15 cm thick are locally observed in *Ttmc* perpendicular to, or at high angles to outcrop strike. Exposures of *Ttmc* in the Punta Chueca block are 30 m thick, which can be sub-divided into a lower ~17 m-thick orange-salmon unit and an upper ~13 m-thick yellow unit. Samples for both geochronology and paleomagnetism were collected from the lower of these two sub-units in *Ttmc*. Bennett et al. (2007) reported an $^{40}Ar/^{39}Ar$ age of 6.39 ± 0.02 Ma on multiple sanidines from *Ttmc* in the study area (Fig. 8C), consistent with isotopic ages from this unit in northeastern Baja California (Stock, 1989; Lewis, 1996; Nagy et al., 1999) and Isla Tiburón (Gastil and Krummenacher, 1977; Oskin, 2002).

In the Punta Chueca and Eco blocks, *Ttmc* overlies group three conglomerates (*Tcl*) and is overlain by group four conglomerates (*Tcu*). In these blocks, both the upper and lower contacts of *Ttmc* are disconformities. In the Guadalupe and Luna blocks, *Ttmc* overlies *Ttsf* and *Taun* in angular unconformable contact and is overlain by group four conglomerates in angular unconformable contact. Where these *Ttmc* contacts are an angular unconformity, they likely transition laterally into disconformable contacts with the underlying and overlying conglomerates. This transition most likely occurs in the down-dip direction and is not exposed in these fault blocks.

Deposits of the Tuffs of Mesa Cuadrada across the northern Gulf of California consistently have a typical down (~54°) to the north-northeast direction of paleomagnetic remanence. This direction was best determined on the *Tmr3b* unit of Lewis and Stock (1998) from Mesa Cuadrada in northeastern Baja California, and is close to the expected Miocene

magnetic field at this latitude. *Ttmc* likely cooled during normal polarity subchron C3An.2n (Lewis and Stock, 1998).

Group 4

Latest Miocene Upper Conglomerates (*Tcu*)

Deposition of group four conglomerates (*Tcu*) spanned from 6.4 Ma to probably latest Miocene time. Deposits of *Tcu* consist of gray, tan, and orange, massive to poorly- to moderately-stratified, poorly- to moderately-sorted, laminated fine-grained sandstone, pebbly sandstone, pebble-conglomerate, clast-supported and matrix-supported cobble-conglomerate, and clast supported boulder-conglomerate, with individual stratified beds up to 2 m thick. *Tcu* also contains few discontinuous and undulatory white airfall ash beds 5 - 15 cm thick between cobble-conglomerate beds.

All sedimentary rocks of *Tcu* are non-marine. Debris-flow deposits dominate *Tcu* with some sheet flood deposits. Thicker sections of *Tcu* (at least 225 m) are found adjacent to the Punta Chueca fault. Dorsey et al. (2008) report restored paleocurrents in *Tcu* that reveal consistent overall transport to the SSW, and have interpreted *Tcu* to record deposition in a 10- to 20-km wide belt of bajadas that formed on the margin of the nascent northern Gulf of California. Using the updated paleomagnetic reference site (discussed later) for restoration, paleocurrent data in *Tcu* reflect a more S-directed overall transport direction (Fig. 10).

The lower contact of *Tcu* varies across the study area from (1) conformable on *Ttmc* (e.g. Punta Chueca block), to (2) a gentle to moderate angular unconformity on underlying units (on *Ttmc* and *Taun* in the San Miguel block, on *Trhe* and *Ttsf* in the Cerro Kino and Granito blocks, and on *Ttmc* and *Ttsf* in the Eco block), to (3) an uncommon and locally

steep angular unconformity on *Ttsf* in the Eco block, where erosion carved small canyons with near-vertical cliffs and *Tcu* filled these canyons in buttress unconformity.

Clast composition of *Tcu* varies across fault blocks and by stratigraphic level (Fig. 10). In the Punta Chueca block adjacent to the Punta Chueca fault, concentrations of foot wall units (e.g. *Kt*) increase towards the fault, evidence for tectonic relief and syntectonic deposition of *Tcu*. Further down section and away from the fault *Tcu* clast composition consists of *Ta2* >> *Ttsf* > *Kgr* ≈ *Kt* ≈ *Pzms* > *Ttmc*. In the Eco block, *Tcu* clast composition changes from rich in *Ttsf* clasts near the basal contact to rich in *Ta2* clasts up section near the Eco fault, which records erosion, stripping, and exposure of progressively older units from the foot wall. Overall, *Tcu* clast composition here consists of *Ttsf* >> *Ta2* > *Kt* > *Kgr*. In the San Miguel block, *Tcu* clast composition consists of *Ta2* > *Ttsf* > *Kgr* ≈ *Kt* ≈ *Ttmc* ≈ *Pzms*. In the Luna block at the basal erosional contact of *Tcu*, large boulders of *Kt* and *Ttsf* up to 2 m in length are observed in a poorly-stratified cobble- to boulder-conglomerate. In the Cerro Kino block *Tcu* clast composition includes *Ta2* >> *Ttsf* > *Ttmc* ≈ *Trhe*. The presence of pumice and salmon-colored fragments of *Ttmc* near the *Tcu* basal contact provide a reliable relative age for a basin with no surface exposures of *Ttmc*; *Tcu* here must be younger than the 6.4 Ma *Ttmc*. *Tcu* is almost absent from the Cerro Tordillo block.

Undifferentiated Conglomerate (*Tcun*)

In the southwestern corner of the Punta Chueca block, an isolated package of undifferentiated basin conglomerate (*Tcun*) is mapped. Because *Ttmc* is not present in either adjacent outcrop or in the clast composition of *Tcun*, *Tcun* cannot be differentiated as either group three (*Tcl*) or group four (*Tcu*) conglomerates. This package is dominated by poorly-sorted poorly-stratified cobble-conglomerate, ranging from coarse-grained sandstone to

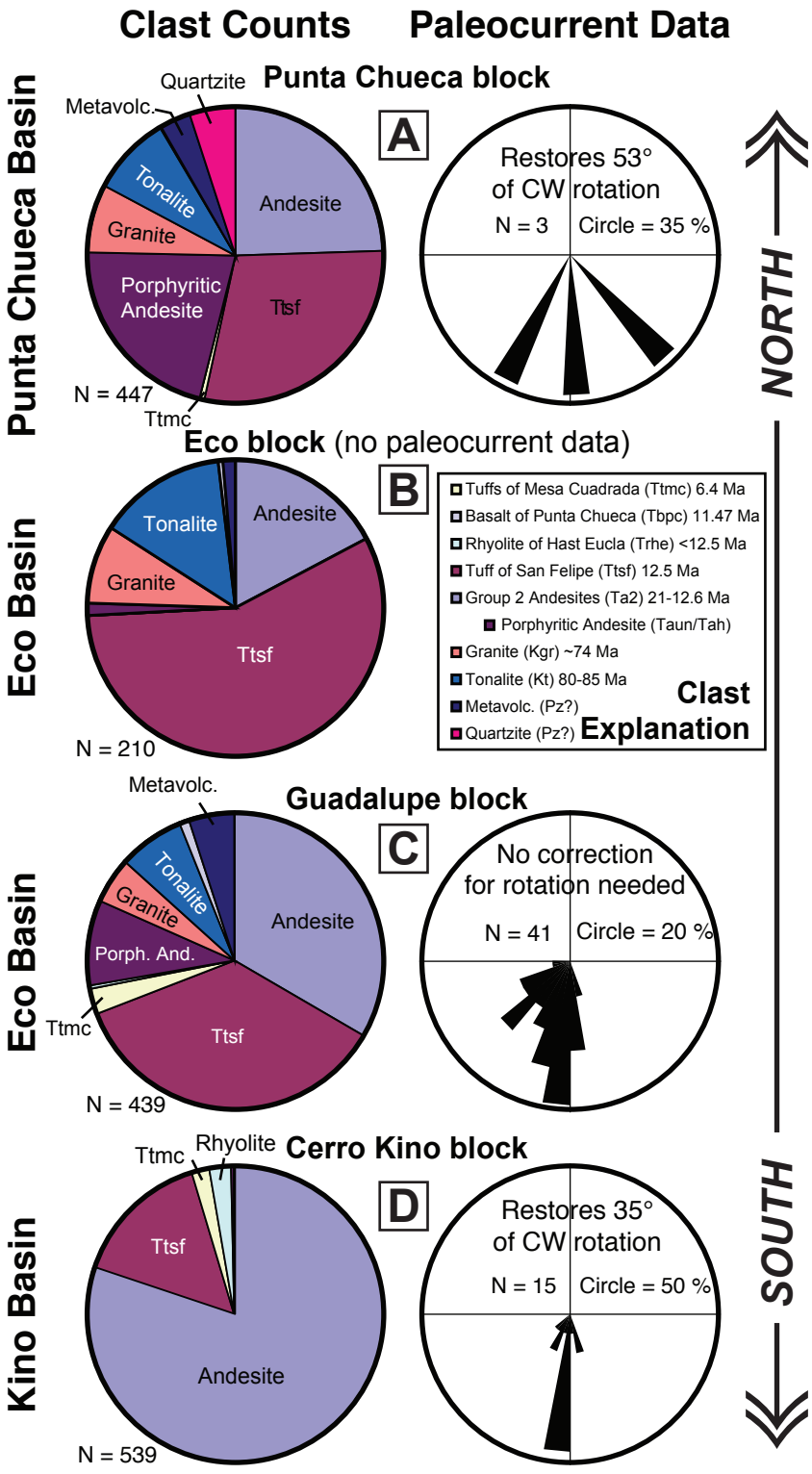

Figure 10. Clast counts and paleocurrent data recorded in the Upper Conglomerate unit (Tcu) from all three coastal Sonora syn-tectonic basins by Dorsey et al. (2008). These published paleocurrent data were corrected for clockwise vertical-axis rotations determined by paleomagnetic sampling from coastal Sonora using the previous reference site of Mesa Cuadrada (Lewis and Stock, 1998) for the Tuff of San Felipe rotation calculations. Additional rotation corrections are applied and shown here using the new paleomagnetic reference site for the Tuff of San Felipe, a regional ignimbrite used for rotation corrections. 'Porphyritic Andesite' is a distinct lithologic subset of the group two andesitic rocks, likely equivalent to both 'Taun' and 'Tah'.

boulder-conglomerate, with subrounded to angular clasts of *Ttsf* >>> *Ta2* ≈ *Tbpc*, with stratified beds up to 1 m thick. This package of *Tcun* appears to have been deposited in a ~1 km-wide drainage with buttress contacts against steep canyon walls carved into *Ttsf*.

Tuff of Cerro Kino (*Ttck*)

The Tuff of Cerro Kino (*Ttck*) is a local airfall tuff that is exposed only in the Cerro Kino block and is interbedded within *Tcu* approximately 200 m stratigraphically above the angular unconformity with the underlying Rhyolite of Hast Eucla.

Ttck is 14 cm thick in the Cerro Kino block and consists of (1) a lower 8 cm thick laminated (reworked?) portion, and (2) an upper 6 cm thick unsorted portion. The upper portion of *Ttck* was sampled for geochronology, which contains quartz, sanidine, and zircon phenocrysts, pink to red rhyolite and welded rhyolitic tuff (*Ttsf*?) lithic fragments up to 0.5 cm in diameter.

A SHRIMP $^{206}Pb/^{238}U$ age on zircons from *Ttck* was attempted (Iriondo, pers. comm; Fig. 9B); however, the zircon age population is dominated by, if not entirely composed of, inherited zircon crystals of older than the expected age of the unit from stratigraphic relations. Individual zircon crystals yield ages that range from 148.8 - 6.75 Ma with multiple clusters of ages that correspond to crystalline basement rocks, arc-related volcanic rocks, and the Tuff of San Felipe. The youngest zircon analyzed for *Ttck* (6.75 ± 0.15 Ma) still does not corroborate its stratigraphic position, because it is interbedded within sedimentary rocks that contain clasts from the 6.4 Ma *Ttmc*. These data indicate that *Ttck* is likely to be fluvially reworked, incorporating exotic zircons from older lithologic units in the area. If the upper 6 cm-thick portion of *Ttck* is a reworked ash deposit, this would corroborate the observation that the underlying lower 8 cm-thick portion of *Ttck* also show evidence that it has been

reworked. This U/Pb age remains unpublished, and an $^{40}Ar/^{39}Ar$ age on sanidines from *Ttmc* is in progress (Iriondo, pers. comm.) that will hopefully resolve the age of *Ttck*. If a consistent age distribution is obtained for *Ttck*, its age will help to better constrain the timing of earliest observed deposition in the Kino basin.

Quaternary Deposits

Active and recently active Quaternary deposits are abundant throughout the study area. Quaternary alluvium (*Qal*) is observed in typically thin, non-marine, sediment bypass environments (pediments) between intervening hillslopes of bedrock outcrops (Plate 1). Adjacent to the modern shoreline, active dissection of *Qal* deposits reveals exposures of the angular, coarse sand to cobbly sand deposits of modern catchment origin, dipping gently seaward. Additional Quaternary deposits include older, dissected alluvium (*Qoa*), recent landslide deposits (*Qls*), beach deposits (*Qb*, *Qcbl*), and recent playa deposits in areas at or below sea level (*Qpl*) (Plate 1).

Marine Strata

Limited evidence for marine strata exists within the study area. Along the shoreline between Punta Ignacio and Punta San Miguel, occasional coquina deposits, too small to map, of likely late Pleistocene age (Ortlieb, 1991) are observed in nonconformable contact with the underlying tonalite basement. This unconformity is a sub-horizontal wave cut bench carved into the underlying basement and is currently observed approximately 2 m above modern-day sea level. These deposits are thin (<3 m) and likely exist as wedge deposits that pinch out to the east beneath the younger overlying thick alluvial deposits (*Qal*). Throughout the study area, abundant evidence exists for higher sea level that likely corresponds with the last largest interglacial maximum ca. 125 ka (MIS Stage 5e; Ortlieb, 1991), including: (1) a

~2 m-elevation horizontal bedrock bench carved into bedrock on the west-facing cliffs of Punta Ignacio, (2) 2 - 3 m-elevation shell-lag shoreface deposits (*Qm*) (flat northeastern portion of Isla Alcatraz), (3) common abandoned non-marine alluvial surfaces with modern drainages dissecting down ~2-5 m, working towards equilibrium with a lower modern-day base level, and (4) observations made by McGee and Johnson (1896) of recent marine shells found in the low-lying areas in the southeastern corner of the study area.

RIFT STRUCTURES

The coastal Sonora region is dissected by normal, dextral, sinistral, and oblique-normal faults (Fig. 6) associated with the Neogene opening of the northern Gulf of California rift (Fig. 4). Within the study area, three tectonic basins are host to group three and four syn-rift deposits that formed over the hanging walls of normal faults systems (Fig. 6). These basins are floored by older group two and earliest group three rocks. Packages of these syntectonic deposits and their basin floor rocks are both tilted down to the east, where average dips of beds shallow from 69° in pre-12.5 Ma rocks (n=93), to 57° in 12.5 - 6.6 Ma rocks (n=248), to 21° in modern Gulf rocks (n=135) (Fig. 11). Where exposed today, these major normal faults systems are N- to NE-striking with dips ranging from very low (<5°) to moderate (~55°) angles. The two southernmost basins (Eco and Kino basins) are cut by sub-vertical NW-striking dextral faults, conjugate NNE-striking sinistral faults, and high-angle N-striking normal faults (Fig. 6).

Gastil and Krummenacher (1977a; 1977b) recognized the study area to be within a northwest-trending strike-slip system and broadly located some of the structures mapped during this study. Oskin (2002) more precisely located the majority of coastal Sonora structures observed within the study area. These rift-related structures are illustrated on the

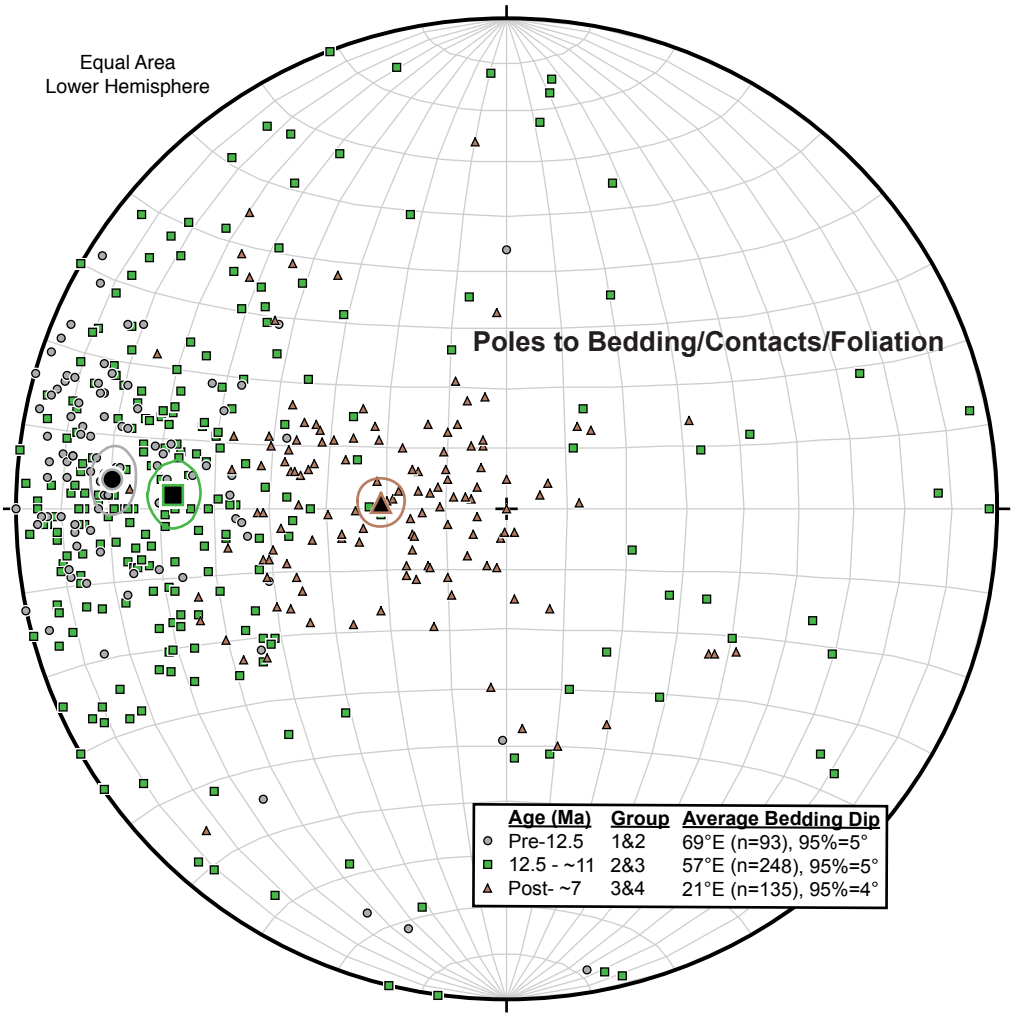

Figure 11. Stereonet plot of poles to planar structures that approximate paleohorizontal (e.g. bedding in sedimentary strata, ignimbrite basal contact, eutaxitic foliation, andesitic flow foliation, andesitic compositional foliation, etc.). Pre-12.5 Ma and 12.5 - ~11 Ma lithologic units are both steeply inclined. The 12° difference between these packages of rocks could: (1) be evidence for minor tilting pre-11 Ma, or (2) be caused by anomalous eutaxitic foliation orientations within the 12.5 Ma Tuff of San Felipe (Ttsf), which display the occasional shallow or even west-dipping foliation, typically where syn-depositional internal rheomorphic flow deformed pumice fiamme away from paleo-horizontal. Syn-tectonic units are typically tilted from ~55° - 5°, while older pre-extension units are tilted from ~40° - 90°.
(Equal Area, Lower Hemisphere projection)

1:10,000-scale geologic map (Plate 1). All mapped structures in the study area lack evidence for Quaternary activity, although evidence for minor Quaternary activity on the Infernillo fault has been reported just northwest of the study area (Ortlieb, 1991). With the exception of the Sacrificio fault, this study assigns new names to previously unnamed rift-related faults, typically with significant amounts (>1 km) of slip (Fig. 6).

Sacrificio Fault Zone

Gastil and Krummenacher (1977a) first identified (but did not name) the Sacrificio fault zone, and reported it as a NW-striking dextral structure with a possible dip-slip component (Gastil and Krummenacher, 1977b). Oskin (2002) named this feature the Sacrificio fault and located it similar to Gastil and Krummenacher (1977a). In the northeastern part of the study area, the Sacrificio fault zone consists of multiple sub-parallel strike-slip faults (Plate 1, Figs. 4 & 6). Total dextral displacement across the Sacrificio fault zone is estimated from matching conglomerate outcrops (Figs. 1 & 4) that bear unique fusulinid-rich limestone clasts exposed in both Baja California (Gastil et al., 1973; Bryant, 1986) and just north of the study area in coastal Sonora (Gastil and Krummenacher, 1977b). After closing the northern Gulf of California across the Upper Delfín basin (Oskin et al., 2001), these matching outcrops from opposite margins of the present-day Gulf of California require less than a few tens of kilometers of dextral restoration across the Sacrificio fault zone (Oskin and Stock, 2003a). The Sacrificio fault zone is likely a significant sub-vertical dextral structure that appears to either absorb displacement from or truncate nearby structures.

Puerto Rico Fault

The Puerto Rico fault is a NW-striking structure near the eastern edge of the study area (Plate 1, Fig. 6). The Puerto Rico fault is poorly exposed and was identified entirely via interpretation of Quickbird satellite imagery where outcrop patterns are truncated, presumably by dextral displacement. The Puerto Rico fault is concealed in the southern study area and appears to merge with the Sacrificio fault zone in the northern study area. The Puerto Rico fault is likely a sub-vertical dextral fault and may be a splay of the Sacrificio fault. Total displacement along the Puerto Rico fault is difficult to estimate due to the lack of exposures to the east that could be used as markers, although an estimate of 2.8 km of dextral displacement is predicted from a structural model presented below.

Bahía Kino Fault

The Bahía Kino fault consists of two vertical, northwest-striking, dextral branches that traverse the central study area (Plate 1, Figs. 4 & 6). Field mapping reveals truncation of all pre-Quaternary map units across both branches of the Bahía Kino fault. Dextral motion and drag folding on the western branch of the Bahía Kino fault is likely the cause of the asymmetric SSE-plunging Kino syncline (Plate 1, Cerro Kino block) where all pre-Quaternary map units are deformed. Deformation associated with the Kino Syncline must post-date 6.4 Ma, because these deformed sedimentary rocks contain *Ttmc* clasts.

Apparent dextral bedrock offsets on the western branch of the Bahía Kino fault vary from 4.55 km (base of group *Ttsf*) in the south to 2.9 km (an average of 2.7 km base of group two, 3.1 km base of *Ttsf*) in the north. On the eastern branch, offsets vary from 0.25 km (base of group two) in the south, to 1.25 km (base of both group two and group four) in the central study area, to 0.75 km (felsic dike in group one) in the north-central study area.

Both *Tat* and the distinctive southern volcanic sequence can be used as a marker for fault slip in the southern study area. These units are observed in the San Miguel, Cerro Kino, Granito, and Rancho Nuevo blocks and strengthen the correlation amongst these southern fault blocks across both branches of the Bahía Kino fault.

El Camino Fault

The El Camino fault is a cryptic NW-striking structure in the south-central study area between the Guadalupe and San Miguel fault blocks (Plate 1, Fig. 6). The El Camino fault is mostly unexposed and its few bedrock locations are entirely inferred by (1) the apparent truncation of the top-of-basement nonconformity observed in the San Miguel block, (2) the disparate group two arc-related volcanic rocks across this boundary, (3) the apparent truncation of Guadalupe block *Ttmc* outcrops across this boundary, and (4) the apparent truncation of San Miguel block *Tvs* outcrops across this boundary (Plate 1). Because multiple units do not match across this boundary, total displacement along the El Camino fault is difficult to estimate, although an estimate of 2.2 km of dextral displacement is predicted from a structural model presented below. It is possible that this boundary is not just a discrete fault boundary, but also corresponds with a gradational lithologic boundary between different suites of arc-related group two rocks (Fig. 5, Plate 1). The El Camino fault is inferred to be a vertical dextral structure, but it could also be a SW-dipping normal fault.

Infernillo Fault

The NW-striking Infernillo fault (Plate 1, Figs. 4 & 6) first appeared on maps by Gastil and Krummenacher (1977a; 1977b) as an inferred, unnamed structure that separates coastal Sonora from Isla Tiburón. This structure continues towards the northwest and may

possibly trend into other northwest-striking structures beneath the Gulf of California (Fig. 4). Although the Infernillo fault is completely submerged by ocean waters, it is inferred as a vertical structure that may continue onshore beneath Quaternary-age alluvial deposits near Punta Chueca (Gastil and Krummenacher, 1977a; Fig. 4). Oskin and Stock (2003a) made the observation that outcrops of *Ttsf* and *Ttmc* are restricted to the northern portion of eastern Isla Tiburón, and suggested that 20 ± 10 km of dextral displacement and/or northwest-directed extension across the intervening channel is required to restore these outcrops to similar outcrops just east of Punta Chueca. Together, the Sacrificio, Bahía Kino, and Infernillo faults comprise a NW-trending shear zone in which the entire study area is contained. This shear zone will be referred to as the Kino-Chueca Shear Zone.

Punta Blanca Fault

The Punta Blanca fault is a NE-striking structure in the south-central study area (Plate 1, Fig. 6). Map-view outcrop patterns suggest that the Punta Blanca fault has ~1.5 km of apparent sinistral displacement of the base of *Ttsf*. The Punta Blanca fault is inferred to be a moderate- to high-angle sinistral-oblique normal fault, though its dip and the slip direction has not been resolved from kinematic data. If a dip angle of 75° towards to northwest is assumed for the Punta Blanca fault, variable amounts of slip are calculated for the various possible slip directions of the Cabra block hanging wall: 1.5 km of slip for pure strike-slip motion, 1.7 km of slip for oblique-slip motion (rake of 045°), and 5.6 km of slip for pure normal motion. Map views restorations of fault blocks (discussed in the Discussion section below) predict 1 -2 km of sinistral displacement along the Punta Blanca fault. The Bahía Kino fault likely truncates the Punta Blanca fault at its northeastern end, while at its

southwestern end it may merge with the normal(?) Guadalupe fault. These fault intersection relationships are not exposed.

Aeropuerto Fault

The Aeropuerto fault in the southeastern study area is an inferred normal fault that is concealed beneath the delta plain of the Rio Sonora (Plate 1, Fig. 6). Normal displacement on the Aeropuerto fault tilted the Rancho Nuevo, Granito, and Cerro Kino blocks down to the east. Both branches of the Bahía Kino fault probably truncate and offset the Aeropuerto fault. Offset along the Aeropuerto fault cannot be determined because no bedrock outcrops are exposed in the foot wall that would match the well exposed rocks of the Cerro Kino block. Additionally, the location of the Aeropuerto fault is very poorly constrained and it could lie well southeast of the southeastern corner of the study area.

Eco Fault

The Eco fault in the east-central portion of the study area is a moderate angle (45-55°) normal fault that juxtaposes group four rocks in the Eco and Luna blocks in the hanging wall against basement rocks in the Rancho Nuevo and Granito blocks in the foot wall (Plate 1, Fig. 6). Total normal displacement on the Eco fault is estimated at 3.0 km, which includes ~0.2 km of displacement on an imbricate fault exposed 1 km northwest of and sub-parallel to the Eco fault. This estimate is poorly constrained, as it is measured on the normal displacement of the base of *Ttsf* from the Eco block to the Puerto Rico block, across the Puerto Rico fault that may have many kilometers of strike-slip displacement. Additional smaller-scale normal faults within the hanging wall of the Eco fault also contribute to the dilation of this portion of the study area. Both branches of the Bahía Kino fault have

subsequently truncated and offset the Eco fault, providing some relative age constraints for extensional and dextral fault systems in the central study area. The Guadalupe fault may be a dextrally offset, southwestern continuation of the Eco fault. However, these fault intersection relationships are not exposed.

Guadalupe Fault

The Guadalupe fault is a NE-striking structure in the south-central study area (Plate 1, Fig. 6). Because the Guadalupe fault is entirely unexposed, its dip angle and relative age with respect to intersecting faults (e.g. western branch Bahía Kino fault, Punta Blanca fault, Infernillo fault) is difficult to assess. Rocks in the hanging wall of the Guadalupe fault (San Miguel block) show 1.2 km of apparent sinistral displacement relative to rocks in the foot wall (Cabra block). This displacement could be the result of pure dip-slip, oblique-sinistral slip, or pure sinistral strike-slip and cannot be readily resolved from the lack of fault exposures. If a dip angle of 50° towards to northwest is assumed for the Guadalupe fault, variable amounts of slip are calculated for the various possible slip directions of the San Miguel block hanging wall: 1.2 km of slip for pure sinistral strike-slip motion, 1.4 km of slip for sinistral oblique-slip motion (rake of 045°), and 6.8 km of slip for pure normal motion. The Guadalupe fault is inferred to be a sinistral-oblique normal fault. The Bahía Kino fault likely truncates the Guadalupe fault at its northeastern end, where it may continue as the Eco fault. At its southwestern end it may merge with the sinistral-oblique normal Punta Blanca fault.

Tordillo Fault

The Tordillo fault in the north-central portion of the study area is a moderate angle (~45°) normal fault that juxtaposes Cerro Tordillo block group two and three rocks in the hanging wall against Eco block basement rocks in the foot wall (Plate 1, Fig. 6). After reconstruction of the base of *Ttsf* in the Eco and Cerro Tordillo blocks, total normal displacement on the Tordillo fault is estimated at 2.2 km. The southwestern end of the Tordillo fault may be a transfer structure and appears to either be truncated by or merges with the Bahía Kino fault (Plate 1). Outcrops in the area of this intersection are either buried or within homogeneous tonalite, obscuring the nature of this fault intersection.

Punta Chueca Fault

The Punta Chueca fault in the northwestern portion of the study area is an undulatory low-angle normal fault with a general west-directed sense of hanging wall motion. Along its trace, Punta Chueca block group two, three, and four hanging wall rocks are juxtaposed against San Miguel and Cerro Tordillo block crystalline foot wall rocks. Locally where well exposed, the Punta Chueca fault consists of shallow (~5°) portions that dip towards the west and shallow (~10°) back-tilted portions that dip towards the southeast (Plate 1). The Punta Chueca fault varies from a N-striking structure in the north to a NE-striking structure along its southwestern portions. This southwestern portion of the Punta Chueca fault may be a transfer structure that either merges with or truncates the Bahía Kino fault. The offset of intrusive basement contacts in the Cerro Tordillo block are used to constrain the location of the base of *Ttsf* in the footwall of the Punta Chueca fault, and total normal offset, measured from the base of *Ttsf* in the hanging wall of the Punta Chueca fault, is estimated at 5.2 km.

FAULT KINEMATICS

Methods

Structural observations and fault kinematic data were collected from fault planes of a variety of scales where preserved fault-slip indicators (slickenlines or mullions) were observed. These kinematic features represent the direction of relative motion between the adjacent bocks on either side of the measured fault surface. A total of 132 fault-slip indicators were measured on small-offset fault plane surfaces throughout the study area within all non-Quaternary map units. Each fault-slip measurement consists of the strike/dip of the fault plane, rake of fault slip indicator, and sense of shear. Where a reliable shear sense indicator was absent, a shear sense direction was systematically assigned to each fault kinematic datum. To do so, the general assumption that these slickenlines formed under extensional stress was implemented. Following this assumption, slickenline data with a significant dip-slip component (slickenline rake from ~20 - 160°) were assigned a shear sense with a component of normal slip (e.g. either a dextral-oblique normal or sinistral-oblique normal shear sense). Slickenline data with a less-significant dip-slip component (slickenline rake from 0 - ~20° and ~160 - 180°) were assigned a shear sense that reflected either dextral motion for NW-striking faults or sinistral motion for NE-striking faults.

Analysis

For this kinematic analysis, slickenlines are assumed to form in the direction of the maximum resolved shear stress on a fault plane (Wallace, 1951; Bott, 1959). Thus, the paleo-stress direction on that fault is a component of the orientation of the fault slickenline or

mullion datum. Together these data should cumulatively be representative of paleo-stress conditions.

Variable amounts of clockwise vertical-axis rotation of fault blocks have occurred across the study area (discussed in the following Paleomagnetism section). Therefore, prior to analysis, all fault kinematic data were rotated counter-clockwise about a vertical-axis by the amount of rotation either determined or predicted by the paleomagnetic results of this study (up to 53°). Principal paleo-stress axes were then determined using FaultKin v.4.3.5 software (Allmendinger et al., 2009), which utilizes the right dihedra geometrical method of Angelier and Mechler (1977) and Pfiffner and Burkhard (1987). Using the well-dated stratigraphy as a chronologic filter, various periods of time were compared for similar or dissimilar paleo-stress vector orientations.

Results

Fault kinematic indicators measured in pre-12.5 Ma rocks (n=89) are generally ignored in this analysis, as they are likely overprinted by and reflect multiple deformational episodes of paleo-stress (e.g. subduction-related shortening, subduction-related back-arc extension, rift-related extension and shear, etc.; Fig. 12B). Fault kinematic indicators measured in 12.5 - 0 Ma rocks (n=43) reflect all Gulf of California deformation, and display WSW-directed extension (T-axis azimuth 254°) with a near-vertical σ1 principal stress vector (Fig. 12C). The well-dated stratigraphy in the study area (Fig. 5) allow for further analysis and division of these Gulf of California fault kinematic into subsets of proto-Gulf rocks. Fault kinematic indicators (n=20) in early proto-Gulf rocks (12.5 to 11.5 Ma), which integrate all subsequent Gulf deformation, display a SW-NE extension direction (T-axis azimuth 232°) with a near-vertical σ1 principal stress vector (Fig. 12D). In latest proto-Gulf

rocks (6.6 to 6.0 Ma), fault kinematic indicators (n=23) suggest an approximate E-W-extension direction (T-axis azimuth 263°) with a near-vertical σ1 principal stress vector (Fig. 12E).

Although the paleo-stress results from the fault kinematic dataset appear to distinguish two distinctly different extension directions for early proto-Gulf and latest proto-Gulf time periods, the stability of these results is not strong. Confidence contours for P- and T-axes for each analysis reflect the low precision of these results (Fig. 12 B,C,D,E). This low precision is indicated by the overlap of contours for P- and T-axes that should theoretically be 90° apart from each other. It also appears that due to the small size of the post-12.5 Ma data set (n=43), the results are quite sensitive to the addition of new data. As this study progressed over three annual field seasons, fault kinematic data were progressively collected, and at the end of each field season all fault kinematic data collected up until that point were analyzed in the fashion explained above. The results changed from each subsequent year as more data were collected. For example, one iteration of analysis increased proto-Gulf data from n=16 to n=20, which resulted in a 26° difference in the T-axis azimuth orientation. Additionally, this kinematic dataset lacks much data from the well-timed 6.4 Ma Tuffs of Mesa Cuadrada due to poor preservation of slickenlines in a nonwelded tuff. Another drawback of this dataset, and possibly the largest one, is that a large portion of proto-Gulf time and all of modern-Gulf time is not preserved in the rock column within the study area (no rocks are present from ~11.5 - 7 Ma and post-6 Ma). Therefore, the kinematic data may not represent the tectonic style during a large portion of proto-Gulf time, and may only be overprinted by modern-Gulf deformation. Therefore, overall, these results should be taken with some level of reservation.

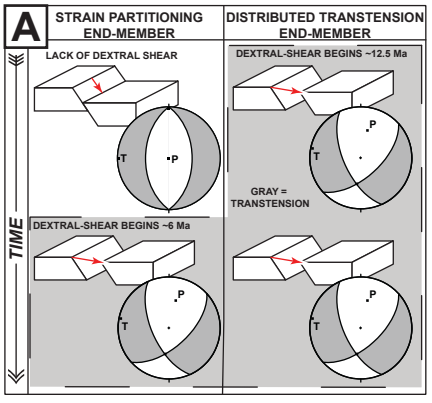

Figure 12. (A) Cartoon of expected fault kinematic results of rift-related structures for both end-member hypothesis. Note that proto-Gulf-age rocks should not only record proto-Gulf tectonics, but also be overprinted by younger modern-Gulf tectonics (possibly via fault reactivation). For rows B-E, kinematic data is sorted by known age of lithologic units. Columns display (left) measured faults and striae, (left-center) P-axes (red circles) and T-axes (blue squares) for individual fault measurements, (right-center) Kamb contour of P-axes (red) and T-axes (blue), and (right) fault plane solution. All analysis conducted with FaultKin software (Allmendinger et al., 2001). (B) Faults measured in pre-12.5 Ma rocks are not relevant to this study, since they may reflect multiple episodes of stress (e.g. subduction-related shortening, subduction-related back-arc extension, rift-related extension and shear, etc.). (C) rift-related fault kinematic data suggest heterogeneous stress is recorded in rocks that post-date 12.5 Ma. For 12.5 - 11.5 Ma rocks, P-axes (green) and T-axes (blue) appear to cluster differently than P-axes (orange) and T-axes (magenta) for 6.6 - 0 Ma rocks. To quantitatively evaluate whether these data represent unique fault kinematics, these data are further subdivided into early proto-Gulf-age (D) and latest proto-Gulf-age (E) rocks. (D) Kinematic data from early proto-Gulf rocks display a SW-NE extension direction (T-axis = 232˚). (E) Kinematic data from latest proto-Gulf rocks display an E-W extension direction (T-axis = 263˚).

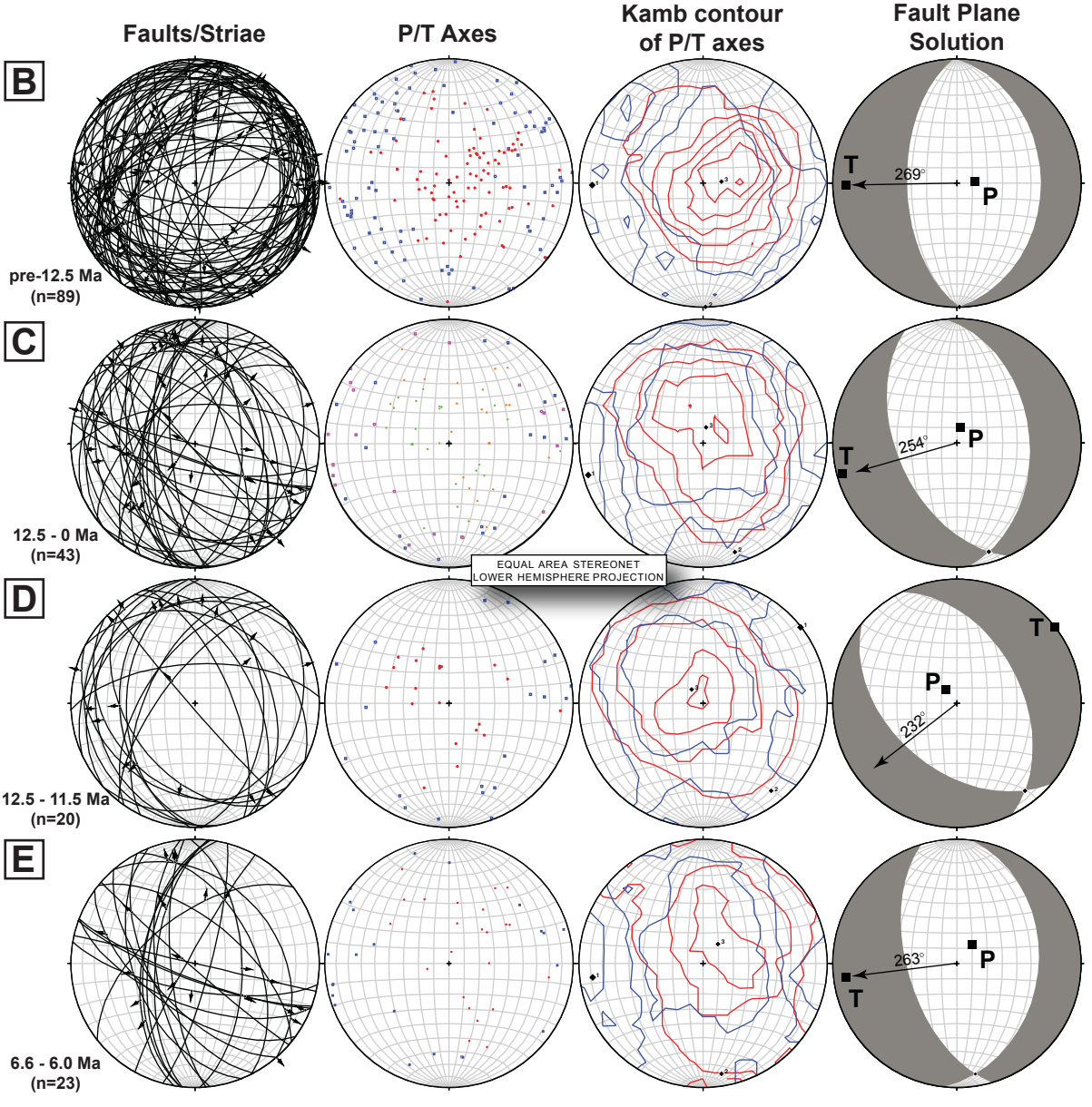

PALEOMAGNETISM

Field and Laboratory Methods

Either *Ttmc* or *Ttsf* was sampled for paleomagnetic analysis at seven sites between the towns of Bahía de Kino and Punta Chueca in coastal Sonora. Additionally, *Ttsf* was sampled at three sites in north-central Baja California to establish a new stable reference site (Fig. 13, Table 2). The isotopic ages determined for *Ttmc* (6.39 ± 0.02 Ma) and *Ttsf* (12.50 ± 0.08 Ma) indicate that these tuffs likely erupted during normal subchron C3An.2n (6.269 - 6.567 Ma) and reverse subchron C5Ar.2r (12.401 - 12.678 Ma) respectively (Cande and Kent, 1995).

206 samples (cores) were collected from these ten paleomagnetic drill sites, and 1-cm tall specimens were prepared from these samples for demagnetization experiments. Samples were oriented in the field using both a magnetic compass and a sun compass, to an accuracy of ±1°. A strict paleomagnetic sampling campaign has been implemented that consistently attempts to sample a high number of randomly oriented samples per paleomagnetic site ($n > 10$, typically $n \approx 20$) in order to improve the 1/sq-root statistics for each paleomagnetic site and to therefore reduce the error in calculated rotation values. Areas prone to secondary magnetization from lightning strikes were also avoided for paleomagnetic sampling, such as topographic promontories (e.g. summit of Cerro Kino, where outcrops of *Ttsf* are currently strongly magnetized to azimuth 302°).

The natural remanent magnetization (NRM) of a specimen is typically the sum vector of at least two components: a primary component acquired during rock formation, and a secondary component acquired after rock formation and prior to analysis in the laboratory (Butler, 1992). Partial demagnetization experiments identify the presence of and remove any

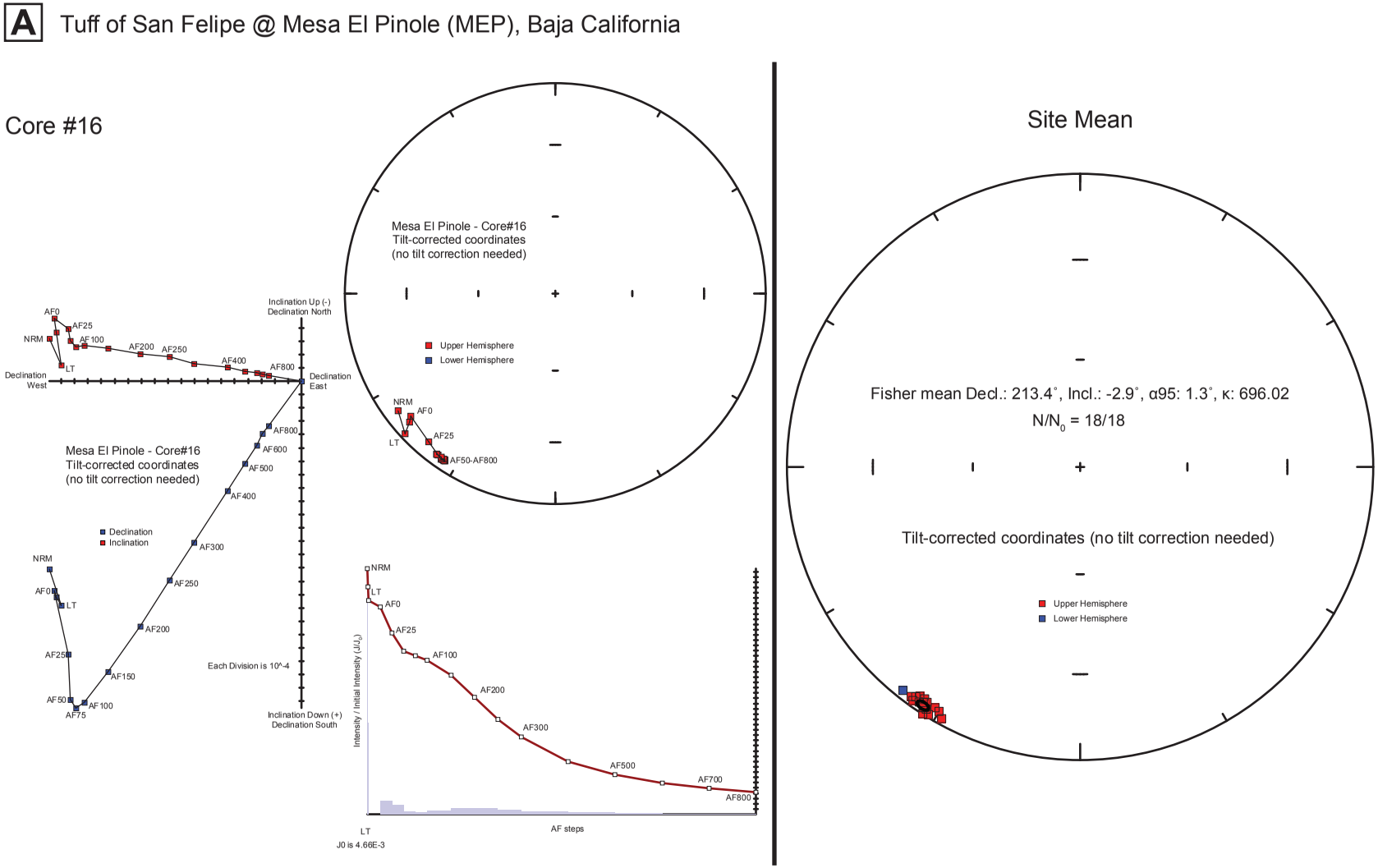

Figure 13. Paleomagnetic results from the 10 paleomagnetic drill sites in central Baja California and coastal Sonora. For each (A-J), vector-component Zijderveld diagram (LEFT) and equal area stereonet (TOP) displays vector orientations for all NRM, LT, and AF partial demagnetization steps conducted. Partial demagnetization steps shown for only one example core at each paleomagnetic site, where multiple cores were sampled. J/J_0 plot also shown for example core (BOTTOM). Site mean was calculated using N of the N_0 cores collected. α 95 confidence ellipse shown. All analysis conducted with PaleoMag v3.1b1 (Jones, 2002).
(A) Typical paleomagnetic results from the Tuff of San Felipe (*Ttsf*) at the Mesa El Pinole drill site in central Baja California. Example core #16 shown.

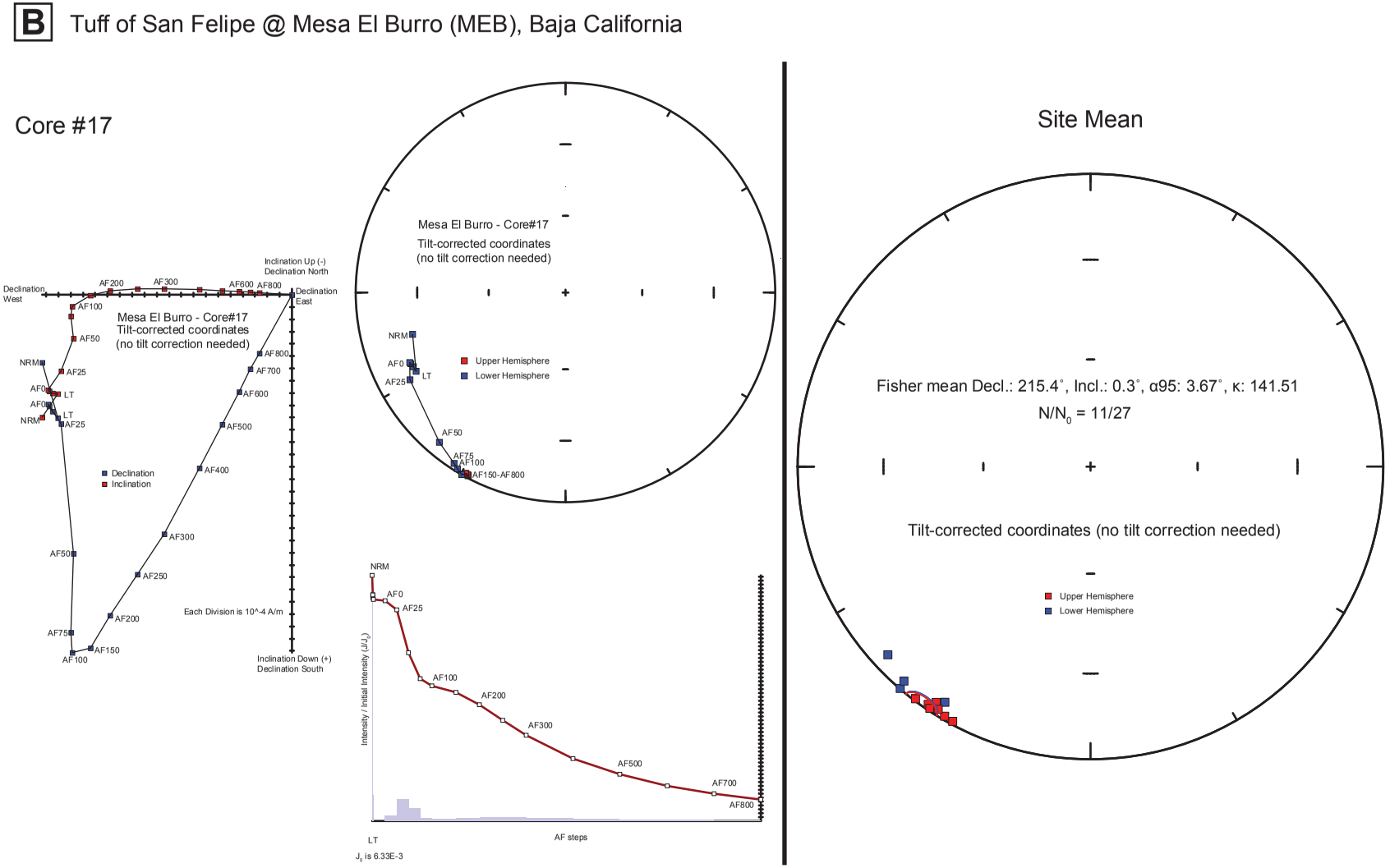

Figure 13. (cont.) (B) Typical paleomagnetic results from the Tuff of San Felipe (*Ttsf*) at the Mesa El Burro drill site in central Baja California. Example core #17 shown.

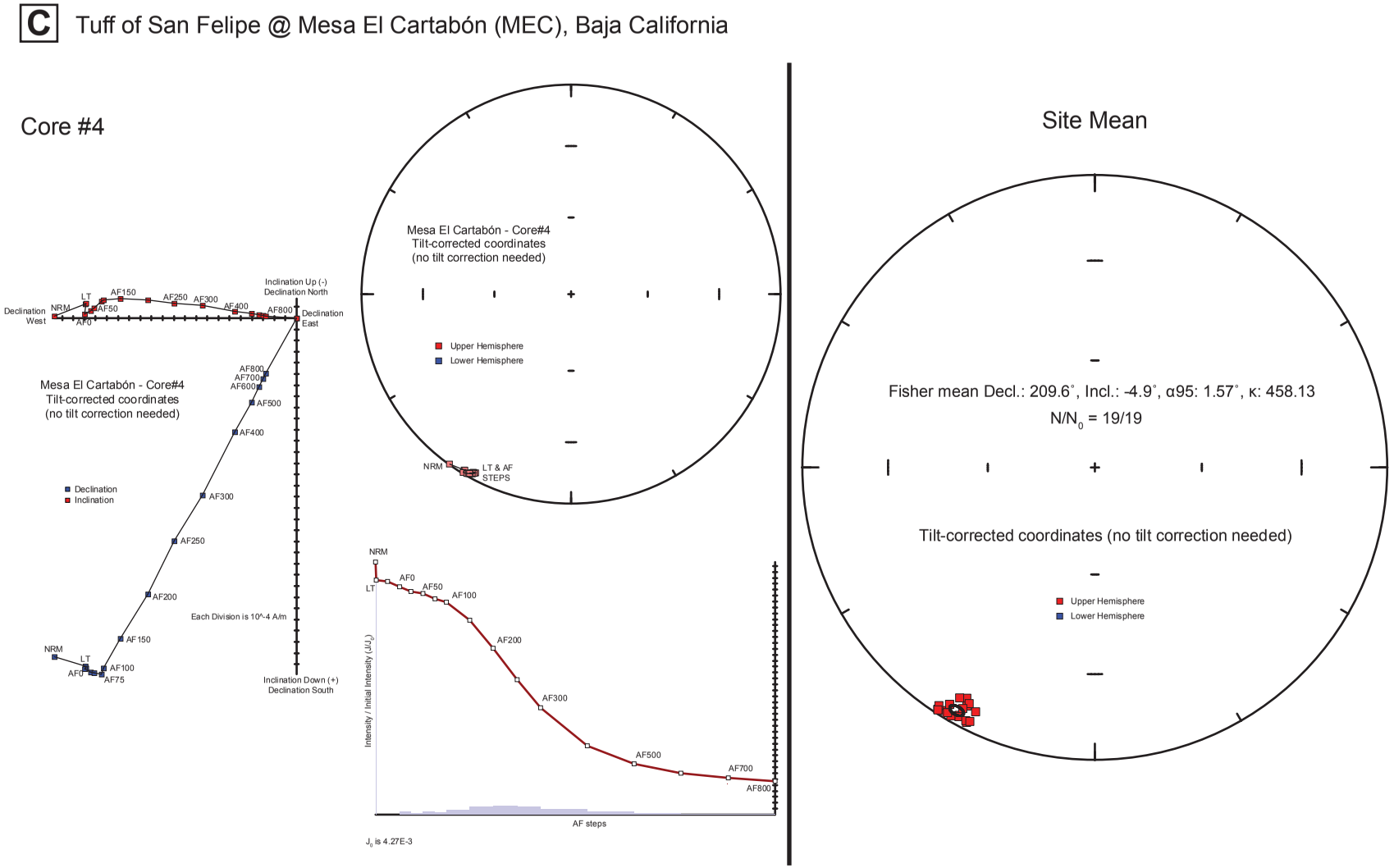

Figure 13. (cont.) (C) Typical paleomagnetic results from the Tuff of San Felipe (*Ttsf*) at the Mesa El Cartabón drill site in central Baja California. Example core #4 shown.

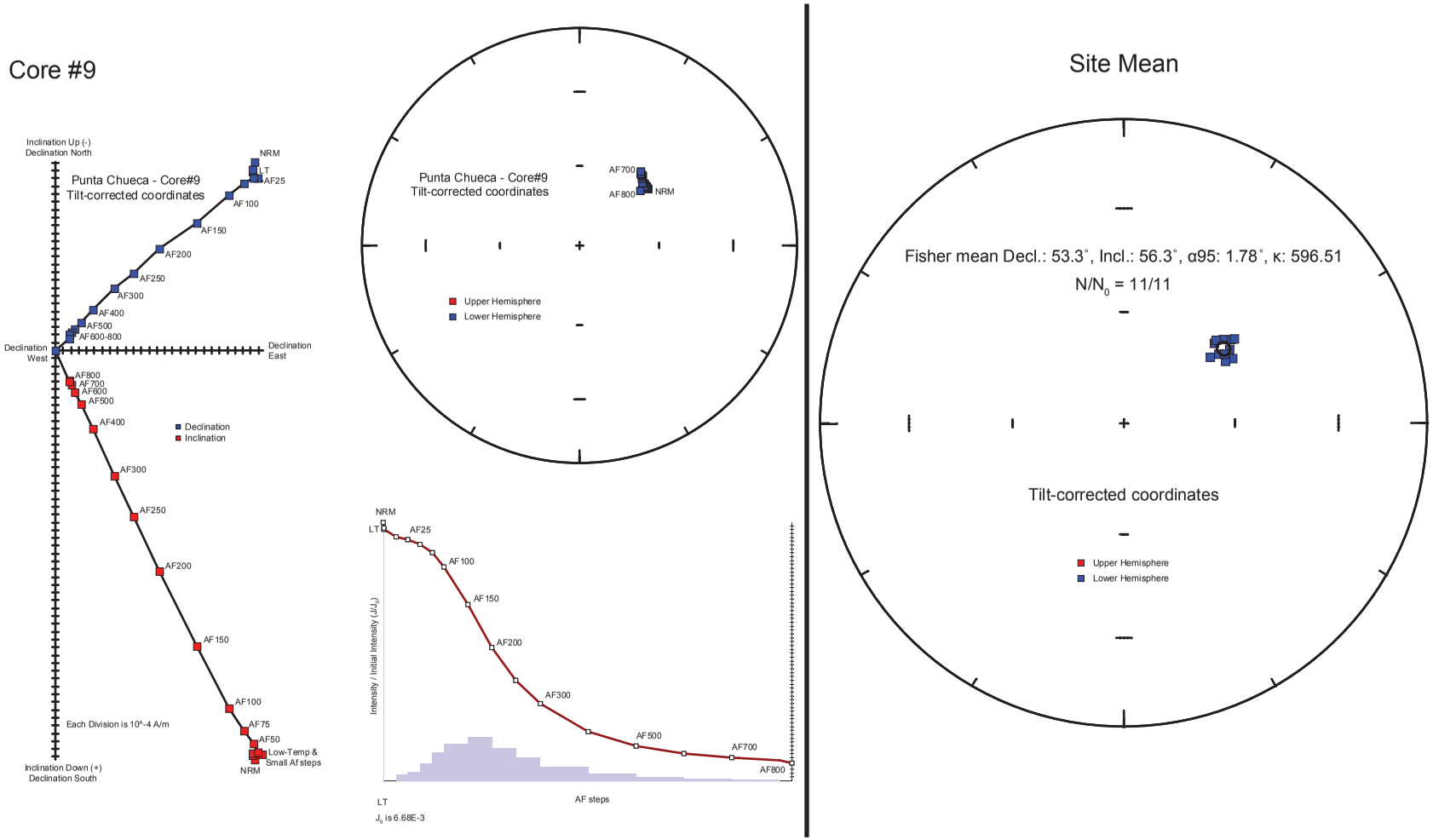

Figure 13. (cont.) (D) Typical paleomagnetic results from the Tuffs of Mesa Cuadrada (*Ttmc*) at the Punta Chueca drill site in coastal Sonora. Example core #9 shown. Drift of data points (visible on stereonet for core #9) is result of minor incremental rotation of sample during analysis. Step AF800 run at correct orientation.

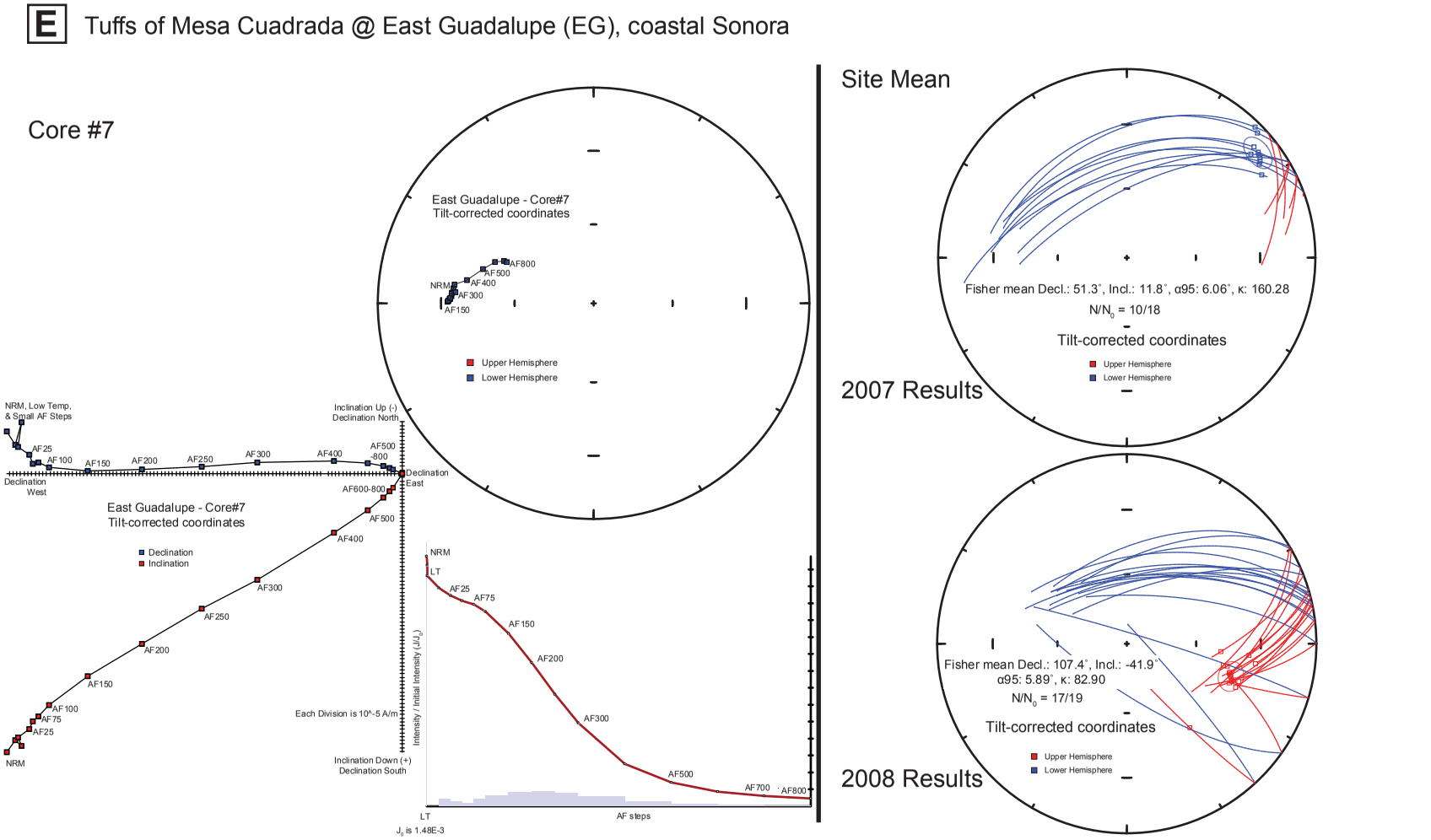

Figure 13. (cont.) (E) Typical paleomagnetic results from the Tuffs of Mesa Cuadrada (*Ttmc*) at the East Guadalupe drill site in coastal Sonora. Results from cores collected from first field season (2007) were unable to completely remove the likely chemical magnetic overprint and planes were fit to the data (upper right). However, the planes do include the expected direction (~north, negative inclination) in their paths. The planes appear to have a direction where many intersect, but this direction is unreliable due to the low accuracy of determining the intersection of planes that are sub-parallel. To attempt to obtain an accurate paleomagnetic direction here, *Ttmc* was sampled again in the 2008 field season approximately 250 meters south of the 2007 site, however, similar results were obtained (lower right) with another unreliable (reverse direction) intersection determined by the PaleoMag software. The open squares on these site mean stereoplots represent the directions of the lines assigned to each plane, that lies on that plane, which is nearest to where the intersection of the multiple planes was determined. Example core #7 shown from 2008 set of samples (left).

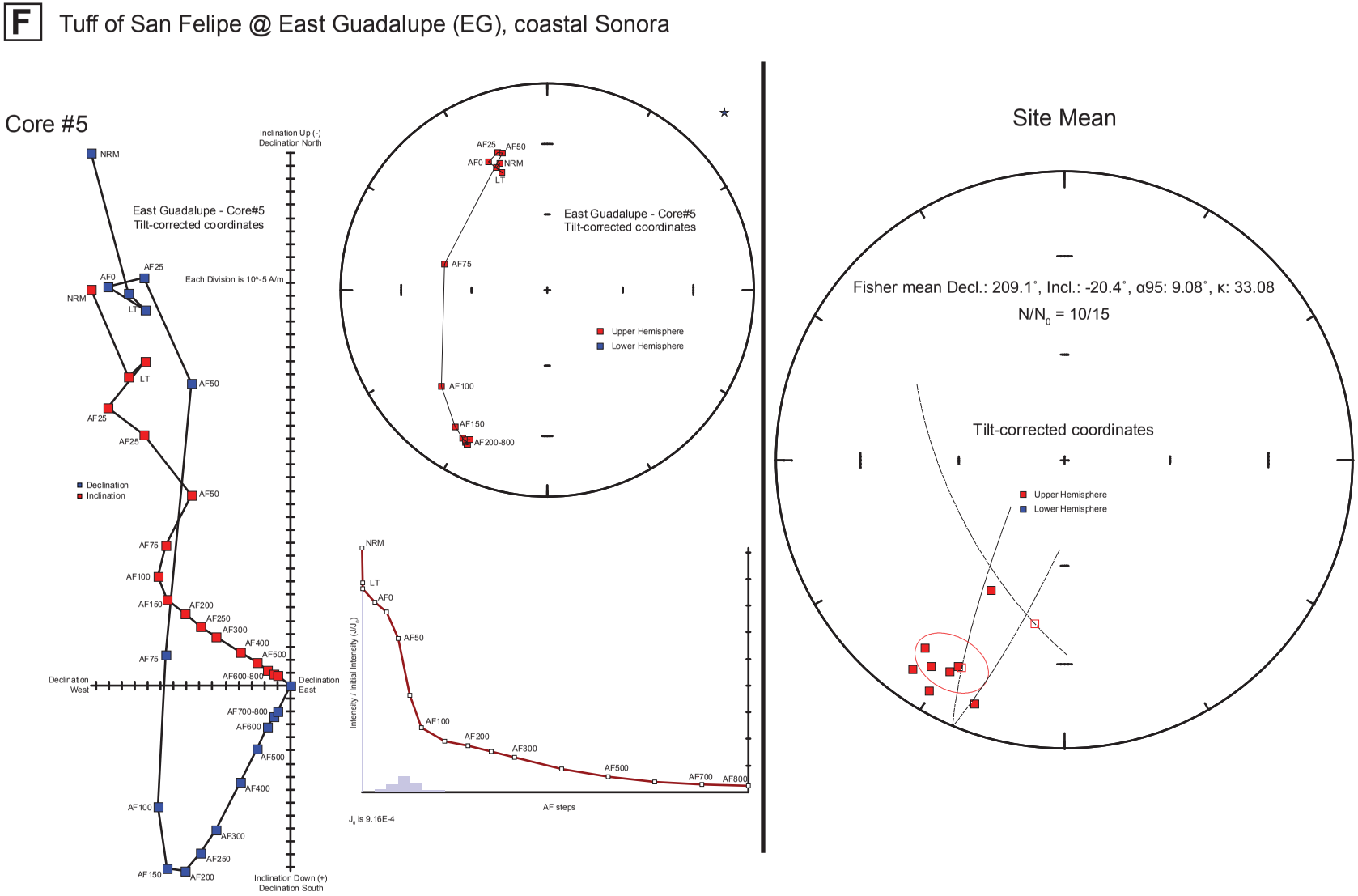

Figure 13. (cont.) (F) Typical paleomagnetic results from the Tuff of San Felipe (*Ttsf*) at the East Guadalupe drill site in coastal Sonora. Example core #5 shown. Open squares on site mean stereoplot same as 13E.

G Tuffs of Mesa Cuadrada @ La Luna (LL), coastal Sonora

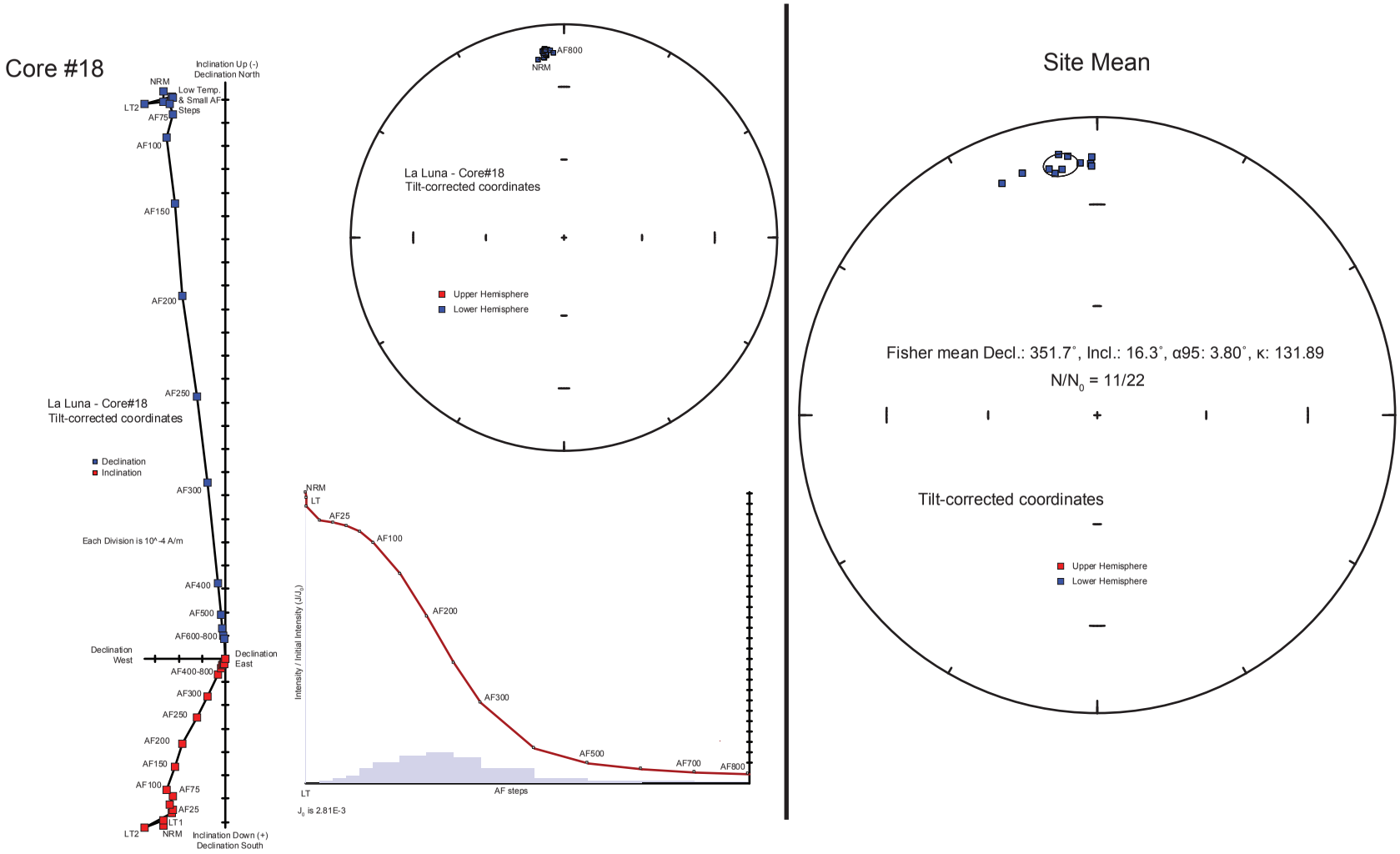

Figure 13. (cont.) (G) Typical paleomagnetic results from the Tuffs of Mesa Cuadrada (*Ttmc*) at the La Luna drill site in coastal Sonora. Example core #18 shown.

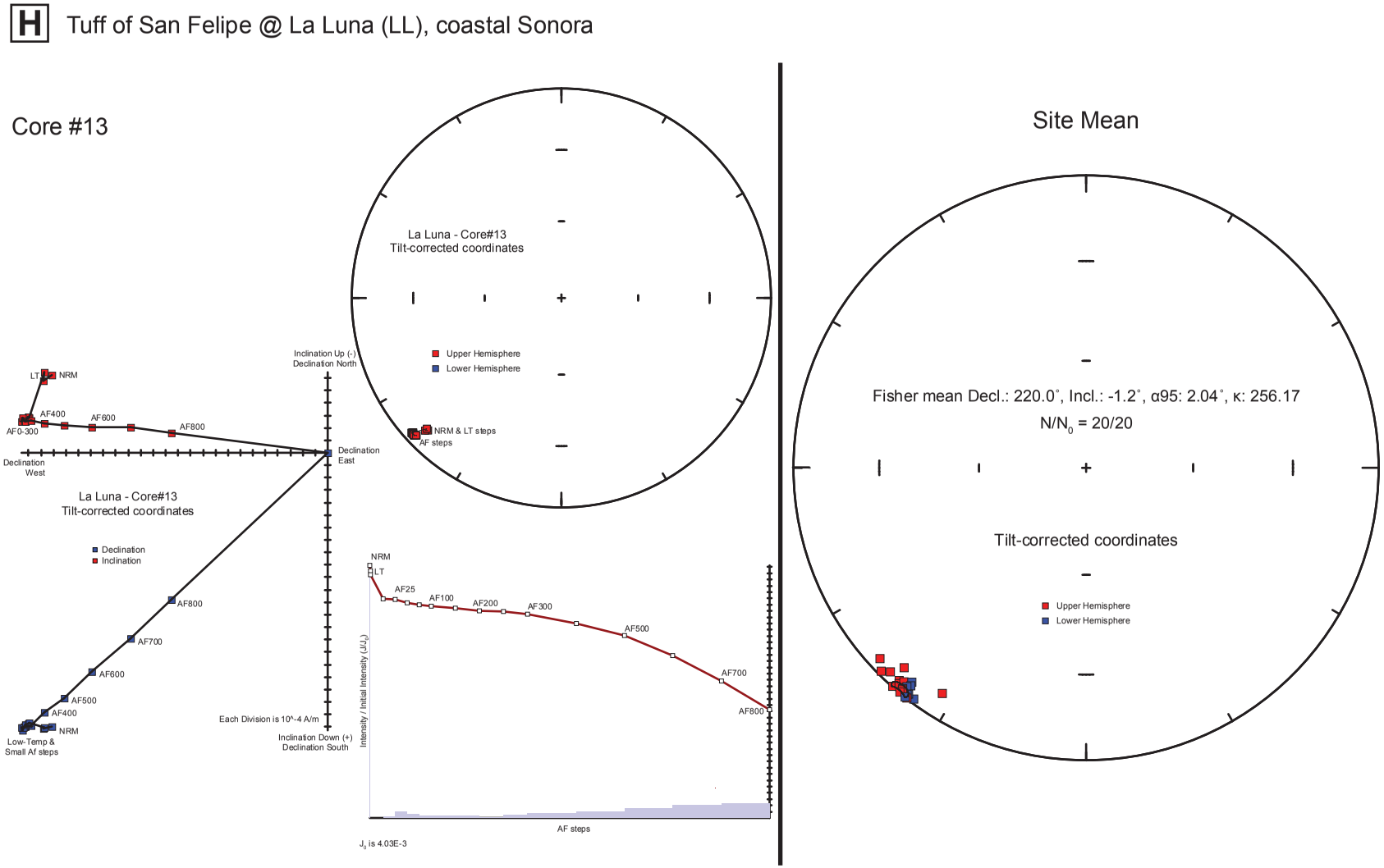

Figure 13. (cont.) (H) Typical paleomagnetic results from the Tuff of San Felipe (*Ttsf*) at the La Luna drill site in coastal Sonora. Example core #13 shown.

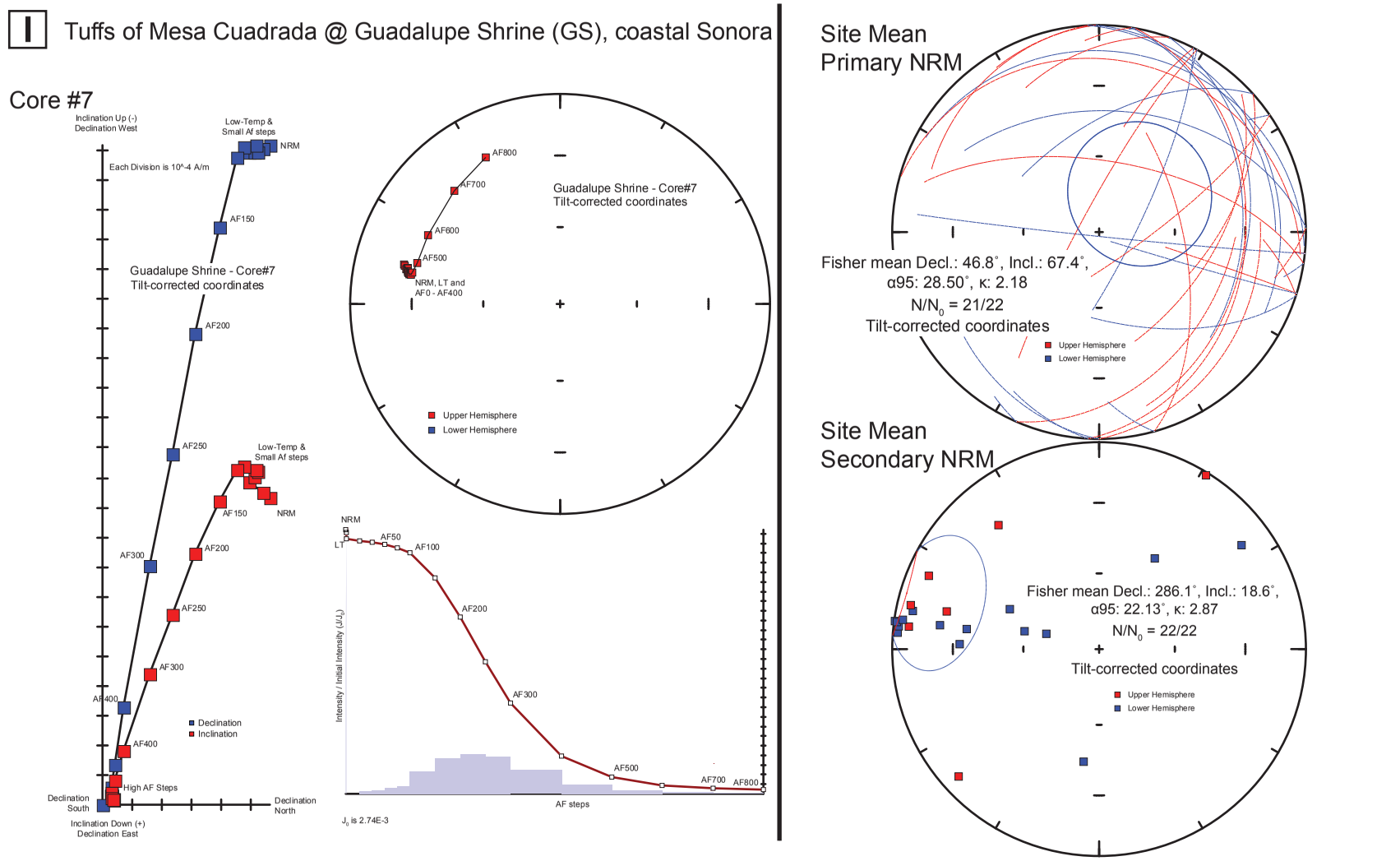

Figure 13. (cont.) (I) Typical paleomagnetic results from the Tuffs of Mesa Cuadrada (*Ttmc*) at the Guadalupe Shrine drill site in coastal Sonora. Example core #7 shown. Note: North is to the right on vector-component plot (left). A strong secondary component of NRM (lower right) complicated isolation of the primary component of NRM (upper right). The secondary NRM component overprinted and was consistently stronger than the primary NRM component until ~400 mT. Typically, the remaining four AF demagnetization steps followed great circles paths (top center stereoplot), presumably migrating towards the primary NRM vector. Out of 22 cores, none displayed a line fit to these higher AF steps, forcing the Fisher statistics to be determined from 21 circles. 1 core was overprinted with secondary NRM for all AF steps. A line fit was possible for all 22 cores using smaller AF steps (lower right), but these line fit directions were only moderately consistent to the WNW.

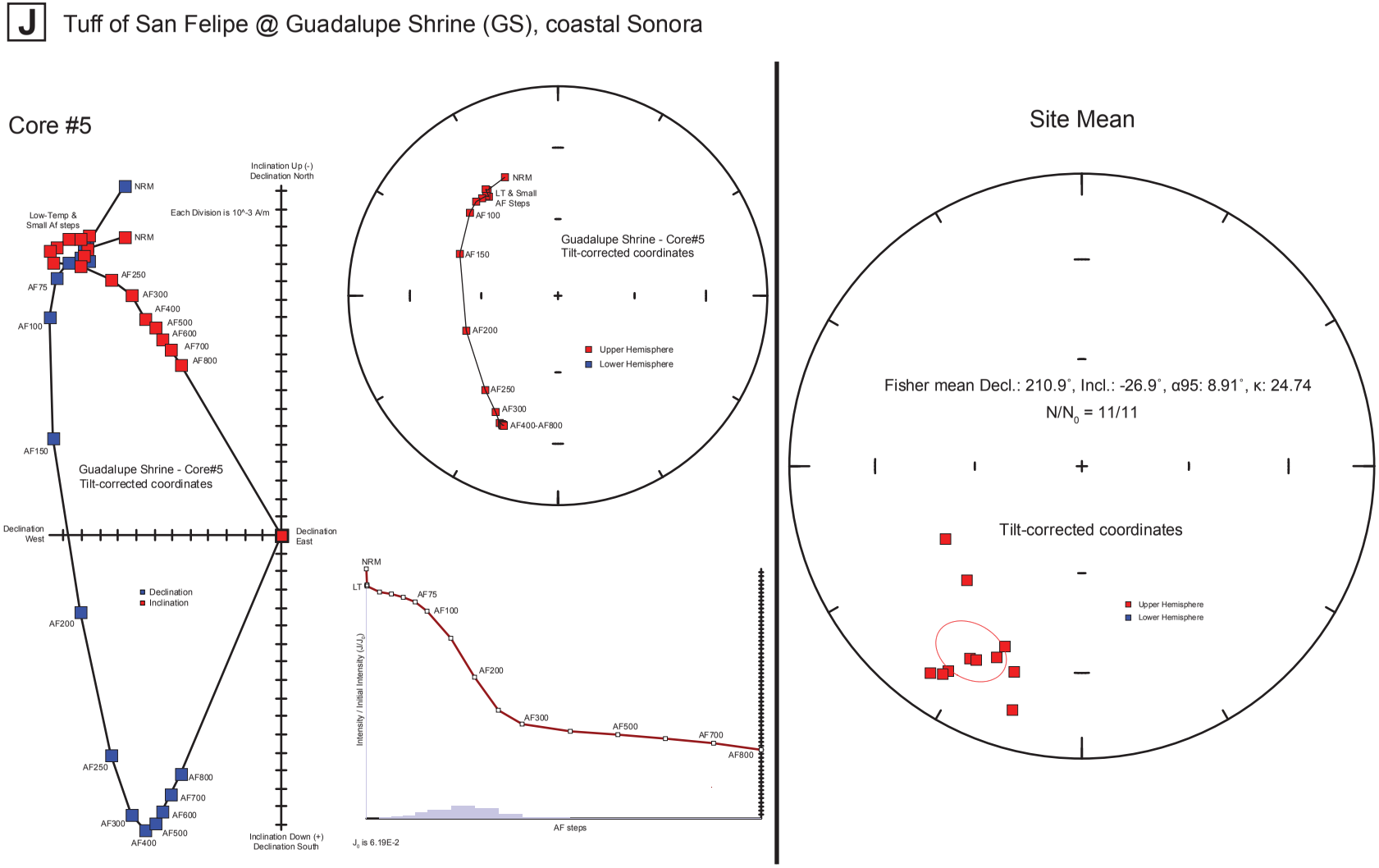

Figure 13. (cont.) (J) Typical paleomagnetic results from the Tuff of San Felipe (*Ttsf*) at the Guadalupe Shrine drill site in coastal Sonora. Example core #5 shown.

Table 2. Paleomagnetic measurements and relative declination and inclination anomalies for the Tuffs of Mesa Cuadrada and Tuff of San Felipe drill sites in central Baja California and coastal Sonora, Mexico.

				Bedding**				Geographic		Tilt Corrected		Fisher Statistics		Bingham Statistics							
	Drill Site/Unit*	°N	°W	Strike	Dip	N/N_0	Corr. Factor	Dec	Inc	Dec	Inc	ά95	κ	κ1	ά95	κ2	ά95	R†	ΔR§	F‡	ΔF§
Baja CA	MEP - Mesa El Pinole																				
	Ttsf	30.32304	115.27470	-	-	18/18	0.79	213.4	-2.9	213.4	-2.9	1.31	696.02	-535.7	1.01	-281.79	1.4		reference locality		
	MEB - Mesa El Burro																				
	Ttsf	30.17822	115.13885	-	-	11/27	0.79	215.4	0.3	215.4	0.3	3.67	141.51	-258.8	1.87	-51.72	4.2		reference locality		
	MEC - Mesa El Cartabón																				
	Ttsf	30.14063	115.20725	-	-	19/19	0.79	209.6	-4.9	209.6	-4.9	1.57	458.13	-416.71	1.12	-170.65	1.75		reference locality		
	REFERENCE SITE																				
	Ttsf			-	-	48/64	0.80	212.4	-3	212.4	-3	1.33	240.33	-319.92	0.8	-76.73	1.65		reference locality		
Sonora	PC - Punta Chueca																				
	Ttmc	28.98549	112.07985	342	37	11/11	0.79	331.6	71.9	53.3	56.3	1.78	596.51	-448.95	1.41	-302.18	1.72	46.1	11.7	-2.4	6.8
	EG - East Guadalupe																				
	******Ttmc***	28.91198	112.03074	25	28	0/37	-	-	-	-	-	-	-	-	-	-	-	-	-	-	-
	Ttsf	28.91927	112.03152	340	76	10/15	0.79	157.3	-38.9	209.1	-20.4	9.08	33.08	-11.10	10.93	-3.85	20.06	-1.0	7.7	17.4	7.3
	LL - La Luna																				
	Ttmc	28.92371	112.02010	354	23	11/22	0.79	346.5	9.8	351.7	16.3	3.8	131.89	-518.19	1.32	-43.58	4.58	-15.5	11.8	37.6	7.3
	Ttsf	28.92361	112.02373	354	65	20/20	0.79	198.3	-40.4	220	-1.2	2.04	256.17	-227.13	1.48	-97.19	2.26	9.9	1.9	-1.8	1.9
	Guadalupe Shrine																				
	Ttmc	28.91925	112.03913	354	62	21/22	0.79	37.7	50.5	46.8	67.4	28.5	2.18	-2.82	22	-1.28	40.72	ND	ND	ND	ND
	Ttsf	28.93141	112.04202	355	72	11/11	0.79	156.9	-37.4	210.9	-26.9	8.91	24.74	-34.09	5.33	-11.17	9.5	0.8	8.0	23.9	7.1

* Ttmc, Tuffs of Mesa Cuadrada; Ttsf, Tuff of San Felipe.

** Bedding is the orientation used for structural correction.

*** No mean site direction was able to be determined. See text for details.

N/N_0, number of samples used to determine site mean vector/number of samples collected.

Correction Factor for various values of N (Demarest, 1983).
Dec., Declination in degrees; Inc., Inclination in degrees.

ά95, cone of 95% confidence about mean direction; κ, the precision parameter (Fisher, 1953).

† R, Rotation in degrees. For *Ttsf* sites in coastal Sonora, calculated relative to *Ttsf* reference site of this study. For *Ttmc* sites, calculated relative to *Tmr3b* reference site at Mesa Cuadrada in Baja California (Lewis and Stock, 1998).
For Sonora sites, 2.3° has been added to R to account for finite rotation of reference locality due to Pacific-North America plate displacement.

‡ F, Flattening in degrees. For *Ttsf* sites in coastal Sonora, calculated relative to *Ttsf* reference site of this study. For *Ttmc* sites, calculated relative to *Tmr3b* reference site at Mesa Cuadrada in Baja California (Lewis and Stock, 1998).

§ ΔR, 95% confidence limits on rotation; ΔF, 95% confidence limits on flattening, both calculated according to Beck (1980) and Demarest (1983).

ND, Due to poor statistics of data from drill site, a rotation calculation is not determinable.

secondary, low-stability component from the NRM. During progressive demagnetization steps, alternating-field (AF) demagnetization procedures (Butler, 1992) gradually remove the low-stability component, and the remaining isolated vector is assumed to represent the high-stability, primary NRM that is representative of Earth's magnetic field at the time the sampled rock cooled below the Curie temperature. Because ignimbrites cool much faster than significant changes in the secular variation of Earth's magnetic field, the NRM directions determined from multiple specimens collected from the same ignimbrite cooling unit should agree within uncertainty (Lewis and Stock, 1998).

Once the NRM and low-temperature (LT) steps were conducted, all specimens from all samples collected from each of the paleomagnetic sites were subjected to this progressive AF demagnetization procedure, typically including 13 steps to a magnetic field strength of 800 millitesla (mT). All experiments were conducted using an automated 2G Enterprises superconducting rock magnetometer in a magnetically shielded μ-metal room at the Paleomagnetics Laboratory of the California Institute of Technology, as described by Kirschvink et al. (2008). No thermal demagnetization steps were performed.

Analysis

Raw paleomagnetic data were analyzed using PaleoMag v3.1b1 (Jones, 2002) to estimate the directions of lines and planes of best least-squares fit for demagnetization paths for each specimen, following on the technique of Kirschvink (1980). Typically, directions resolved from higher AF steps were utilized to obtain best-fit lines, while NRM, LT, and low AF steps displayed anomalous directions, indicative of variable magnitudes of a secondary NRM component (Fig. 13).

Results

New Reference Site for the Tuff of San Felipe

In central Baja California, a new high-precision paleomagnetic reference vector for *Ttsf* has been measured (Bennett and Oskin, 2008). This new reference location is west of both the main Gulf topographic escarpment and the San Pedro Martír fault that marks the western edge of the Gulf Extensional Province (Fig. 4). Because this reference location has remained tectonically stable since the eruption and deposition of *Ttsf*, the paleomagnetic vector measured here is a good estimate of the magnetic field at the time *Ttsf* cooled below the Curie temperature. Representative examples of paleomagnetic measurements from this new central Baja California paleomagnetic reference site(s) are shown in Figures 13A through 13C, and their relative declination and inclination anomalies are summarized in Table 2. 1:20,000-scale and 1:50,000-scale geologic mapping was conducted in the Baja California study area (Fig. 14) and three mesas capped by *Ttsf* were selected for paleomagnetic sampling: Mesa El Pinole (MEP) 20 km northwest of El Metate (Fig. 14C), Mesa El Burro (MEB) 1 km south of El Metate (Fig. 14D), and Mesa El Cartabón (MEC) 9 km southwest of El Metate (Fig. 14E). These mesas are capped by 10-30 m of the Tuff of San Felipe and are amongst the most western exposures of this ignimbrite documented in Baja California. Evidence for two cooling units within *Ttsf* exists in the northern and northeastern portions of this study area. In the area of these mesas, *Ttsf* was deposited on a generally flat landscape with minor paleo-topography incised into a 15 - 110 m-thick section of sedimentary rocks. These Oligo-Miocene strata (Dorsey and Burns, 1994) nonconformably overlie a variety of plutonic and metamorphic basement rocks. Locally, *Ttsf* infills westward-draining paleo-drainages carved into the near-horizontally dipping

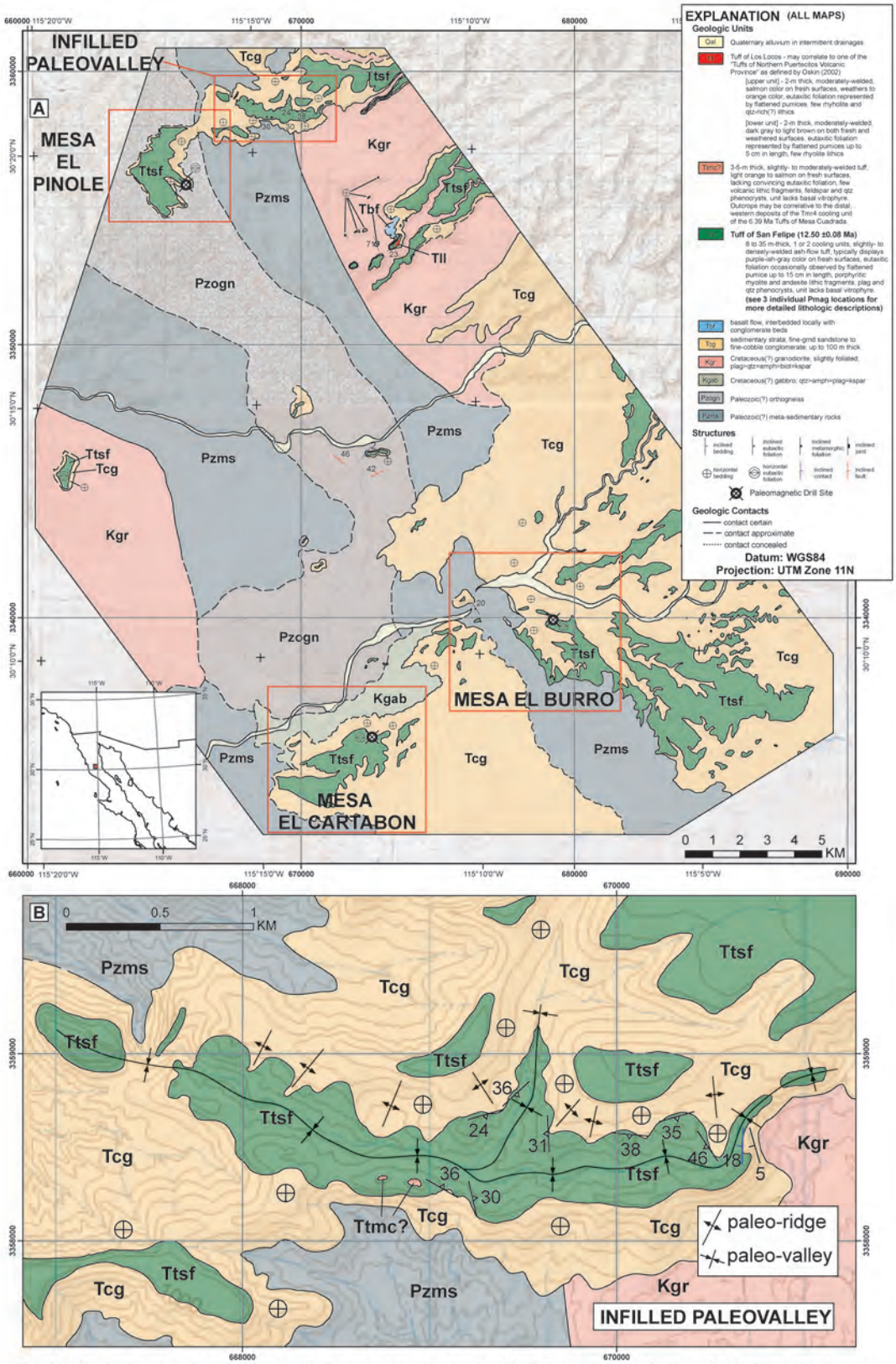

Figure 14. (A) Geologic map of new paleomagnetic reference site for the 12.5 Ma Tuff of San Felipe, Central Baja California, Mexico. Inset map and Figure 4 shows location on Baja California peninsula. (B) 12.5 Ma paleo-valley preserved by ignimbrite deposits of the Tuff of San Felipe, See following page for three additional map insets and paleomagnetic results.

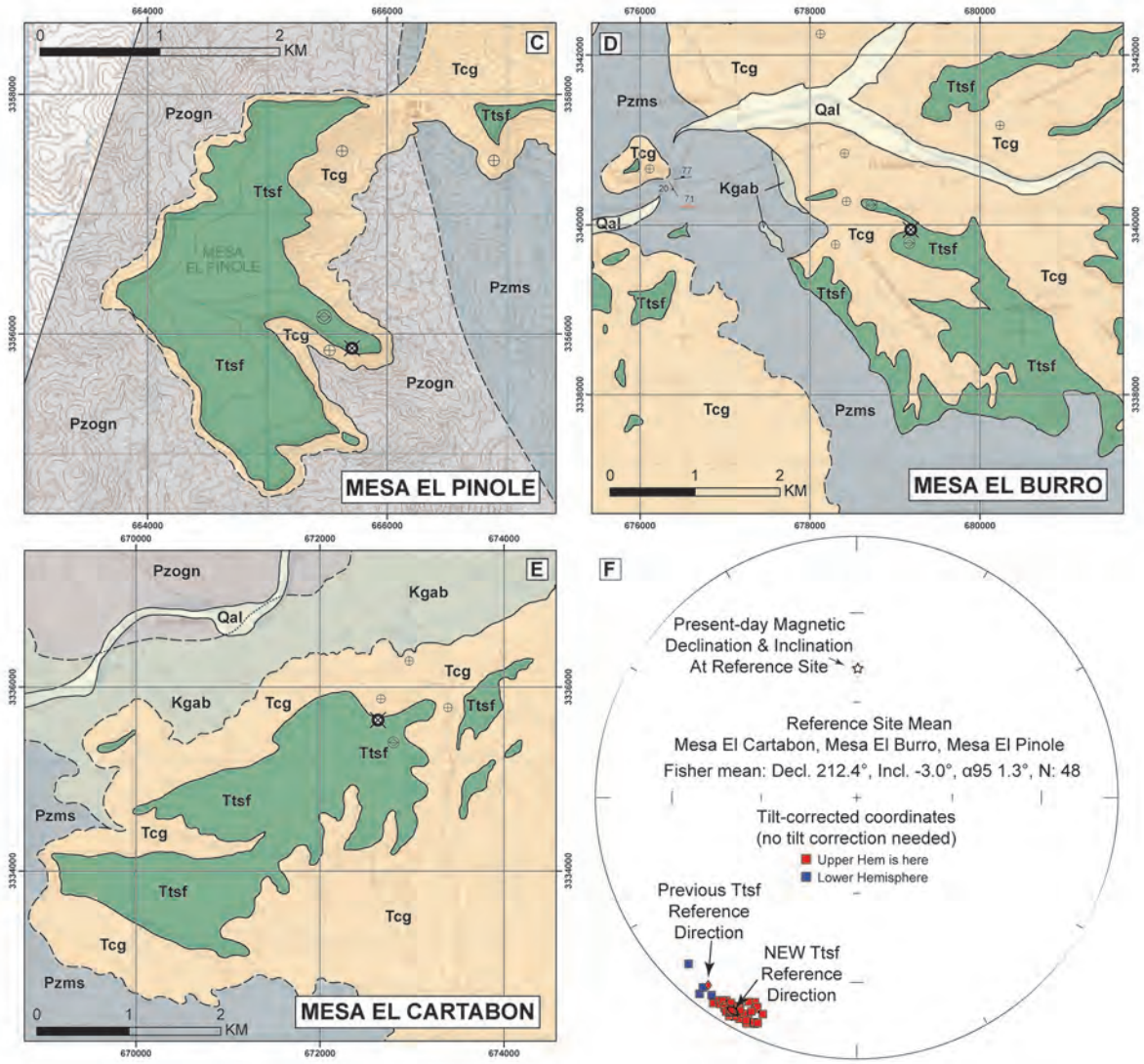

Figure 14. (cont.) Geologic inset maps and paleomagnetic results of new paleomagnetic reference site for the 12.5 Ma Tuff of San Felipe, Central Baja California, Mexico. See previous page for main geologic map, explanation, and location of insets. (C) Paleomagnetic drill site at Mesa El Pinole, (D) Paleomagnetic drill site at Mesa El Burro, (E) Paleomagnetic drill site at Mesa El Cartabon, (F) 48 of 64 cores used for new reference vector for the 12.5 Ma Tuff of San Felipe. Present-day magnetic field (black star) and previous Ttsf reference site direction from the Mesa Cuadrada locality (red-black diamond; Lewis and Stock, 1998) shown for comparison. See text for discussion of paleomagnetic methods and analysis.

underlying conglomerates (Fig. 14B).

64 randomly oriented core samples were drilled in *Ttsf* at these three mesas, including 19 samples from MEC, 27 samples from MEB, and 18 samples from MEP (Table 2). At MEC, samples were drilled from the lower cooling unit of *Ttsf*, and at MEB and MEP, samples were drilled from the upper cooling unit of *Ttsf*. At each paleomagnetic site, samples were collected in two or three clusters spaced from 10 to 600 meters apart, permitting partial exclusion of data from a paleomagnetic site if one cluster appeared to be overprinted (e.g. by a lightning strike). The majority of samples from these three mesas appear to lack any significant magnetic overprint and primary remanent magnetization directions were successfully extracted from these samples (Fig. 13A-C). However, at MEB, 14 of the 27 samples were sampled near the western tip of a protruding mesa-top; the remaining 13 samples were collected ~600 m to the east at the same elevation but within a protected drainage. These 14 western samples were discarded from the analysis for anomalous directions likely due to lightning strike at the sampling location. Of the remaining 13 cores, 11 appear to retain their Miocene direction and were included in the analysis. These 16 samples from MEB are the only samples discarded prior to calculation of the mean paleomagnetic vector for *Ttsf*.

48 of these 64 samples together yield a mean direction of 212.4° declination, -3.0° inclination with an α-95 confidence of 1.3° (Fig. 14F, Table 2). This direction lies well off of the expected Miocene paleo-pole position (Fig. 14F) and records an apparent geomagnetic excursion during reversed polarity subchron C5Ar.2r (Stock et al., 1999). This unique magnetic signature only strengthens the utility of the Tuff of San Felipe as a regional tectonic marker. The declination measured at these mesas is ~6° counter-clockwise of the Mesa Cuadrada *Ttsf* reference site in the Sierra San Felipe (Lewis and Stock, 1998), indicating that

at the previous *Ttsf* paleomagnetic reference site a minor amount of clockwise vertical-axis rotation has occurred since 12.5 Ma. Therefore, clockwise vertical-axis rotation values for all previously published *Ttsf* paleomagnetic sites from both margins of the Gulf of California are updated here and further discussed later (Fig. 15; Table 3).

Deformed Sites in Coastal Sonora

Data from paleomagnetic remanence directions measured on pyroclastic flows in coastal Sonora indicate vertical-axis rotations range from ~15° counter-clockwise to ~53° clockwise relative to their respective reference locations in stable Baja California. Representative examples of paleomagnetic measurements from these coastal Sonora paleomagnetic sites are shown in Figures 13D through 13J, and their relative declination and inclination anomalies are summarized in Table 2. For all *Ttsf* paleomagnetic sites, rotation values are calculated with respect to the new reference site of this study (Bennett and Oskin, 2008). For all *Ttmc* paleomagnetic sites, rotation values are calculated with respect to the *Tmr3b* unit of Lewis and Stock (1998) from Mesa Cuadrada in northeastern Baja California. Additionally, a correction of +4.6° has been applied to all published rotation values for *Ttsf* from Oskin et al. (2001).

At the Punta Chueca (PC) paleomagnetic site in the Punta Chueca block (Fig. 13D), *Ttmc* displays a clockwise vertical-axis rotation of 46.1° ± 11.7°. *Ttsf*, previously sampled in this fault block by Oskin et al. (2001), displays a vertical-axis rotation of 52.8° ± 2.1°. At the East Guadalupe (EG) paleomagnetic site in the Guadalupe block, a magnetic vector direction was unable to be determined for *Ttmc* (Fig. 13E), while *Ttsf* displays a clockwise vertical-axis rotation of -1.0° ± 7.7° (Fig. 13F). A secondary chemical overprint of the primary magnetic vector direction of *Ttmc* at EG is likely to be the cause of the inconclusive results

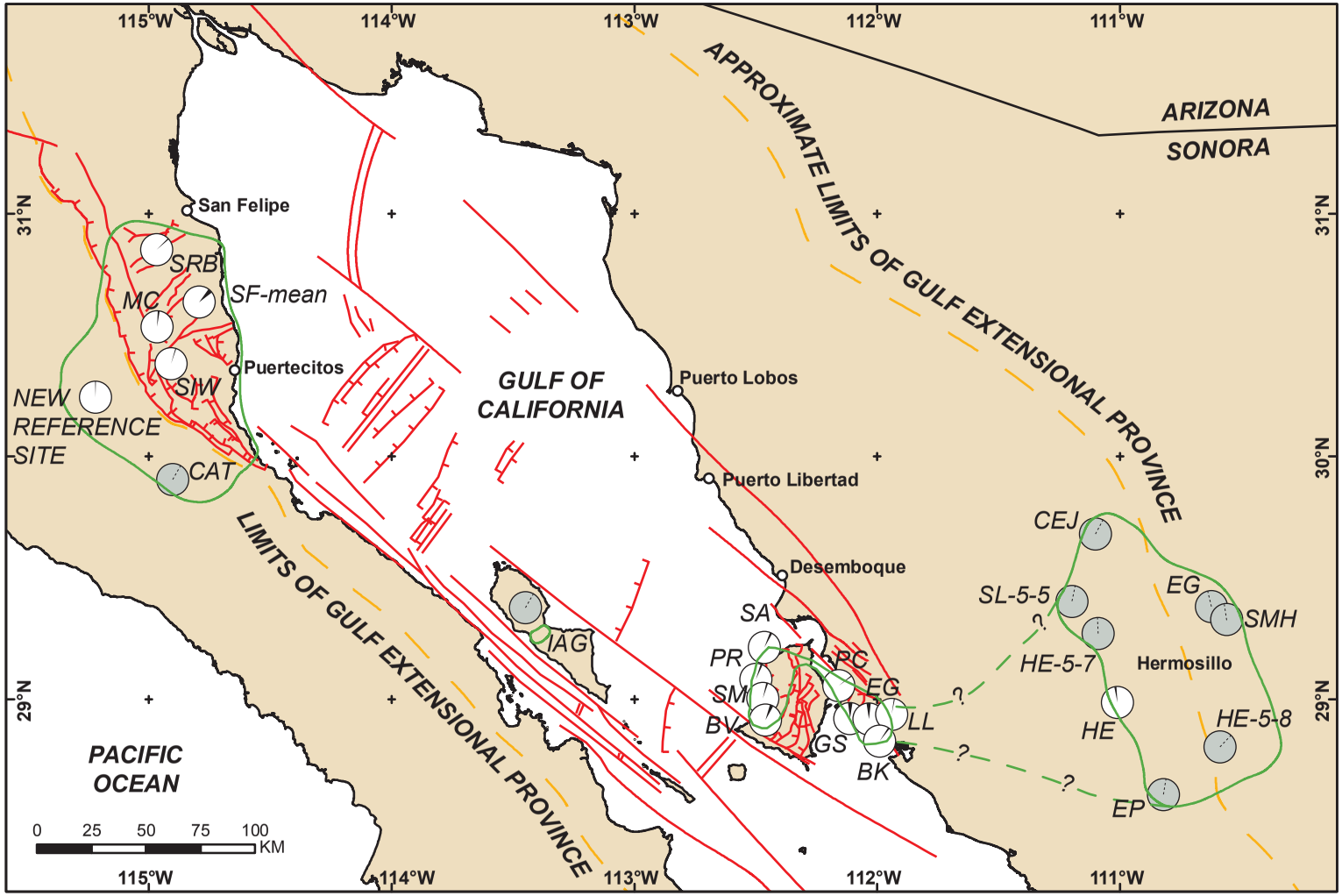

Figure 15. Paleomagnetic summary and update map for the Tuff of San Felipe across the northern Gulf of California. All unpublished (this study) and published (Lewis and Stock, 1998; Stock et al., 1999; Oskin et al., 2001; Oskin, 2002; Oskin and Stock, 2003a; Stock et al., 2006; Hernández-Ménez et al., 2008; Stock et al., 2008) paleomagnetic drill sites of the Tuff of San Felipe are shown here, with their rotation values updated to the new stable paleomagnetic reference site in Baja California from this study. Rotation values are shown relative to north as an arbitrary datum. Clockwise vertical-axis rotations are shown east of north, counter clock-wise vertical-axis rotations are shown west of north. Magnitude of rotation error values are shown by greater arc length ('wider') pie slices. Gray 'pie tins' lack rotation error values due to unavailability of raw paleomagnetic data (drill site results only recently published in conference abstracts) and rotations are represented by dashed line, not 'pie slice'. Approximate extent of Tuff of San Felipe outcrops (solid green lines) and highly speculative extent of Tuff of San Felipe outcrops buried by alluvium (dashed green lines) indicated. See Table 3 for details of rotation calculations and paleomagnetic site name abbreviations.

Table 3. Updated paleomagnetic relative declination and inclination anomalies for published Tuff of San Felipe drill sites across northwest Mexico.

						Tilt-Corrected		Using Mesa Cuadrada as Reference Site				Using new Reference Site from This Study			
	Reference	Drill Site	°N	°W	N/N_0	Dec.	Inc.	R†	ΔR§	F‡	ΔF§	R†	ΔR§	F‡	ΔF§
Baja CA	This Study	MEC-MEB-MEP grouped	30.213962	115.206932	48/64	212.4	-3.0		reference locality				reference locality		
	This Study	MEC - Mesa El Cartabon	30.14063	115.207248	19/19	209.6	-4.9		reference locality				reference locality		
	This Study	MEB - Mesa El Burro	30.178217	115.138845	11/27	215.4	0.3		reference locality				reference locality		
	This Study	MEP - Mesa El Pinole	30.32304	115.274704	18/18	213.4	-2.9		reference locality				reference locality		
	Lewis and Stock (1998)	MC - Mesa Cuadrada	30.53	114.96	5/6	218.3	-6.9		former reference locality			5.9	3.4	3.9	3.3
	Lewis and Stock (1998)	SFD - San Fermin	30.73	114.85	8/8	253.0	1.8	34.7	6.0	-8.7	6.0	40.6	5.2	-4.8	5.2
	Lewis and Stock (1998)	SFE - San Fermin	30.66	114.83	7/7	253.4	-2.8	35.1	5.5	-4.1	5.5	41.0	4.6	-0.2	4.6
	Lewis and Stock (1998)	SFB - San Fermin	30.65	114.79	3/6	258.5	-3.1	40.2	7.8	-3.8	7.8	46.1	6.9	0.1	6.9
	Lewis and Stock (1998)	SFF - San Fermin	30.6	114.79	5/5	276.7	-3.0	58.4	5.9	-3.9	5.9	64.3	5.0	0.0	5.0
	Lewis and Stock (1998)	SFJ - San Fermin	30.54	114.83	6/6	255.4	-11.2	37.1	6.5	4.3	6.4	43.0	5.7	8.2	5.6
	Lewis and Stock (1998)	SFH - San Fermin	30.55	114.74	4/5	288.6	10.6	70.3	11.0	-17.5	10.8	76.2	10.6	-13.6	10.4
	Lewis and Stock (1998)	SF - unit_mean	30.61	114.83	-	259.4	-3.7	41.1	8.6	-3.2	8.6	44.0	8.5	7.0	8.4
	Stock et al. (1999)	SIW - Santa Isabel Wash	30.38	114.92	11/11	229.7	-9.1	11.4	4.0	2.2	3.6	17.3	1.9	6.1	1.9
	Stock et al. (1999)	SRB - Santa Rosa Basin	30.85	114.97	11/11	259.4	-11.5	41.1	3.9	-4.6	3.8	47.0	2.4	8.5	2.4
	Stock et al. (2008) AGU poster	CAT - Catavina*	29.898	114.904	8	242.0	-16.0	-	-	-	-	29.6	-	13.0	-
Western Midriff Islands	Stock et al. (2008) AGU poster	IAG - Isla Angel de la Guarda	29.265	113.395	9	242.2	-9.5	-	-	-	-	29.8	-	6.5	-
Eastern Midriff Islands**	Oskin et al. (2001)	SA - NW Isla Tiburon***	29.18	112.46	6/7	235.1	-15.8	14.5	6.0	8.9	5.4	25.0	4.5	12.8	4.3
	Oskin et al. (2001)	PR - Central Isla Tiburon***	29.07	112.49	10/12	231.3	-1.3	10.7	5.0	-5.6	4.9	21.2	3.8	-1.7	3.8
	Oskin et al. (2001)	SM - S.Central Isla Tiburon***	28.98	112.46	11/13	226.0	2.7	5.4	5.0	-9.6	4.6	15.9	3.3	-5.7	3.3
	Oskin and Stock (2003a)	BV - Isla Tiburon***	28.92	112.47	16/18	232.9	16.4	12.3	7.0	-23.3	7.0	22.8	6.5	-19.4	6.3
Coastal Sonora**	This Study	EG - East Guadalupe	28.91927	112.03152	10/15	209.1	-20.4	-6.9	8.3	13.5	7.8	-1.0	7.7	17.4	7.2
	This Study	LL - La Luna	28.92361	112.02373	20/20	220.0	-1.2	4.0	3.6	-5.7	3.5	9.9	1.9	-1.8	1.9
	This Study	GS - Guadalupe Shrine	28.93141	112.04202	11/11	210.9	-26.9	-5.1	8.5	20.0	7.7	0.8	8.0	23.9	7.1
	Oskin et al. (2001)	BK - Bahia Kino***	28.88	112.01	10/11	245.6	-10.4	25.0	5.0	3.5	4.5	35.5	3.3	7.4	3.3
	Oskin et al. (2001)	PC - Punta Chueca***	29.02	112.08	13/13	262.9	-11.6	42.4	4.0	4.7	3.7	52.8	2.1	8.6	2.0
Central Sonora**	Oskin (2002)	HE - Hermosillo	28.98	111.00	5/7	202.5	-10.0	-18.1	5.0	3.1	5.1	-7.6	3.9	7.0	3.8
	Hernandez-Mendez et al. (2008)	SMH - San Miguel de Horcasitas*	29.34	110.57	10	201.5	4.0	-	-	-	-	-8.6	-	-7.0	-
	Hernandez-Mendez et al. (2008)	EG - El Gavilan	29.38	110.62	6	196.6	-11.3	-	-	-	-	-13.5	-	8.3	-
	Hernandez-Mendez et al. (2008)	EP - Rancho El Pilar (Sierra Libre)*	28.6	110.82	5	219.4	1.0	-	-	-	-	9.3	-	-4.0	-
	Hernandez-Mendez et al. (2008)	CEJ - Cerro la Ceja*	29.68	111.1	5	238.2	-1.8	-	-	-	-	28.1	-	-1.2	-
	Stock et al. (2006) NSF workshop	SL-05-05 - Sierra Lopez*	29.4	111.2	4	222.0	-8.1	-	-	-	-	11.9	-	5.1	-
	Stock et al. (2006) NSF workshop	HE-05-08 - La Colorado*	28.8	110.59	16	253.5	2.6	-	-	-	-	43.4	-	-5.6	-
	Stock et al. (2006) NSF workshop	HE-05-07 - northwest of Hermosillo*	29.27	111.09	7	207.8	-5.9	-	-	-	-	-2.3	-	2.9	-

N/N_0, number of samples used to determine site mean vector/number of samples collected. When N_0 is not known, only N is reported.

Dec., Declination in degrees; Inc., Inclination in degrees.

† R, Rotation in degrees. Calculated relative to *Ttsf* reference site of this study.

‡ F, Flattening in degrees. Calculated relative to Ttsf reference site of this study.

§ ΔR, 95% confidence limits on rotation; ΔF, 95% confidence limits on flattening, both calculated according to Beck (1980) and Demarest (1983).

* Drill sites are published in conference abstracts and presented on posters without detailed results necessary to calculate confidence limits. Rotations relative to the former Mesa Cuadrada reference site have not been previously published for these sites.

** For sites on Isla Tiburon and in Sonora, 2.3° has been added to R to account for finite rotation of reference locality on the Pacific plate around Euler pole of the North America plate.

*** 4.6° (clockwise) correction made to these published values, in addition to the recalculation relative to new reference site of this study.

from this site. At the La Luna (LL) paleomagnetic site in the Luna block, *Ttmc* (Fig. 13G) and *Ttsf* (Fig. 13H) display clockwise vertical-axis rotations of -15.5° ± 11.8° and 9.9° ± 1.9°, respectively. At the Guadalupe Shrine (GS) paleomagnetic site in the Guadalupe block, *Ttmc* (Fig. 13I) displays ~40° of clockwise vertical-axis rotation with at least 70° of error. Due to only partial removal of a shallow WNW-oriented secondary NRM component, both the direction of the primary NRM component and the relative rotation value for *Ttmc* at GS have low precision, ± 28.5° and at least 70°, respectively (Fig. 13I), and this rotation value is not reliable. Also at this site, *Ttsf* (Fig. 13J) displays a clockwise vertical-axis rotation of 0.8° ± 8.0°. *Ttsf* in the Cerro Kino fault block, previously sampled at the Bahía Kino (BK) paleomagnetic site by Oskin et al. (2001), displays a vertical-axis rotation of 35.5° ± 3.3°. *Ttmc* is not exposed in the Cerro Kino fault block.

DISCUSSION

The results from detailed geologic mapping, geochronology, paleomagnetism, and fault kinematic analysis begin to suggest a tectonic history in the study area of a rapid, single transtensional stage with progressive localization of strike-slip faulting. Palinspastic reconstructions of both cross section and map view help to further clarify the tectonic evolution of the Kino-Chueca Shear Zone since Middle Miocene time. The results from these restorations help to constrain the timing, direction, and magnitude of both extensional and strike-slip faulting within the study area related to the opening of the Gulf of California.

Extensional Faulting in Coastal Sonora

Evidence for extensional faulting is observed throughout all pre-Quaternary map units within the study area. Generally, two distinct styles of extensional faulting are observed: (1) a

larger magnitude extension style that was WSW-directed on NNW-striking normal faults, expressed present-day by low- to high-angle N- to NNE-striking normal faults that have been variably rotated in a clockwise direction, and (2) a smaller magnitude extension style expressed present day by high-angle N-S-striking and WNW-striking normal faults. Paleo-horizontal datums of *Ttmc* and *Ttsf* are exploited to assist cross-section restoration of fault blocks back to 6.4 and 12.5 Ma, respectively (Fig. 16).

The larger-magnitude style of WSW-directed faulting consists of normal faults with dips that range from very low (<5°), to moderate (~60°), to high (~90°) angles. Pre-extension hanging wall rocks are tilted down to the east up to 90°. These relationships produce greater than 90° hanging wall cutoff angles, which is the angle measured between tilted hanging wall rocks and the normal fault surface, down towards the normal fault. Typically, both the steepest plausible normal fault dip (90°) and the more likely normal fault dip (60°) produce hanging wall cutoff angles ≤90°. Therefore, the observed >90° hanging wall cutoff angles are impossible to palinspastically restore with one generation of normal faults, and require that a more complex multi-phase extensional history has acted to tilt these rocks to such steep angles (e.g. Proffett, 1977). In this multi-stage model for extended continental crust, first-generation normal faults slip and rotate to low angle. As this first fault generation becomes less mechanically favorable to slip (Anderson, 1942; Proffett, 1977; Forsyth, 1992; Buck, 1993), new second-generation faults initiate, allowing for continued continental extension. These younger second-generation faults may sole into older first-generation faults that continue to slip at moderate to low angles (e.g. Brady et al., 2000).

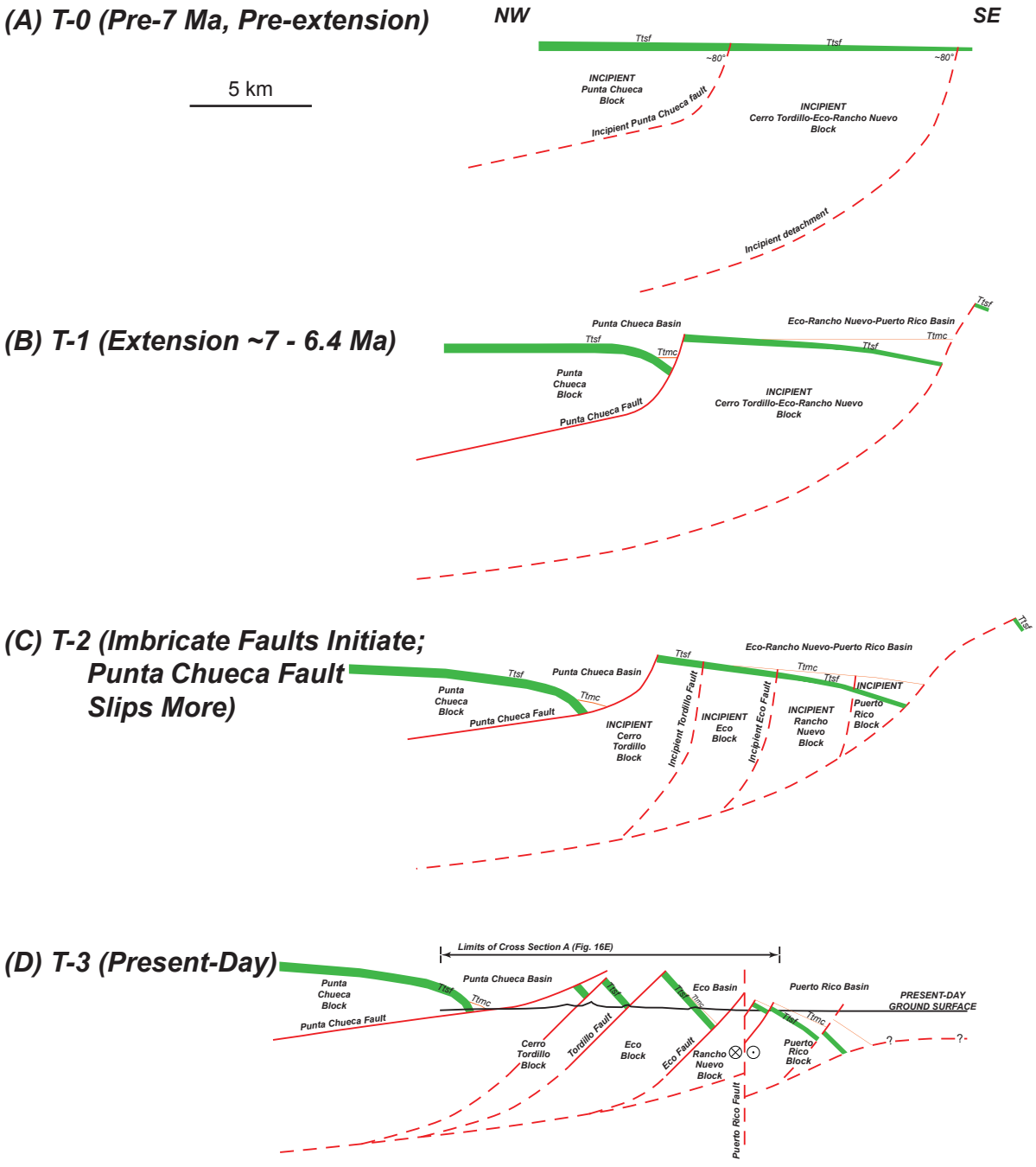

Figure 16. Incremental restoration of extension fault systems along cross section A-A' (see Plate 1 for location). (A) At 12.5 Ma, coastal Sonora was blanketed by the Tuff of San Felipe (green). At ~7 Ma, transtension initiated in the study area. (B) After some slip on the Punta Chueca fault, the 6.4 Ma Tuffs of Mesa Cuadrada (orange) is deposited in these basins as syn-rift record of extension. The Punta Chueca Fault is low-angle fault relative to the Eco and Tordillo faults and likely initiated slip prior the more moderate-angle faults towards the southeast. This early slip on the Punta Chueca fault is supported by the larger dip difference between the Tuff of San Felipe (Ttsf) and the Tuffs of Mesa Cuadrada (Ttmc) in the Punta Chueca basin. (C) The foot wall of the Punta Chueca fault is dissected by high-angle imbricate Eco and Tordillo faults. (D) Continued slip on the Punta Chueca fault and moderate slip on the Eco and Tordillo fault characterize the present-day fault relationships.
All restoration steps are the same scale. No vertical exaggeration.

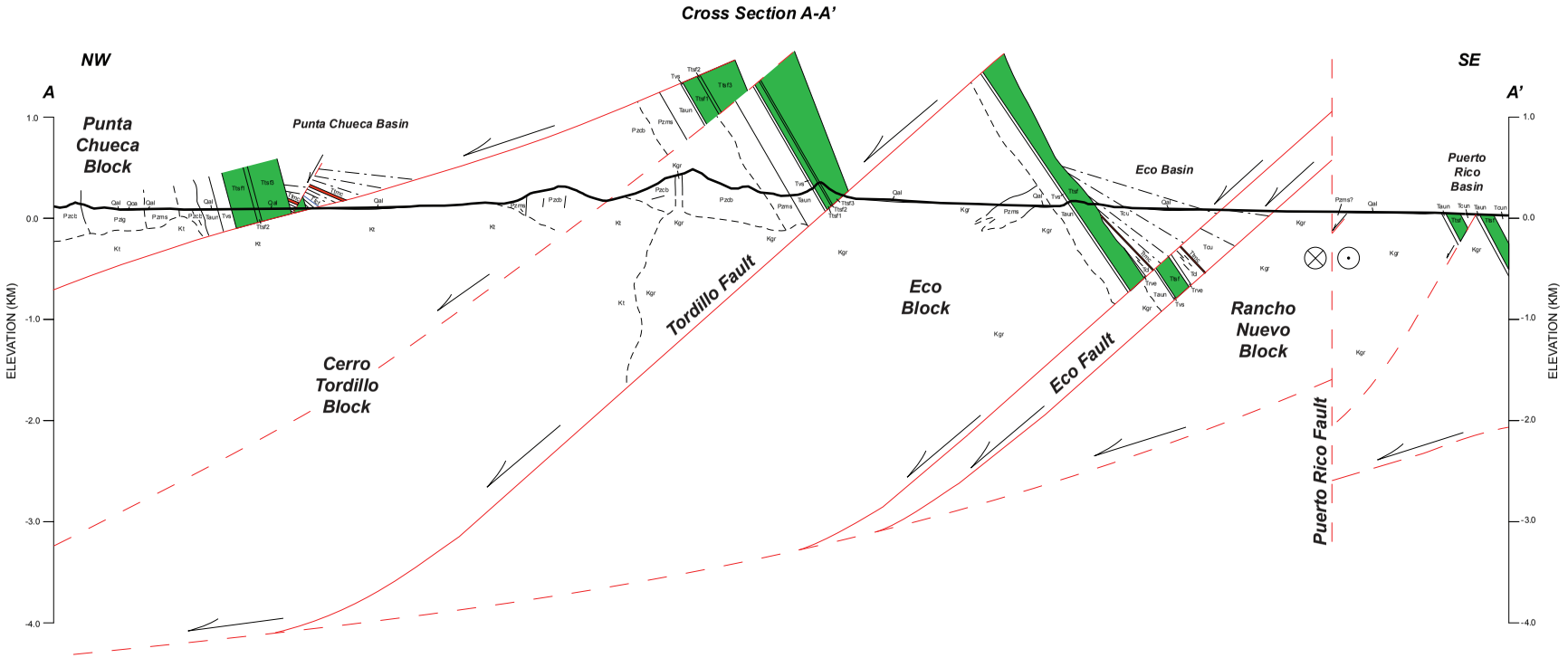

Figure 16. (cont.) (E) Cross section A-A' is drawn across multiple extensional basins of the northern part of the study area. See PLATE 1 for location. See text for unit descriptions.

Timing of Extensional Faulting

Stratigraphic Constraints

Block tilting and basin deposition prior to the eruptions of both the 6.4 Ma Tuffs of Mesa Cuadrada and the 6.5 Ma Tuff of Cerro Tordillo constrain the timing of the earliest activity on these extensional fault systems. Thus, *Tcl* is an exceptionally important lithologic unit to this study, in that it helps to date the earliest presence of tectonic basins related to the Gulf of California rift in the study area.

In order to quantitatively determine the timing of this earliest extension, conglomerate sedimentation rates, constrained by isotopically-dated interbedded tuffs, are extrapolated to resolve earliest basin formation and deposition. In the Punta Chueca block, the 6.39 ± 0.02 Ma Tuffs of Mesa Cuadrada is 166 m above the 6.53 ± 0.18 Ma Tuff of Cerro Tordillo, yielding a sedimentation rate of 1.2 ± 0.2 mm/yr for *Tcl* (Dorsey et al., 2008). When this *Tcl* sedimentation rate is applied to the ~50 m of *Tcl* below the Tuff of Cerro Tordillo that is exposed at the surface, the timing of basin initiation, accommodation, and sediment deposition in coastal Sonora is estimated at ca. 6.6 Ma. This is a minimum age estimate for basin initiation because there is presumably thicker *Tcl* deposits in the Punta Chueca basin at depth than the ~50 m exposed at the surface.

Slip on the Punta Chueca fault is interpreted to have created the tectonic accommodation for these basin conglomerates and tuffs. This dip-slip occurred coeval with deposition and is demonstrated by: (1) fanning dip sections in the hanging wall of large-scale normal faults (e.g. Punta Chueca and Eco faults), and (2) growth strata thickening towards the faults (e.g. Punta Chueca fault) (Plate 1, Fig. 16). Additional evidence for syn-tectonic deposition of *Tcl*, *Ttmc*, and *Tcu* is that the upper and lower contacts of *Ttmc* are either both

disconformities above an actively tilting hanging wall (Punta Chueca block), or both angular unconformities, suggesting tilting began prior to and was ongoing after 6.4 Ma. Extensional faulting likely terminated coeval with or shortly after the end of conglomerate deposition, because the youngest conglomerate deposits are relatively undeformed (dipping <5°).

Structural Constraints

Relative amounts of tilting of pre- and syn-rift strata can also constrain the timing of the earliest activity on these extensional fault systems. In order to quantitatively determine the timing of this earliest extension, the relative structural tilt of isotopically-dated tuffs interbedded within extensional basins are evaluated.

In the Punta Chueca block, the 6.39 ± 0.02 Ma Tuffs of Mesa Cuadrada is inclined 34°, while the stratigraphically lower 6.53 ± 0.18 Ma Tuff of Cerro Tordillo is inclined 50°. This yields a rapid tilting rate of 0.11°/kyr for the intervening *Tcl* deposits. When this tilting rate is extrapolated to the >50 m *Tcl* deposits that underlie the Tuff of Cerro Tordillo and overlie the 71°-inclined Tuff of San Felipe, the timing of basin initiation, accommodation, and sediment deposition in coastal Sonora is estimated at ca. 6.7 Ma. Because this tilting rate is rather high, a more conservative age of 7 Ma is assigned to initiation of extensional deformation determined from structural inclinations.

When this conglomerate deposition rate and tilting rate are forward projected to the thickest exposures of *Tcu* (~225 m in the Punta Chueca block), cessation of conglomerate deposition and extensional faulting is estimated at ca. 6.2 Ma. This is a maximum estimate because *Tcu* deposits likely exceed 225 m and are not completely observed due to the likely erosion of the upper portions of these youngest deposits. Therefore, a more conservative estimate of 6 Ma is assigned to cessation of extensional deformation in coastal Sonora.

Direction of Extensional Faulting

The direction of extension for a normal fault can be constrained from the structural strike of the tilted units within its hanging wall. This assumes that typical orthogonal extension ingrains a structural strike into tilted strata that is 90° clockwise from the direction of tectonic transport (right-hand rule). Vertical-axis block rotations will alter these results. Thus, any subsequent block rotation associated with strike-slip motion must be corrected for prior to this analysis.

After first grouping the structural strike of the 12.5 Ma Tuff of San Felipe by fault blocks, a dominant pattern of approximate NNW- to NNE-oriented strike ridges is observed across the study area (gray arrows, Fig. 17). Next, variable amounts of clockwise vertical-axis rotations determined by the paleomagnetic results of this study were removed from the average structural strike in four fault blocks (Punta Chueca, Guadalupe, Luna, and Cerro Kino blocks). As a result, a consistent pre-rotation strike direction of azimuth ~334° is determined (red arrows, Fig. 17). Thus, a WSW orthogonal extension direction of azimuth ~244° is assumed to have tilted these fault blocks down to the ENE along NNW-striking west-dipping normal faults (blue arrows, Fig. 17). This extension direction corroborates well with published extension directions throughout the Gulf Extensional Province (Henry, 1989; Stewart et al., 1998).

When this technique is applied to basin fill deposits (e.g. *Tcl*, *Ttmc*, *Tcu*), a broadly similar extensional direction emerges (Fig. 17). This result indicates that the WSW extension direction remained broadly constant from the inception of extensional basins and throughout the duration of basin activity. One notable exception is within the Guadalupe block, where basin fill were tilted down to the east via WNW-directed extension, not by WSW-directed

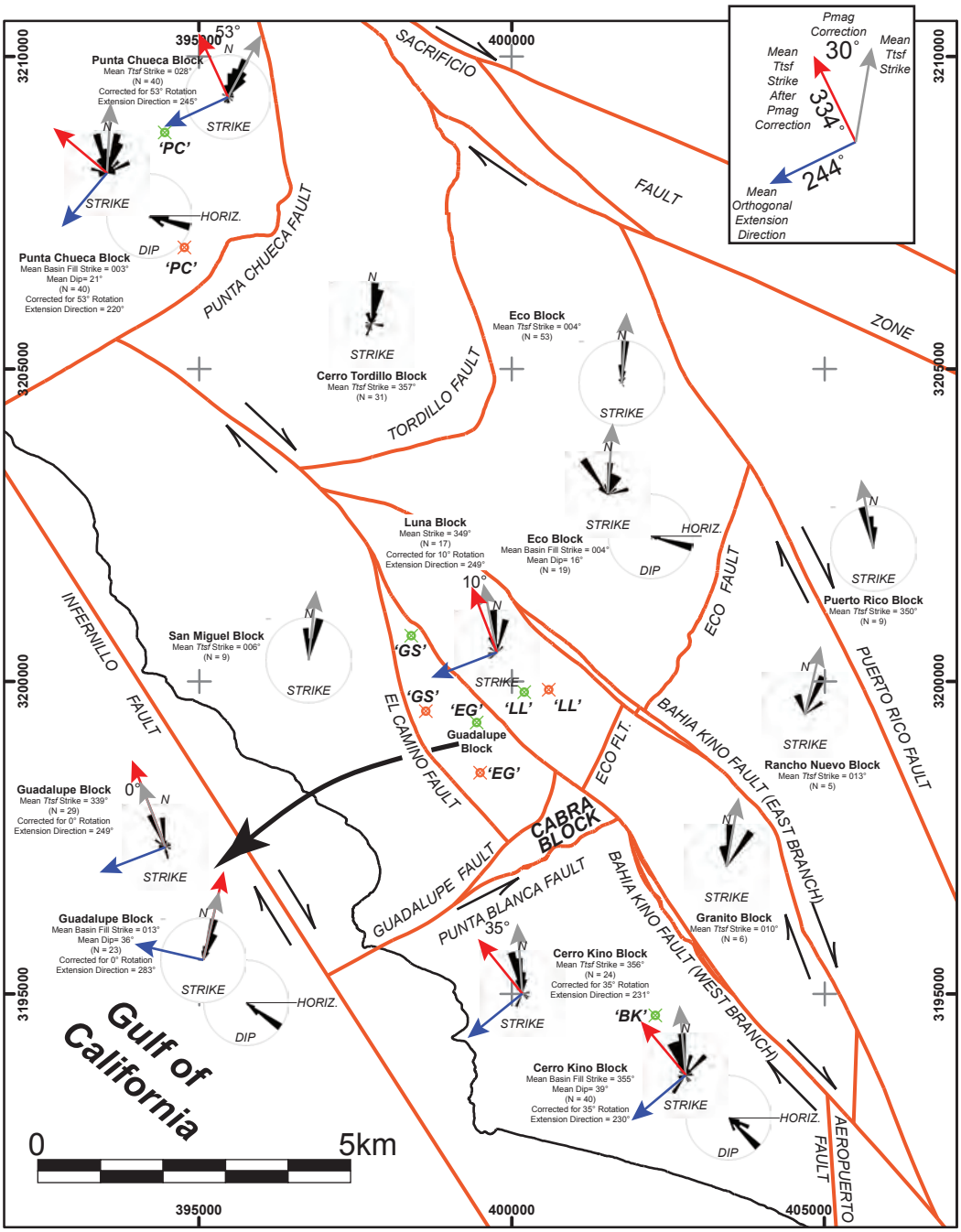

Figure 17. Rose diagrams of structural strike for the Tuff of San Felipe (*Ttsf*) for each fault block, and strike and dip for basin fill sediments and tuffs (gray arrows). These structures were then corrected for variable amounts of clockwise vertical-axis rotations determined from paleomagnetism (solid red arrows) for the Cerro Kino, Guadalupe, Luna, and Punta Chueca blocks. From these corrected strike directions, orthogonal extension directions were independently determined for both packages of *Ttsf* and basin fill (blue arrows). A consistent WSW-ENE extension direction emerges (average extension azimuth = 244˚) for *Ttsf*. Extension directions for basin fill are similar to that of *Ttsf* within the Cerro Kino, Punta Chueca, and Eco blocks. However, basin fill in the Guadalupe block appears to have filled a portion of the Eco basin that was extending in a more WNW direction (extension azimuth = 283˚). Calculated clockwise vertical-axis rotation amounts shown in degrees. Paleomagnetic drill sites in *Ttsf* (green) and *Ttmc* (orange) shown with bullseye. Pmag sites: 'PC' - Punta Chueca, 'LL' - La Luna, 'GS' - Guadalupe Shrine, 'EG' - East Guadalupe, 'BK' - Bahia Kino. Pmag sites for *Ttsf* at 'PC' and 'BK' from Oskin et al. (2001).

extension (Fig. 17). Because this block underwent 0° of rotation (Fig. 15 and 17; Table 2), this extension direction more likely reflects a local structural complexity between the two branches of the Bahía Kino fault.

Paleocurrent data collected from conglomerate deposits within these three coastal Sonora basins (Dorsey et al., 2008) have been corrected for the paleomagnetic rotations determined from this study (Fig. 10). These corrected paleocurrents data reveal a consistent south-draining direction. These results are broadly consistent with an extensional model in which the WSW- and WNW-directed extension forms axial drainages that are approximately N-S-oriented. Thus, a southerly paleo-flow direction within these normal fault-controlled axial drainages would drain towards the extensional depression of the nascent Gulf of California.

A later stage of WNW- or NW-directed extension may have further deformed the northwestern-most portion of the study area. The NE-striking portion of the Punta Chueca fault in the southwestern Punta Chueca block was likely the transfer (i.e. transform) portion of the early history of the Punta Chueca fault while it was accommodating WSW-directed extension. Multiple lines of evidence suggest that this portion may have later become a zone of WNW-directed extension: (1) An isolated package of undifferentiated conglomerate (*Tcun*) in the Punta Chueca block displays a consistent southeast dip direction. This dip direction suggests deposition during NW-directed extension and tilting along the southwestern portion of the Punta Chueca fault. This uncharacteristic orientation of these basin conglomerates may also indicate their relative age is younger than *Tcu*, being deposited while the Punta Chueca fault continued to slip as it rotated, (2) In the northern study area, a general WNW-ESE tectonic transport direction of a similar rock package is apparent across the Eco, Cerro Tordillo, and Punta Chueca blocks (Plate 1, Fig. 16E). This packages consists

of (1) crystalline basement (*Kt* and *Kgr*) and the wall rocks they intrude (*Pz*), (2) undifferentiated andesite (*Taun*), (3) volcaniclastic deposits (*Tvs*), (4) all three cooling units of the Tuff of San Felipe (*Ttsf1*, *Ttsf2*, and *Ttsf3*), and (5) basin fill (*Tcl*, *Ttmc*, and *Tcu*) (Plate 1, Fig. 16), (3) Slickenline orientations measured on the Punta Chueca fault reflect dip-slip and sinistral oblique-normal slip, (4) For the Punta Chueca fault, a relative greater amount of basement rocks are exhumed in the San Miguel block foot wall (~6 km in map view), compared to the ~4.5 km (map view) of basement exhumed in the Cerro Tordillo block foot wall.

Magnitude of Extensional Faulting

Estimates of the magnitudes of slip on extensional faults are calculated from restoration of cross section 'A' (Fig. 16; Plate 1). Along this line of section, total dip-slip displacements on significant normal faults since 12.5 Ma are as follows: Eco fault (3.0 km), Tordillo fault (2.2 km), and Punta Chueca fault (5.2 km). Dip-slip displacements on these faults since 6.4 Ma are: Eco fault (3.0 km), Tordillo fault (2.2 km), and Punta Chueca fault (3.8 km). Although restoration of cross section 'A' infers structures beyond the boundaries of the study area and at depth, estimates of % extension are calculated only from data collected within the study area, along the line of cross section 'A'. From these measurements, 11% extension occurred across the northern study area between 12.5 and 6.4 Ma. Extrapolation of sedimentation rates in the Punta Chueca basin suggests this extension began ca. 7 Ma, and thus likely occurred over ~0.6 Ma. This earlier extension is assumed to have occurred on the Punta Chueca fault because restoration of cross section 'A' requires the Tordillo and Eco faults to be a set of later stage faults, rooting into a deeper inferred detachment fault (Fig. 16). Total extension since 12.5 Ma is estimated at 75%. This estimate accounts for extension

on the Punta Chueca, Tordillo, and Eco faults and two minor imbricate structures discussed above.

Generally, patterns emerge from *Tcu* clast count data (Dorsey et al., 2008) that support a depositional model where local sources, which reflect nearby lithologic units, were actively being tilted and exposed due to extensional faulting (Fig. 10). Specific examples supporting this depositional model include: (1) *Kgr*, *Pzms*, *Pzcb*, and *Pzig* clasts decrease to the south where these units are not present, and (2) *Ta2* clasts increase to the south where the thickest sections of andesite are present. This depositional model suggests that small-scale (~2 km wide) extensional basins focused axial flow within relatively small (~10 - 20 km^2), disconnected, tectonically-controlled drainage basins with local sources. No evidence suggests far-traveled exotic clast compositions that would support larger-scale, connected extensional basins.

In summary, extension directions determined from the structure and paleomagnetism of coastal Sonora basins reveal a consistent WSW direction of extension across the study area as blocks were rotated. These basins were actively extending from ~7 to 6 Ma and accommodated a total of 10.4 km of dip-slip displacement along discrete normal faults that caused 4.5 km and 75% of extension across the northern part of the study area since 12.5 Ma, and likely during the period from 7 - 6 Ma. Approximately half of this displacement occurred on the Punta Chueca fault, which appears to have been an active structure throughout the extensional history of the study area, likely accommodating extensional strain at moderate to low angles prior to becoming inactive. These estimates of percent extension are approximately double the estimate of 36% made by Oskin (2002) along an almost identical transect. However, this previous transect included one more extensional basin towards the northwest, beyond the study area. Additionally, these estimates of percent extension along

cross section 'A' fall within the range of theoretical estimates of extension along listric faults with the observed hanging wall cutoff angles (Wernicke and Burchfiel, 1982).

The Punta Chueca fault may represent one example of a major, low-angle, moderate-offset, detachment fault that facilitated strain localization along the nascent margins of the northern Gulf of California. Structural and paleomagnetic data from the study area suggest that the Punta Chueca fault was an active WSW-extending structure by 7 Ma and likely rotated clockwise and evolved into a NW-directed low-angle structure by ca. 6 Ma. The Punta Chueca fault may be an earlier example of the large-magnitude extension proposed to have opened the Upper Tiburón basin (González-Fernández et al., 2005) shortly after 6.1 Ma (Oskin et al., 2001; Oskin and Stock, 2003a).

Dextral Faulting in Coastal Sonora

Evidence for dextral and conjugate sinistral faulting is observed throughout all pre-Quaternary map units and is associated with dextral shear across the Kino-Chueca Shear Zone. Extensional basins in the central and southern study area are cut by sub-vertical NW-striking dextral faults, conjugate NNE-striking sinistral faults, and high-angle N-striking normal faults (Plate 1, Fig. 6). Generally, NW-striking dextral structures display larger displacements than their conjugate NNE-striking sinistral counterparts. Additional evidence for dextral deformation includes clockwise vertical-axis rotations of fault blocks determined from the paleomagnetic results of this study (Fig. 15, Table 2), and originally NNW-striking normal faults that have been rotated to a present-day N to NE strike (Fig. 17).

Timing of Dextral Faulting

Stratigraphic and Structural Constraints

Displacement of multiple geochronologically constrained stratigraphic features constrain the timing of the earliest activity on these strike-slip fault systems, including:

(1) The base of the syn-extensional basins (*Tcl*, *Tmc*, or *Tcu* on 11.5 Ma or older rocks) displays both dextral and sinistral offsets. This feature is a time-transgressive angular unconformity that grades laterally into a disconformity, with an estimated age range of 7 to 6 Ma from stratigraphic constraints. No direct evidence exists for active dextral faulting during deposition of the ~11.5 Ma packages of rocks that overlie the Tuff of San Felipe, therefore, a very conservative maximum age of 11.5 Ma is assigned to earliest dextral faulting in the central study area. However, the minor clockwise block rotation (10°) of the Luna block and the observation that the majority of (if not all) dextral bedrock displacement post-dates the deposition of the 6.4 Ma Tuffs of Mesa Cuadrada, both indicate that any pre-6.4 Ma dextral motion was minor and likely occurred immediately prior to 6.4 Ma, rather than immediately following 11.5 Ma.

(2) Where the Luna and Eco blocks are juxtaposed in the central study area, 1.25 km apparent dextral offsets are measured on both the base of group two (*Taun*) and base of group four (*Tcu*) rocks across the eastern branch of the fault (Plate 1). Assuming little or no vertical displacement along this vertical strike-slip structure, these identical magnitude offsets of group two and group four rocks suggest that earliest strike-slip faulting here post-dates the age of the base of *Tcu* (6.4 Ma).

(3) In the Eco fault block, dextral faults consistently truncate and offset N-striking normal faults (Plate 1). These normal faults cut post-6.4 Ma conglomerates, and are therefore

constrained as post-6.4 Ma structures. Thus, these strike-slip faults must also post-date 6.4 Ma.

Paleomagnetic Constraints

Clockwise vertical-axis rotations of fault blocks are evidence for distributed dextral deformation (e.g. Lewis and Stock, 1998). In coastal Sonora, paleomagnetic results indicate that many fault blocks have undergone clockwise rotations (Fig. 15, Table 2) in response to the NW-directed oblique divergence between the Pacific and North America plates.

A paleomagnetic drilling campaign was designed to not only quantify block rotations due to dextral faulting, but to also attempt to determine the timing of earliest dextral faulting. Towards this goal, paleomagnetic sites were chosen within fault blocks where both the 12.5 Ma Tuff of San Felipe and the 6.4 Ma Tuffs of Mesa Cuadrada were exposed (Fig. 17, Plate 1). Rotation values for these tuffs could then be compared for an individual fault block. If rotations from both tuffs were similar, rotation and dextral deformation of that fault block is assumed to post-date the younger tuff. Alternatively, if the older tuff displayed larger amounts of rotation relative to the younger tuff, rotation and dextral deformation is assumed to have initiated prior to deposition of the younger tuff. A cartoon representation of these hypothesized results and their interpretations are summarized in Figure 18A.

At the Punta Chueca (PC) paleomagnetic site in the Punta Chueca block, *Ttmc* (this study, Fig. 13D) and *Ttsf* (Oskin et al., 2001) display clockwise vertical-axis rotations of 46.1° ± 11.7° and 52.8° ± 2.1°, respectively. Because these values are indistinguishable within error, these correlated paleomagnetic sites are interpreted to be evidence that earliest distributed dextral deformation of the Punta Chueca block began after the deposition of the 6.4 Ma Tuffs of Mesa Cuadrada (Fig. 18B). However, up to ~20° of this rotation could have

occurred prior to 6.4 Ma. At the La Luna (LL) paleomagnetic site in the Luna block, *Ttmc* (Fig. 13G) and *Ttsf* (Fig. 13H) display clockwise vertical-axis rotations of -15.5° ± 11.8° and 9.9° ± 1.9°, respectively. *Ttmc* at LL is interpreted as rotated slightly counter-clockwise, and *Ttsf* at is interpreted as rotated moderately clockwise. These values and their error ranges do not overlap (Fig. 18C), which is evidence for minor clockwise rotation of the Luna block that pre-dates the eruption of the 6.4 Ma Tuffs of Mesa Cuadrada. At the Guadalupe Shrine (GS) paleomagnetic site in the Guadalupe block, *Ttsf* (Fig. 13J) displays a clockwise vertical-axis rotation of 0.8° ± 8.0°, while a reliable rotation estimate could not be determined for *Ttmc* (Fig. 13I, Table 2). Also in the Guadalupe block, at the East Guadalupe (EG) paleomagnetic site, no magnetic vector direction was determined for *Ttmc* (Fig. 13E), while *Ttsf* displays a clockwise vertical-axis rotation of -1.0° ± 7.7° (Fig. 13F). The results from both the GS and EG paleomagnetic sites suggest the Guadalupe block is not rotated. At the Bahía de Kino (BK) paleomagnetic site in the Cerro Kino block, *Ttsf* displays a clockwise vertical-axis rotation of 35.5° ± 3.3° (Oskin et al., 2001). This value is updated to the new reference site and also reflects a 4.6° correction (clockwise) made to the published rotation value. Because *Ttmc* is not exposed in Cerro Kino fault block, dextral deformation of the Cerro Kino can only be constrained to post-date 12.5 Ma, although it is likely that this dextral deformation began sometime between ca. 7 and 6 Ma, similar to remainder of the study area.

The relatively smaller fault blocks immediately adjacent to where the Bahía Kino fault branches interact with multiple normal faults display little to no clockwise vertical-axis rotation (0 - 10°). In contrast, fault blocks where this complex fault interaction in not present (e.g. Cerro Kino block) or where the Bahía Kino fault is not present (e.g. Punta Chueca block) display higher rotation values (≥35°). These small rotation values of small fault blocks may be the result of a local region of constriction adjacent to a zone of complex dextral and

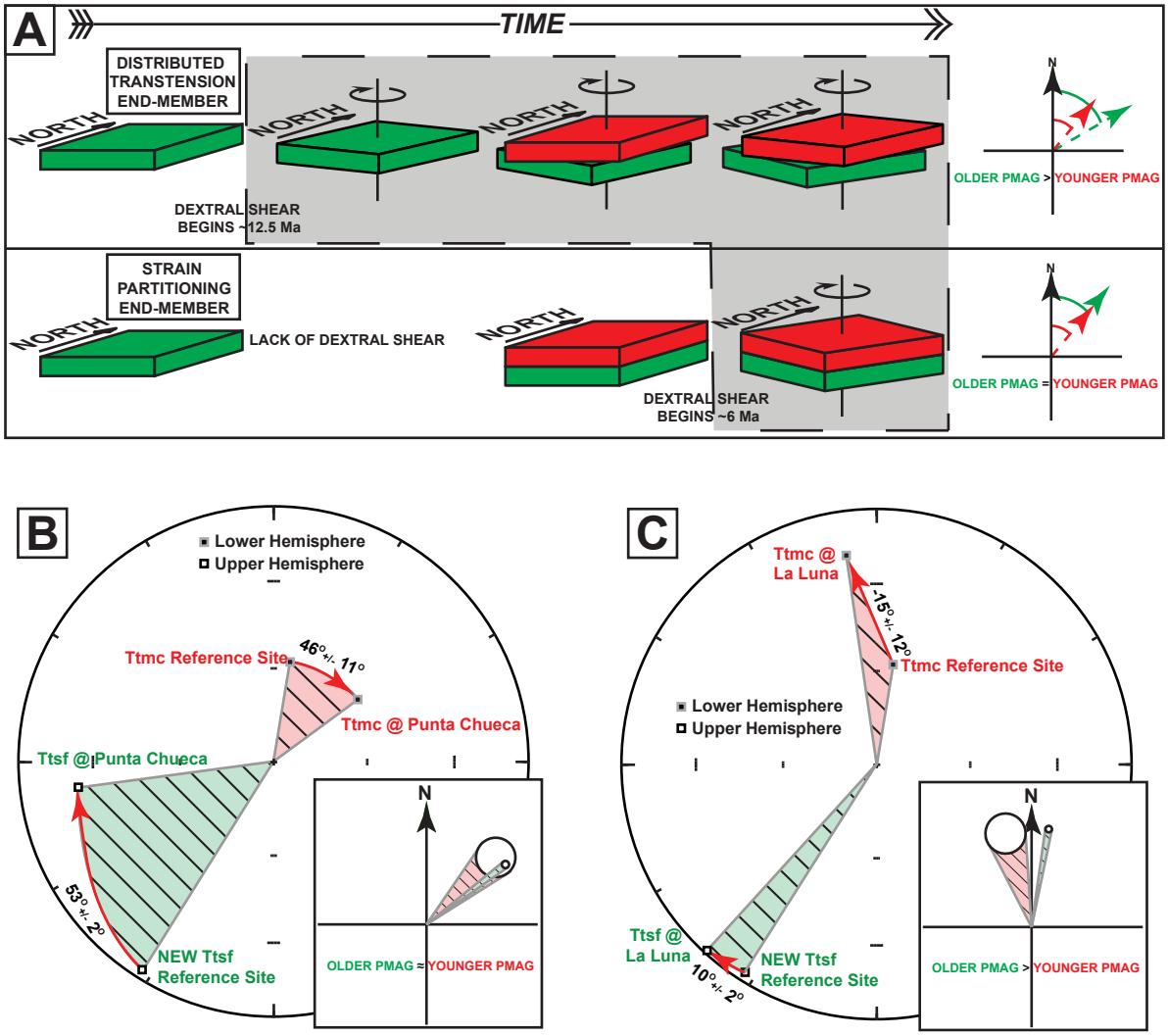

Figure 18. (A) Cartoon of expected paleomagnetic results for two tuff deposits erupted at the beginning and the end of proto-Gulf time. The 'Distributed Transtension' model predicts greater rotation of older tuff deposits due to proto-Gulf dextral shearing. The 'Strain Partitioning' model predicts similar rotation values for these deposits. (B) Results from Punta Chueca (PC) paleomagnetic drill sites, where both the 12.5 Ma Tuff of San Felipe (*Ttsf*) and the 6.4 Ma Tuffs of Mesa Cuadrada (*Ttmc*) were sampled. At PC, both tuffs display similar magnitudes of clockwise vertical-axis rotation (within error) within the same fault block (inset). These results suggest that rotation in the Punta Chueca block due to dextral shearing likely post-dates the eruption of the 6.4 Ma Tuffs of Mesa Cuadrada. (C) Results from La Luna (LL) paleomagnetic drill sites, where both tuffs were again sampled. At LL, *Ttsf* displays ~10˚ of clockwise rotation, while *Ttmc* is essentially not rotated. Even when rotation errors (white error ellipses on inset) are considered, these tuffs in the Luna fault block do not display similar rotations. These results suggest that minor rotations due to dextral shearing may pre-date the eruption of the 6.4 Ma Tuffs of Mesa Cuadrada. The significant flattening of the measured paleomagnetic vector for *Ttmc* at LL (F=38˚) remains unresolved. However, the paleomagnetic samples from the *Ttmc* reference site at Mesa Cuadrada in Baja California may have also undergone minor rotation, similar to the *Ttsf* samples at Mesa Cuadrada. If this is the case, and the *Ttmc* reference site requires ~6˚ of correction, *Ttmc* at LL may only be rotated -9˚ ± 12˚. This would reduce the difference between *Ttsf* and *Ttmc* rotation values (including their errors) from ~12˚ to ~6˚. A correction of this magnitude for the *Ttmc* reference site would only strengthen the similarity of paired paleomagnetic sites (PC) in the Punta Chueca fault block. Further explorations for a new *Ttmc* paleomagnetic reference site in central Baja California, but beyond the limits of the Gulf Extensional Province, should be pursued to resolve this.

normal fault interactions, allowing blocks to translate while preventing large amounts of rotation.

The results from the paired paleomagnetic drill sites from the Punta Chueca block and from the paired sites of the Luna block are inconsistent and suggest that earliest dextral shear accommodated by fault block rotation was not coincident across the study area. In the Punta Chueca block dextral shearing commenced following the 6.4 Ma eruption of *Ttmc*, while in Luna block, shearing and ~10º of clockwise rotation appears to have occurred after 12.5 Ma and ceased prior to 6.4 Ma. These results suggest that dextral shear may have been coeval with, rather than post-dating, orthogonal extension, and these transtensional stresses created the rift-related Punta Chueca, Eco, and Kino basins.

With a new paleomagnetic reference site for the Tuff of San Felipe, all published rotation values from this ignimbrite and their resulting interpretations require an update. Therefore, all published rotations from paleomagnetic site on both sides of the northern Gulf of California, including the Midriff Islands, are recalculated and summarized in Figure 15 and Table 3. Specifically, interpretations from paleomagnetic results of the Tuff of San Felipe from northeastern Baja California require an update. These interpretations by Lewis and Stock (1998) estimated 23 km of shear and 7 km of extension in the direction of relative plate motion (315°) in the rotated region between the dextral Valle de San Felipe fault and a postulated, parallel offshore dextral fault. When the calculations of Lewis & Stock (1998) are reproduced using the new rotation values, 27 km of NNW-directed dextral shear and 7 km of ENE-directed extension is calculated to have occurred in the Sierra San Fermin, Baja California. This result increases the amount of distributed dextral shear via block rotation in northeastern Baja California by 4 km. Lewis and Stock (1998) determined that a statistically

insignificant amount of block rotation occurred from 12.5 - 6 Ma, and thus these updated values of shear and extension probably occurred largely during modern-Gulf time.

In summary, dextral faulting predominantly post-dates deposition of the 6.4 Ma *Ttmc* and a significant portion, if not all, of the overlying latest Miocene basin conglomerates (*Tcu*). Paleomagnetic evidence is also consistent with dextral shear via clockwise vertical-axis rotation post-6.4 Ma in the northern study area, although up to 20° of this 53° rotation could pre-date 6.4 Ma within uncertainty. In the central study area, minor amounts of dextral deformation must pre-date 6.4 Ma, based on the greater clockwise rotation of *Ttsf* versus *Ttmc*.

Direction of Dextral Faulting

Map pattern of dextral faults (Fig. 6, Plate 1) demonstrate the direction of dextral faulting related to Gulf opening. The general trends of dextral faults across the study area, including the large-scale Bahía Kino fault, are towards the northwest (azimuth 315° to 320°). These trends coincide well with azimuths measured from modern-Gulf dextral structures within the active rift basins (Fenby and Gastil, 1991), and also with, and are likely extensions of, offshore faults (e.g. De Mar fault) that are known to have been a component of Gulf opening (Fig. 4; Aragón-Arreola and Martín-Barajas, 2007).

Magnitude of Dextral Faulting

Magnitudes of dextral faulting are calculated from map-view restorations of geologic structures (Plate 1). Across the Kino-Chueca Shear Zone, dextral faulting occurred on discrete dextral faults amongst a distributed zone of dextral shear that involved clockwise vertical-axis block rotations.

Multiple strike-slip faults display evidence for dextral bedrock displacements. Dextral displacement across both branches of the Bahía Kino fault is at least 5.8 km, based on restoration of units between the Cerro Kino and Granito blocks. Temporal slip alternation between dextral and normal fault systems appears to add additional slip to the western branch of the Bahía Kino fault. Restoration of this extension (Fig. 19) to realign the northern end of the San Miguel-Cabra block with the southern end of the Granito block adds 2.2 km of additional dextral displacement. Therefore, the total slip estimate for the Bahía Kino fault zone is 7.0 km. Slip along the Bahía Kino fault likely diminishes to zero at its northwestern end where it intersects the Punta Chueca fault (Plate 1). Predictions from map view block restorations suggest that total displacement along the Puerto Rico fault may be up to 2.8 km. Therefore, between the Sacrificio and Infernillo faults (i.e. within the Kino-Chueca Shear Zone), 9.8 km of total discrete displacement is estimated.

In addition to dextral faulting within the Kino-Chueca Shear Zone, evidence also exists for dextral faulting along the faults that bound this shear zone. Total dextral displacement along the Infernillo fault is estimated at 20 ± 10 km, and is less than a few tens of kilometers for the Sacrificio fault (Oskin and Stock, 2003a).

In summary, dextral deformation across the Kino-Chueca Shear zone consists of both discrete dextral displacements and distributed dextral deformation via block rotation. From the study area, total maximum dextral displacement along faults within the Kino-Chueca Shear Zone is estimated to be 9.8 km.

A Transtensional Model for the Kino-Chueca Shear Zone

Field observations and geochronology suggest that transtensional strain within the study area associated with activity across the Kino-Chueca Shear Zone initiated ca. 7 Ma.

Because stratigraphic and structural constraints suggest that the Bahía Kino fault became active after 6.4 Ma, strain likely evolved from extension-dominated transtension ca. 7 Ma, to shear-dominated transtension sometime after 6.4 Ma. That basin sedimentation appears to have ceased ca. 6 Ma further supports this transition from extension-dominated transtension to shear-dominated transtension, as basin-subsidence caused by extension gave way to crustal deformation in the form of strike-slip faults.

The much higher relative amount of clockwise rotation determined from paleomagnetism distinguishes the Punta Chueca block in the northern part of the study area from the remaining fault blocks to the south. This high rotation of the Punta Chueca block was likely caused due to the distributed dextral deformation between the Sacrificio and Infernillo faults, and the lack of intervening discrete dextral faults that would accommodate focused dextral shear. In contrast, in the central and southern portions of the study area, the Bahía Kino fault is a significant structure to accommodate dextral shear, therefore, reducing the need to distribute dextral deformation across these faults blocks in the form of clockwise vertical-axis block rotation. As a result, fault blocks in the central and southern area are rotated by smaller amounts.

Thus, a tectonic model of the gradual evolution of partitioned strain may be envisioned for the Kino-Chueca Shear Zone. In this model (Fig. 19), the NW-striking Sacrificio and Infernillo faults serve as the boundaries of an intervening zone of both discrete and distributed dextral deformation. For the duration of this model, the orientation and location of the Sacrificio fault remains fixed. Additionally, the location of the eastern rotational pivot point of the Rancho Nuevo fault block also remains fixed. The amounts and timing of extension determined from palinspastic reconstructions along the line of cross section ‘A’ (Fig. 16) constrain the separations of the Rancho Nuevo, Eco, Tordillo, and Punta

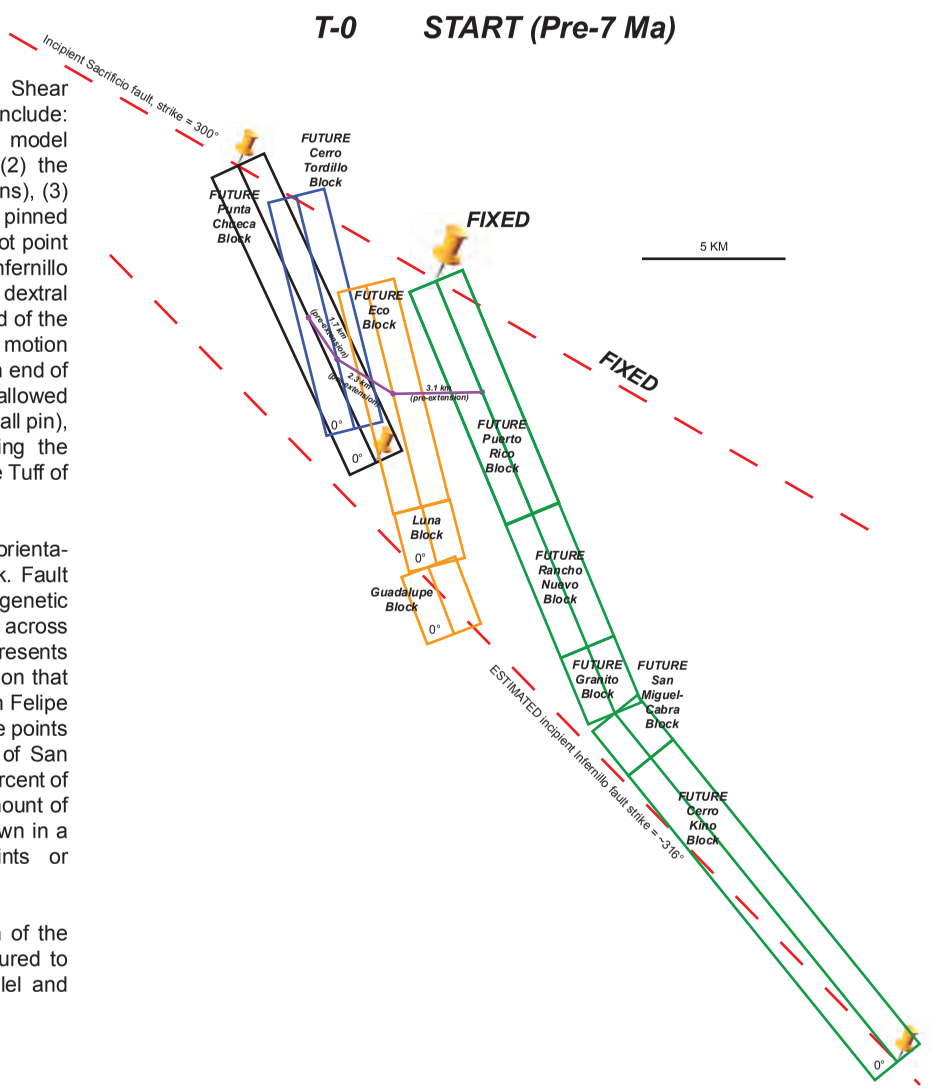

Figure 19. (A) Transtensional model for the Kino-Chueca Shear Zone of coastal Sonora. Model parameters at initial step (T-0) include: (1) the NW-trending Sacrificio and Infernillo faults are the model boundaries of a zone of distributed dextral transtension, (2) the location and orientation of the Sacrificio fault is fixed (large pins), (3) the pivot point at the northern end of the Puerto Rico block is pinned to a fixed location on the Sacrificio fault (large pin), (4) the pivot point at the southern end of the Cerro Kino block is pinned to the Infernillo fault, but allowed to move with the fault in response to dextral transtension (small pin), (5) the pivot point at the southern end of the Punta Chueca is not pinned to a fault in this model, however its motion is tracked through the model, (6) the pivot point at the northern end of the Punta Chueca block is pinned to the Sacrificio fault, but is allowed to move along the fault in response to dextral transtension (small pin), (7) orientations of fault blocks are constrained by removing the documented clockwise rotations from the average strike of the Tuff of San Felipe in each fault block (Fig. 18).

The center-line of each rectangle represents the location and orientation of the Tuff of San Felipe strike ridge for each fault block. Fault blocks are color-coded in all model steps by their common genetic relation formed by initial tilting and segmentation of blocks across multiple normal faults. In all model steps, the purple line represents the location of cross section 'A', and the small purple circles on that line represent the location of the intersection of the Tuff of San Felipe strike ridge with the line of section. Initial spacing (T-0) of these points were measured from pre-extension bed lengths of the Tuff of San Felipe determined from the restored cross section (Fig. 17). Percent of total extension on each segment is shown. The estimated amount of clockwise block rotation complete by each model step is shown in a southern corner of blocks with paleomagnetic constraints or estimates. See text for discussion of paleomagnetic results.

As the documented deformation is forward modeled, motion of the moveable pinned locations are tracked and ultimately measured to determine estimates of shear and extension resolved parallel and perpendicular to published plate motion vectors.

Figure continues on next few pages.

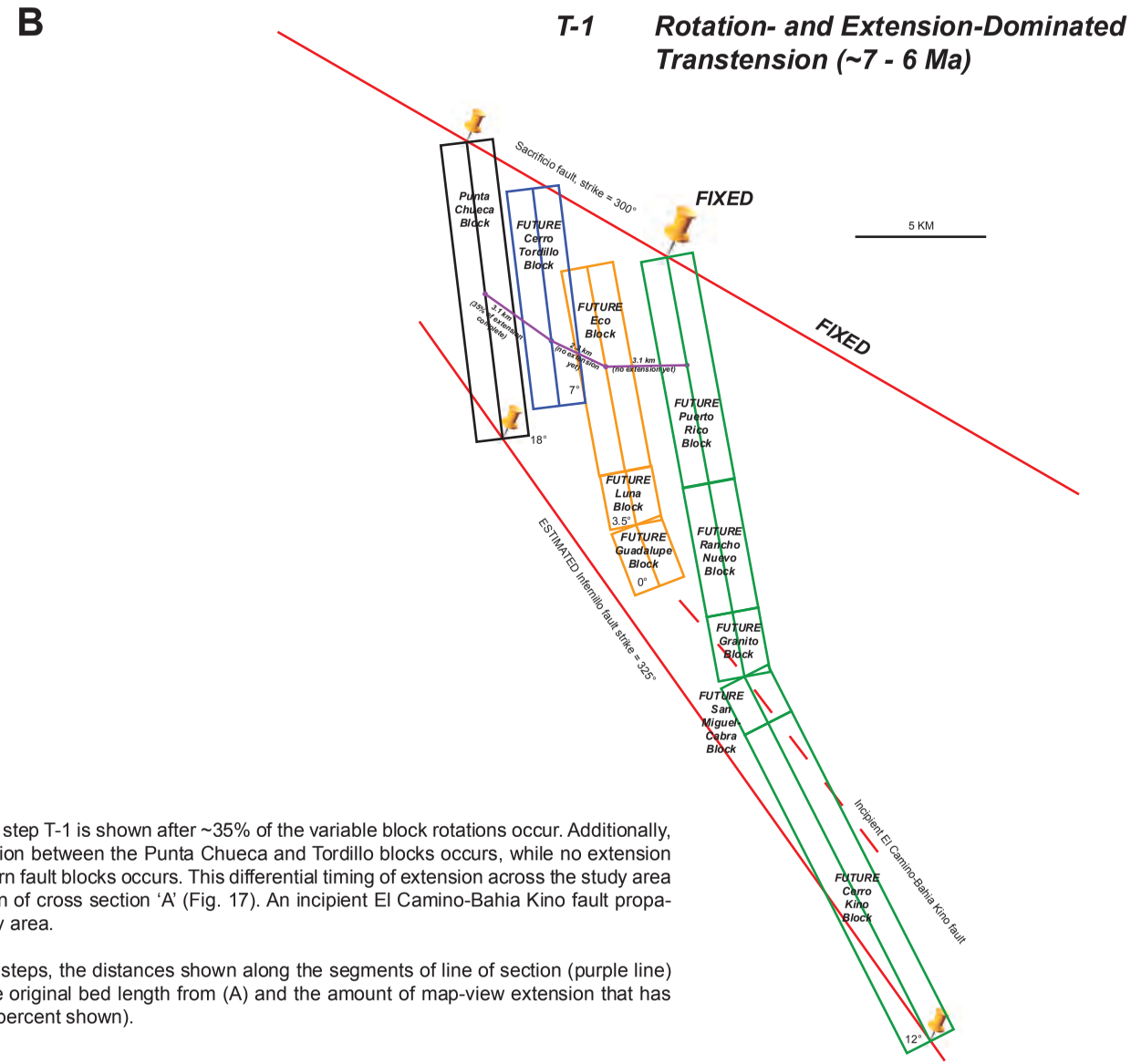

Figure 19. (cont.) (B) Model step T-1 is shown after ~35% of the variable block rotations occur. Additionally, ~35% of the observed extension between the Punta Chueca and Tordillo blocks occurs, while no extension between the remaining northern fault blocks occurs. This differential timing of extension across the study area is demonstrated by restoration of cross section 'A' (Fig. 17). An incipient El Camino-Bahia Kino fault propagates northward into the study area.

For T-1 and remaining model steps, the distances shown along the segments of line of section (purple line) represent the sum of both the original bed length from (A) and the amount of map-view extension that has occurred by that model step (percent shown).

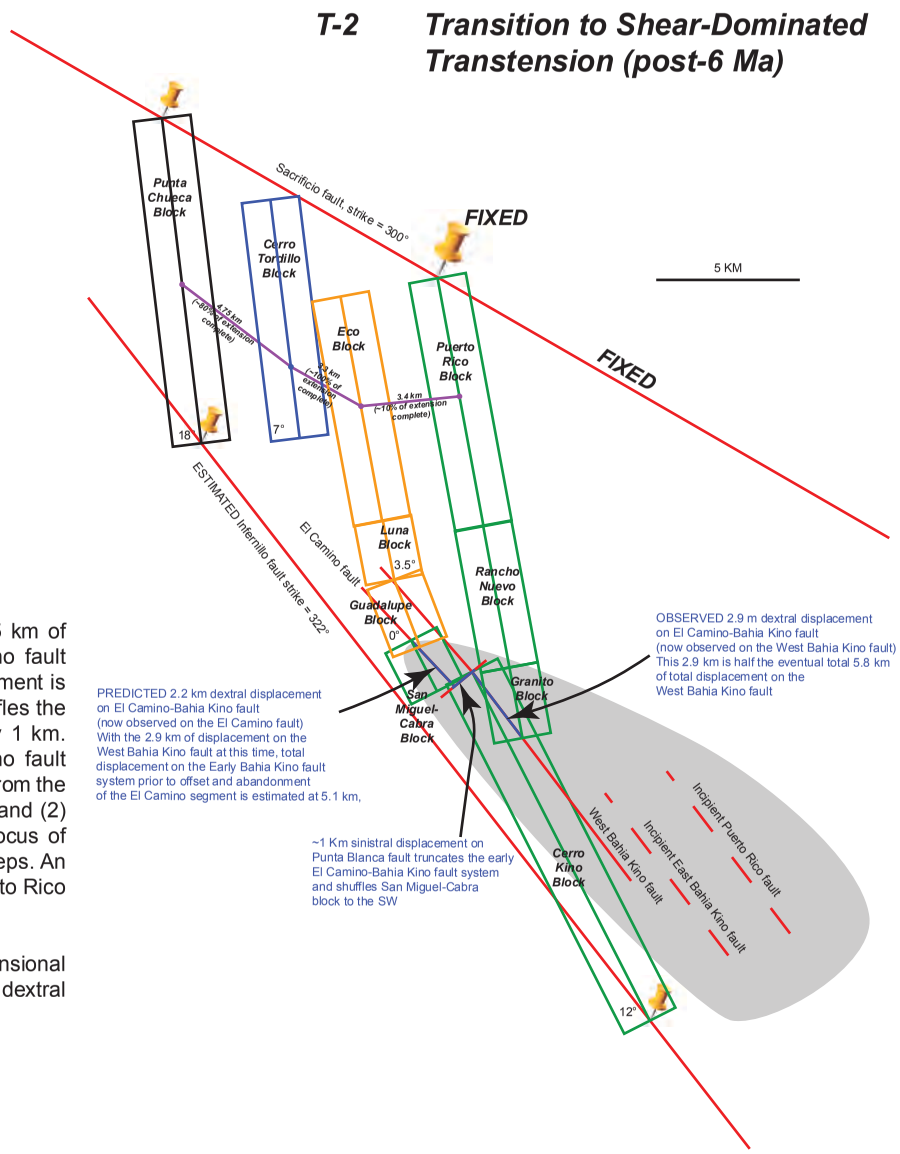

Figure 19. (cont.) (C) Model step T-2 is shown after ~5 km of discrete dextral offsets occur on the El Camino-Bahia Kino fault system. This fault system and the observed dextral displacement is truncated by the Punta Blanca fault, a sinistral fault that shuffles the San Miguel-Cabra block to the southwest by approximately 1 km. This sinistral displacement splits the El Camino-Bahia Kino fault system into (1) the El Camino fault, which is translated away from the locus of strain and accommodates no further displacement, and (2) the Western branch of the Bahia Kino fault, which is the locus of strain and remains active throughout the remaining model steps. An incipient Eastern branch of the Bahia Kino fault and the Puerto Rico fault propagate north into the study area.

Gray area represents encroaching area where transtensional deformation is accommodated increasingly by discrete dextral displacement along strike slip faults.

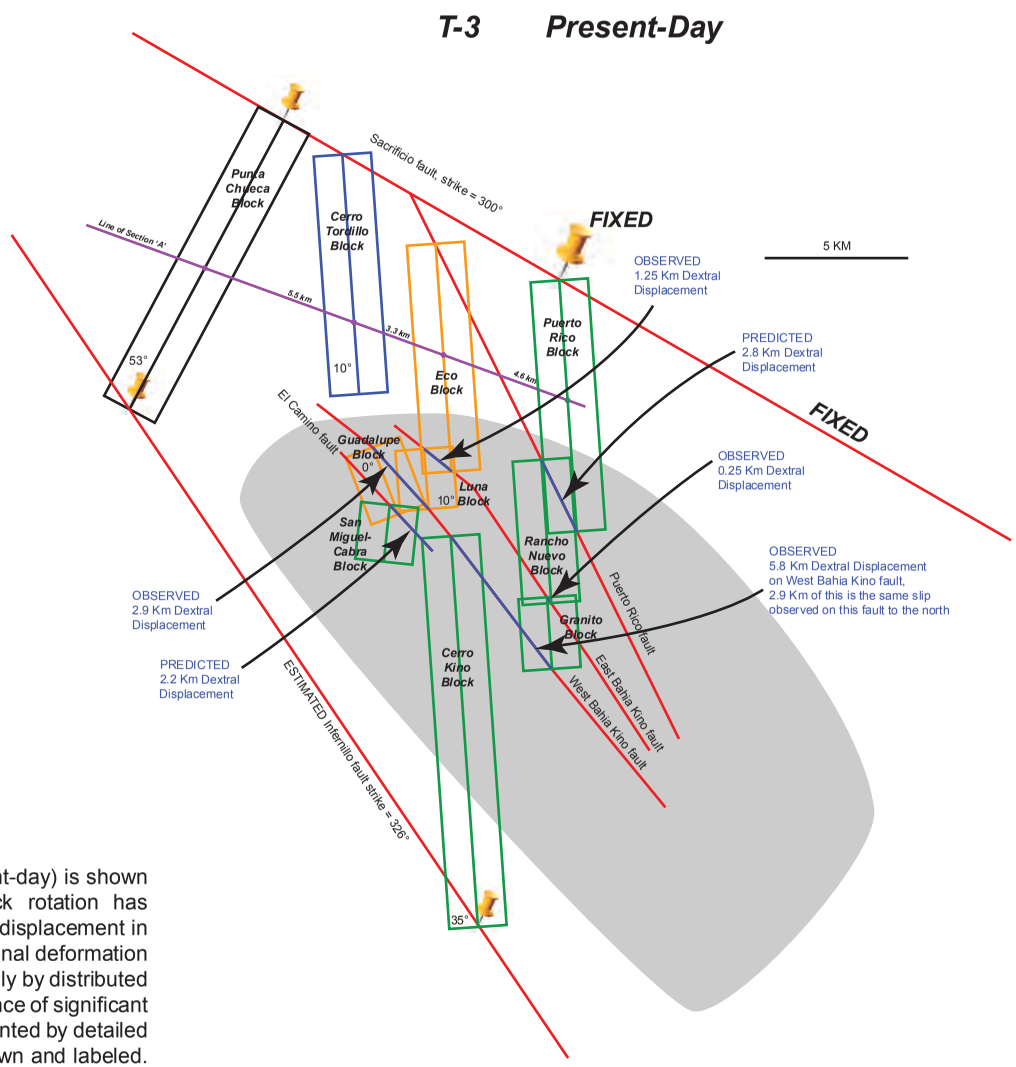

Figure 19. (cont.) (D) Model step T-3 (present-day) is shown after ~65% of the remaining clockwise block rotation has occurred, coeval with a zone of discrete dextral displacement in the southern and central study area. Transtensional deformation in the northern study area is accommodated solely by distributed clockwise vertical-axis block rotation in the absence of significant strike-slip faulting. Dextral displacement documented by detailed mapping and predicted from this model are shown and labeled. Area of encroaching deformation via strike-slip faulting (gray) has propagated further north in to the study area.

Figure 19. (cont.)

(E) Estimates of transtension from comparison of model steps T-0 (initial) and T-3 (present-day) across the Kino-Chueca Shear Zone. These estimates are made in a reference frame parallel to the published PAC-NAM plate motion direction (317°). From this model, the amount and direction of transtension varies across the study area (from NW to SE) due to the non-parallel nature of the faults that bound the shear zone. The net motion across the study area is towards the west-northwest. Estimates are 13.1 km @ 278° in the northern study area, and 15.7 km @ 294° in the southern study area. This model requires 3.1 km of extension between the Punta Chueca and Puerto Rico blocks, in a direction parallel to the Sacrificio fault.

Motion on the southernmost observable end of the Cerro Kino block (where it dives into the ocean) is a good representation of the magnitude and direction of transtensional strain within the study area. The 15.7 km @ 294° vector obtained from this location is further decomposed into 14.5 km of shear strain parallel to the relative PAC-NAM plate motion direction (317°) and 6.0 km of extensional strain perpendicular to this direction. This deformation occurred during a ~1 Myr period, from ~7 to 6 Ma.

(F) Inset shows relation of the deformation from the study area (15.7 km @ azimuth 294°) to the Pacific-North America plate motion since the inception of the Gulf of California rift ca. 11 Ma. If additional proto-Gulf deformation in coastal Sonora is assumed to be transtensional and oriented at a similar orientation (~294°), the amounts and directions of this unaccounted deformation can be estimated at ~105 km. With this assumption, total proto-Gulf offset on the Tosco-Abreojos fault is predicted at ~225 km.

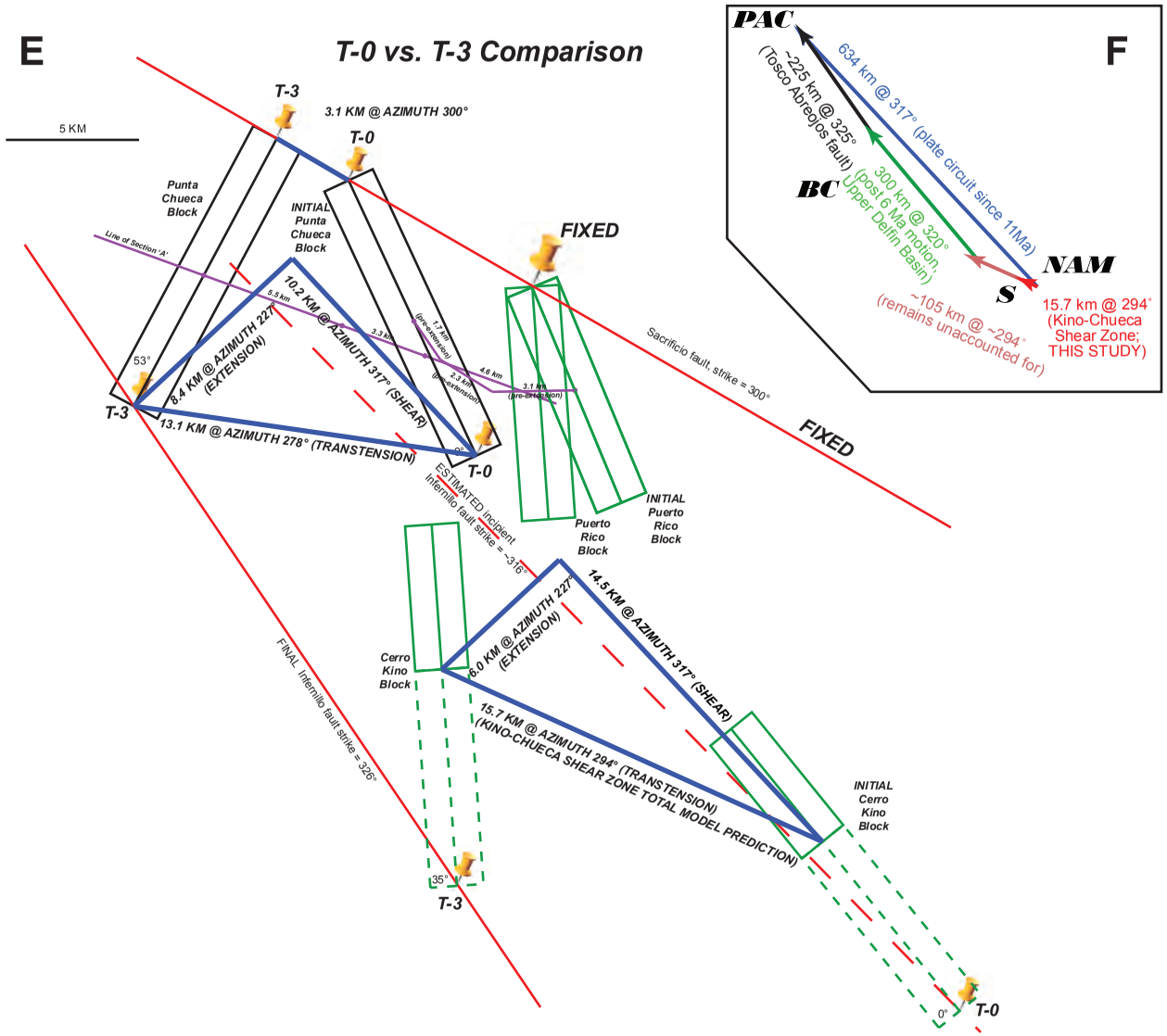

Chueca blocks. Initial block orientations are predicted from correcting the average structural strike of present-day fault blocks by the amount determined from the paleomagnetic results of this study (Fig. 18), and their sizes are approximated by projecting mapped exposures of strike ridges within these fault blocks to the model-bounding faults.

This model predicts rotation of four initial fault blocks (Fig. 19A). Each fault block consists of up to five smaller blocks defined by the present-day geology. The center lines of these blocks at the initial model step (T-0) represent the former locations of strike ridges of the Tuff of San Felipe, which are well documented (Plate 1). At T-0, these strike ridges are assumed to not yet be tilted, therefore, these blocks of horizontal tuff deposits are spaced out by their pre-extension bed lengths calculated from cross section 'A'.

Due to the larger (i.e. longer strike direction length) of the southern fault blocks at T-0, ~35% of the total clockwise block rotations operate to rotate the Infernillo fault clockwise, to a more northerly structural strike in model step T-1 (Fig. 19B). Thus the original sub-parallel relationship of the Sacrificio and Infernillo faults is not preserved. WSW-directed extension with a minor component of dextral deformation dominates the initial rotational deformation of these fault blocks (Fig. 19B). At T-1, an incipient El Camino-Bahía Kino fault propagates northward, approximately at the former location of the Infernillo fault. This northward propagation of the incipient Bahía Kino fault system introduces a change in the style that dextral deformation is accommodated between the model-bounding faults. As the Bahía Kino fault propagates northward in model step T-2, areas that previously accommodated dextral deformation entirely in the form of clockwise block rotation, instead accommodate some of this deformation along discrete strike-slip structures (Fig. 19C). Also at T-2, the incipient East Bahía Kino and Puerto Rico dextral faults begin to propagate into the study area from the south. Generally, as rotation continues (Fig. 19 C,D), the extensional

component is progressively reduced as the dextral component increases. Thus, with time, extensional basins that formed between fault blocks are subsequently rotated, and eventually, some are cut by newly-formed strike-slip faults. In the final model step (T-3), the majority of dextral deformation occurs along discrete dextral faults in the southern and central study area, while in the northern study area this dextral deformation continues to be accommodated entirely via clockwise rotation of the Punta Chueca block and continued slip on the low-angle Punta Chueca fault (Fig. 19D, Fig. 16).

The model presented here predicts amounts of total shear and extension that vary slightly across the study area (Fig. 19E). These differences are a result of the dissimilar incipient fault block sizes and non-parallel model-bounding faults. At the end of the model, transtensional deformation is resolved into a shear component parallel to and an orthogonal extensional component perpendicular to 317°, the approximate PAC-NAM vector (Stock, 2007). In the northern study area, the model predicts 8.4 km of extension towards azimuth 227° and 10.2 km of shear towards azimuth 317°, together yielding 13.1 km of transtension towards azimuth 278° (Fig. 19E). In the southern study area, the model predicts 6.0 km of extension towards azimuth 227° and 14.5 km of shear towards azimuth 317°, together yielding 15.7 km of transtension towards azimuth 294°. These estimates are for the zone bound between the Sacrificio and Infernillo faults and do not account for discrete dextral deformation along these model-bounding structures.

The orientations of large-scale strike-slip structures within the study area (315-320°) agree well with PAC-NAM relative plate motion vectors (317°; Stock, 2007), however, the strain direction for the Kino-Chueca Shear Zone is towards 294°. This WSW direction indicates that, although this coastal Sonoran belt deformed in a transtensional style, only a

component of this deformation directly contributed to the overall 317°-directed PAC-NAM relative plate motion vector.

During proto-Gulf time, as much as 300 km of 310°-directed PAC-NAM relative plate motion is unaccounted for, distributed somewhere across the GEP (Fig. 3). Approximately 14.5 km of shear across the Kino-Chueca Shear Zone accounts for a portion of this missing proto-Gulf shear (Fig. 19E). Offset on the Sacrificio and Infernillo faults likely account for additional components of proto-Gulf shear. Proto-Gulf-age offsets across the Infernillo fault are limited to 20 ± 10 km from matching exposures of tuffs on Isla Tiburón. Slip on the Sacrificio fault is less well constrained. After restoration of the post-6.1 Ma opening of the Upper Delfín basin ('T' on Figure 1; Oskin et al., 2001; Oskin and Stock, 2003a), realignment of exposures of the pre-15 Ma fusulinid-clast bearing conglomerate ('F' on Figure 1; Bryant, 1986; Gastil and Krummenacher, 1977b) supports anywhere from zero to perhaps up to 100 km of additional strike-slip on the Sacrificio fault. Because little or no evidence exists for significant deformation prior to 12.5 Ma, what additional offset occurred on the Sacrificio fault most likely accrued entirely during proto-Gulf time. Thus it is possible that anywhere from 25-155 km of proto-Gulf shear may have occurred in coastal Sonora, together across the Sacrificio fault, Kino-Chueca Shear Zone, and the Infernillo fault. The upper estimate of 155 km would require approximately 3 Myr of plate motion. However, only 1 Myr of activity is recorded in the Kino-Chueca Shear Zone, which is more consistent with a shorter life span and less slip on the adjacent Sacrificio fault.

Implications for Continental Rupture Mechanisms

Data from well-dated stratigraphy, detailed structural mapping, and paleomagnetic analysis of isotopically-dated regional ignimbrites reveal that transtension was initiated

within the Kino-Chueca Shear Zone during latest proto-Gulf time, approximately 1 Myr prior to lithospheric rupture of the northern Gulf of California. Throughout this period, transtension appears to have evolved from extension-dominated to shear-dominated transtension. Extensional strain rates likely grew within Kino-Chueca Shear Zone in response to initial transtensional rifting and WSW-directed extension. As transtension progressively evolved to a more shear-dominated transtension, the extensional strain rates likely accelerated in response to the amplified presence of transform faulting. By ca. 6 Ma, strike-slip faults were well developed and embedded within a zone of rotating extensional fault systems. These results are consistent with a scenario in which elevated extensional strain rates may have acted to weaken the lithosphere.

The Kino-Chueca Shear Zone was probably not unique. Similar deformation was likely occurring elsewhere in the northern Gulf of California, acting as coeval zones of transtension just prior to lithospheric rupture. A strong candidate for another late proto-Gulf transtensional shear zone flanking the Kino-Chueca Shear Zone is the La Cruz fault that transects southwestern Isla Tiburón to the west of the study area (Fig. 4). Both of these zones of combined shear and extension probably acted together to accelerate strain rates and allowed for focused extensional strain. Conceivably, following at least 1 Myr of focused transtensional deformational along these shear zones, strain rates reached a level high enough to focus extensional strain at a location somewhere between these shear zones, and rupture of the lithosphere occurred along a N-striking normal fault system just offshore of the western edge of Isla Tiburón (Oskin and Stock, 2003a; González-Fernández et al., 2005) beginning ca. 6.1 Ma (Oskin et al., 2001; Oskin and Stock, 2003a). This zone of narrow rifting and rupture is bound on the northeast by the De Mar fault --the northwestern projection of the Kino-Chueca Shear Zone-- and on the southwest by the La Cruz fault and Tiburón transform

(Fig. 4). These NW-trending shear zones appear to have operated like transform faults, similar to transform faults between oceanic rift segments, and connected the zone of rupture west of Isla Tiburón to other extensional regions further to the north and south. Thus, once extensional strain migrated from within the study area to the western side of Isla Tiburón ca. 6 Ma, activity within the Kino-Chueca Shear Zone likely diminished or became inactive, broadly similar to how oceanic transforms become inactive when they cease to connect active spreading centers.

To place this into the perspective of the Gulf of California kinematic puzzle (Fig. 3), a significant portion of proto-Gulf dextral shear is still unaccounted for (Fig. 19F). The geological constraints from coastal Sonora suggest that transtensional strain occurred in coastal Sonora during latest proto-Gulf time, although the direction of this strain was WNW-directed (Fig. 19E). Therefore, only a small component of proto-Gulf dextral shear parallel to PAC-NAM plate motion (~14.5 km) was located along the eastern margin of the Gulf of California rift at this latitude. An alternative location for proto-Gulf shear may include regions east of the study area now concealed by the modern delta plain of the Rio Sonora. Further examination of the distribution and timing of proto-Gulf basins, possibly from borehole data east of the study area, may shed light on missing proto-Gulf shear. Also, examination of the magnitude of dextral translation of pre-rift deposits (e.g. geographic extent of the Tuff of San Felipe ignimbrite deposit) will also help to determine if significant additional proto-Gulf shear existed within inland Sonora (Oskin and Stock, 2003a).

CONCLUSIONS

This study documents a ~1 Myr period of relatively rapid, focused transtensional deformation in coastal Sonora preceding continental rupture in the Gulf of California. This

result in part addresses the unaccounted for history of the proto-Gulf (~12.5 - 6 Ma) dextral component of the PAC-NAM plate boundary motion. In coastal Sonora, stratigraphic and geochronologic data indicate that extensional basins, floored by the 12.5 Ma Tuff of San Felipe, began to open to the WSW ca. 7 Ma in response to the onset of transtensional deformation. These basins continued to subside and record deposits of the 6.4 Ma Tuffs of Mesa Cuadrada, and display up to 75% extension across the northern part of the study area. A new model for the Kino-Chueca Shear Zone demonstrates that transtension progressively evolved from extension-dominated to shear-dominated over a ~1 Myr interval. The majority of this interval was comprised of distributed dextral deformation via clockwise block rotations up to 53°. Paleomagnetic data from both 6.4 Ma and 12.5 Ma ignimbrites suggest that the majority of this rotation post-dates 6.4 Ma. The end of this interval integrated discrete dextral offset along NW-striking dextral faults in the south (e.g. the Bahía Kino fault), while in the north shear continued via clockwise vertical-axis rotation of fault blocks and slip on the low-angle Punta Chueca fault. Overall this fault accommodated a total of 5 to 6 km of normal slip. A transtensional model for deformation across the Kino-Chueca Shear Zone resolves 15.7 km of transtensional deformation at an azimuth of 294° through a combination of block rotation and faulting. 14.5 km of shear deformation is resolved in the PAC-NAM relative plate motion direction (317°), and occurred over a span of ~1 Myr, from 7 to 6 Ma. This deformation rate, ~1.5 cm/yr, represents a substantial fraction (~28%) of PAC-NAM plate motion during this period.

Focused transtension in the Kino-Chueca Shear Zone from 7 - 6 Ma may represent an acceleration of extensional strain rate in coastal Sonora. Such a co-location of extension and shear at lithospheric scale may have helped to focus deformation on the NW-striking De Mar fault, and possibly elsewhere, such as the La Cruz fault along southwestern Isla Tiburón.

This focused deformation was followed shortly by lithospheric rupture along intervening N-striking extensional structures west of Isla Tiburón ca. 6 Ma. Hence, this study documents an early phase of westward migration of plate boundary strain. The timing for the onset of transtensional deformation in coastal Sonora agrees well with a model of progressive westward migration of plate boundary strain and related depocenters. In this model, ~1.5 cm/yr of plate boundary strain initiated ca. 7 Ma in coastal Sonora and formed the Punta Chueca, Eco, and Kino basins. Subsequently at ca. 6 Ma, strain and related basin formation migrated westward to the Upper Tiburón basin (Oskin et al., 2001), and ultimately migrated to the Upper Delfín basin by 2 to 3 Ma (Fig. 4; Aragón-Arreola and Martín-Barajas, 2007). This westward migration ultimately formed an asymmetric rift geometry in the northern Gulf of California where the active rift axis today is located near the western edge of a ~300 km-wide, mostly submerged extensional province. This is remarkably similar to observations of other, more mature rifted continental margins (Louden and Chian, 1999) and to model predictions of asymmetric continental break-up during rupture (Bassi, 1995; Huismans and Beaumont, 2003).

In summary, results from geologic mapping, geochronology, and paleomagnetism in coastal Sonora, support the hypothesis that incorporation of dextral shear into a broad region of extension may have been the catalyst for lithospheric rupture in the northern Gulf of California, and support the concept of a causal link between rift obliquity and the potential for lithospheric rupture. In the study area dextral shear progressively localized within a zone of transtension. This shear preceded localization of strain in the axis of the Gulf of California by at least 1 Myr, and represents the latest interval of proto-Gulf deformation. It remains uncertain whether earlier proto-Gulf dextral motion occurred east of the study area. If, as according to the 'distributed transtension' model, dextral shear occurred primarily within

Sonora, additional older dextral shear zones are predicted to lie east of the study area. Alternatively, the results of this study are also consistent with a 'progressive localization' model where shear deformation accelerated and focused along transtensional shear zones embedded within the broader Gulf Extensional Province during latest proto-Gulf time.

REFERENCES

Abbott, P.L., and Smith, T.E., 1989, Sonora, Mexico, Source for the Eocene Poway Conglomerate of Southern California: Geology, v. 17, p. 329-332.

Al-Zoubi, A., and ten Brink, U., 2002, Lower crustal flow and the role of shear in basin subsidence: an example from the Dead Sea basin: Earth and Planetary Science Letters, v. 199, p. 67-79.

Allmendinger, R.W., Marrett, R.A., and Cladouhos, T., 2009, FaultKin, version 4.3.5, a Program for Analyzing Fault Slip Data for the Mac.

Anderson, C.A., 1950, Geology of Islands and Neighboring Land Areas, Geological Society of America Memoir 43: 1940 E.W. Scripps Cruise to the Gulf of California: Boulder, CO, Geological Society of America, p. 53.

Anderson, E.M., 1942, The dynamics of faulting and dyke formation with application to Britain: Edinburgh, Oliver and Boyd, 191 p.

Angelier, J., and Mechler, P., 1977, Sur une méthode graphique de recherche des contraintes principales également utilisable en tectonique et en séismologie: la méthode des dièdres droits: Bull. Soc. géol. France, v. 7, p. 1309-1318.

Aragón-Arreola, M., and Martín-Barajas, A., 2007, Westward migration of extension in the northern Gulf of California, Mexico: Geology, v. 35, p. 571-574.

Artemjev, M.E., and Artyushkov, E.V., 1971, Structure and Isostasy of the Baikal Rift and the Mechanism of Rifting: Journal of Geophysical Research, v. 76, p. 1197-1211.

Atwater, T., 1970, Implications of plate tectonics for the Cenozoic evolution of western North America: Geological Society of America Bulletin, v. 81, p. 3513-3536.

Atwater, T., 1989, Plate tectonic history of the northeast Pacific and western North America, *in* Winterer, E.L., Hussong, D.M., and Decker, R.W., eds., The Eastern Pacific Ocean and Hawaii, Volume N: Boulder, Colorado, The Geological Society of America, p. 21-72.

Atwater, T., and Stock, J.M., 1998, Pacific North America plate tectonics of the Neogene southwestern United States: An update: International Geology Review, v. 40, p. 375-402.

Bassi, G., 1995, Relative importance of strain rate and rheology for the mode of continental extension: Geophys. J. Int., v. 122, p. 195-210.

Beal, C.H., 1948, Reconnaissance of the Geology and Oil Possibilities of Baja California, Mexico, Geological Society of America Memoir 31: Baltimore, MD, Geological Society of America, 138 p.

Beck, M.E., 1980, Paleomagnetic record of plate-margin tectonic processes along the western edge of North America: Journal of Geophysical Research, v. 85, p. 7115-7131.

Bennett, S.E.K., and Oskin, M., 2007, Transition From Proto-Gulf Extension to Transtension, Coastal Sonora, Mexico: Eos Transactions American Geophysical Union, v. 88, p. Abstract S31A-10.

Bennett, S.E.K., and Oskin, M.E., 2008, A New High-Precision Paleomagnetic Reference Vector from Mesa El Burro, Mesa Cartabón, and Mesa El Pinole, Baja California for the Tuff of San Felipe, a Miocene Ignimbrite Marker Bed Exposed in Baja California and Sonora, México, AGU Fall Meeting: San Francisco, American Geophysical Union.

Bialas, R.W., Buck, W.R., Studinger, M., and Fitzgerald, P.G., 2007, Plateau collapse model for the Transantarctic Mountains–West Antarctic Rift System: Insights from numerical experiments: Geology, v. 35, p. 687-690.

Block, L., and Royden, L., 1990, Core complex geometries and regional scale flow in the lower crust: Tectonics, v. 9, p. 557-567.

Bott, M.H.P., 1959, The mechanics of oblique slip faulting: Geological Magazine, v. 96, p. 109-117.

Brady, R., Wernicke, B., and Fryxell, J., 2000, Kinematic evolution of a large-offset continental normal fault system, South Virgen Mountains, Nevada: Geological Society of America Bulletin, v. 112, p. 1375-1397.

Bryant, B.A., 1986, Geology of the Sierra Santa Rosa Basin, Baja California, Mexico [Masters thesis]: San Diego, San Diego State University.

Buck, R.W., 1991, Modes of continental extension: Journal of Geophysical Research, v. 96, p. 20161-20178.

Buck, W.R., 1993, Effect of lithospheric thickness on the formation of high- and low-angle normal faults: Geology, v. 21, p. 933-936.

Buck, W.R., Lavier, L.L., Poliakov, A.N.B., Rohr, K., Jackson, J., Chadwick, A., Osmaston, M., Kusznir, N., Brun, J.-P., Roberts, A., and Geli, L., 1999, How to Make a Rift Wide: Philosophical Transactions: Mathematical, Physical and Engineering Sciences, v. 357, p. 671-693.

Butler, R.L., 1992, Paleomagnetism: Cambridge, MA, Blackwell Scientific Publications, 319 p.

Cande, S.C., and Kent, D.V., 1995, Revised calibration of the geomagnetic polarity timescale for the late Cretaceous and Cenozoic: Journal of Geophysical Research, v. 100, p. 6093-6096.

Coleman, D.S., and Walker, J.D., 1994, Modes of Tilting During Extensional Core Complex Development: Science, v. 263, p. 215-218.

deBoer, J.Z., and Clifton, A.E., 1988, Mesozoic tectogenesis. development and deformation of `Newark' rift zones in the Appalachians (with special emphasis on the Hartford basin, Connecticut), *in* Manspeizer, W., ed., Triassic-Jurassic Rifting, Continental Breakup and the Origin of the Atlantic and Passive Margins, Part A, Developments in Geotectonics, Volume 22: Amsterdam, Elsevier, p. 275-302.

Demarest, H.H., 1983, Error analysis for the determination of tectonic rotation from paleomagnetic data: Journal of Geophysical Research, v. 88, p. 4321-4328.

Dorsey, R.J., and Burns, B., 1994, Regional stratigraphy, sedimentology, and tectonic significance of Oligocene-Miocene sedimentary and volcanic rocks, northern Baja California, Mexico: Sedimentary Geology, v. 88, p. 231-251.

Dorsey, R.J., Peryam, T.C., Bennett, S., Oskin, M.E., and Iriondo, A., 2008, Preliminary Basin Analysis of Latest Miocene Conglomerate Near Bahía Kino, Coastal Sonora: A New Record of Crustal Deformation During Initial Opening of the Northern Gulf of California, Fall Meeting, Volume Abstract T11A-1851: San Francisco, American Geophysical Union.

Driscoll, N.W., and Karner, G.D., 1998, Lower crustal extension across the Northern Carnarvan basin, Australia: Evidence for an eastward dipping detachment: Journal of Geophysical Research, v. 103, p. 4975-4991.

England, P., 1983, Constraints on extension of continental lithosphere: Journal of Geophysical Research, v. 88, p. 1145-1152.

Fenby, S.S., and Gastil, R.G., 1991, A seismo-tectonic map of the Gulf of California and surrounding areas, *in* Dauphin, J.P., and Simoneit, B.R., eds., The Gulf and Peninsular Provinces of the Californias , American Association of Petroleum Geologists Memoir 47, American Association of Petroleum Geologists, p. 79-83.

Fisher, S.R., 1953, Dispersion on a Sphere: Proceedings of the Royal Society of London. Series A, Mathematical and Physical Sciences, v. 217, p. 295-305.

Fletcher, J.M., Grove, M., Kimbrough, D., Lovera, O., and Gehrels, G.E., 2007, Ridge-trench interactions and the Neogene tectonic evolution of the Magdalena shelf and southern Gulf of California: Insights from detrital zircon U-Pb ages from the Magdalena fan and adjacent areas: Geological Society of America Bulletin, v. 119, p. 1313-1336.

Forsyth, D.W., 1992, Finite extension and low-angle normal faulting: Geology, v. 20, p. 27-30.

Gans, P., Wong, M., Macmillan, I., Blair, K., Roldan, J., Till, C., and Herman, S., 2006, Cenozoic structural and magmatic evolution of the Sonoran basin-range and Gulf of California rift system: Geological Society of America Abstracts with Programs - Backbone of the Americas, Paper 10-9.

Gans, P.B., 1997, Large-magnitude Oligo-Miocene extension in southern Sonora: Implications for the tectonic evolution of northwest Mexico: Tectonics, v. 16, p. 388-408.

Gastil, R.G., 1993, Prebatholithic history of peninsular California, *in* Gastil, R.G., and Miller, R.H., eds., The prebatholithic stratigraphy of peninsular California, Geological Society of America Special Paper 279, Volume 279: Boulder, CO, Geological Society of America, p. 145-156.

Gastil, R.G., and Krummenacher, D., 1977a, Reconnaissance geologic map of coastal Sonora between Puerto Lobos and Bahia Kino, GSA Map and Chart Series MC-16: Boulder, CO, Geological Society of America.

Gastil, R.G., and Krummenacher, D., 1977b, Reconnaissance geology of coastal Sonora between Puerto Lobos and Bahia Kino: Geological Society of America Bulletin, v. 88, p. 189-198.

Gastil, R.G., Krummenacher, D., and Minch, J.A., 1979, The record of Cenozoic volcanism around the Gulf of California: Geological Society of America Bulletin, v. 90, p. 839-857.

Gastil, R.G., Lemone, D.V., and Stewart, W.J., 1973, Permian fusulinids from near San Felipe, Baja California: AAPG Bulletin, v. 57, p. 746-747.

Gastil, R.G., Phillips, R.P., and Allison, E.C., 1975, Reconnaissance geology of the State of Baja California, Geological Society of America Memoir 140: Boulder, CO, Geological Society of America, 170 p.

González-Fernández , A., Danobeitia, J.J., Deldago-Argote, L., Michaud, F., Cordoba, D., and Bartolome, R., 2005, Mode of extension and rifting history of upper Tiburon and upper Delfin basins, northern Gulf of California: Journal of Geophysical Research, v. 110, p. 1-17.

Hamilton, W., 1961, Origin of the Gulf of California: Geological Society of America Bulletin, v. 72, p. 1307-1318.

Hausback, B.P., 1984, Cenozoic volcanic and tectonic evolution of Baja California Sur, Mexico, *in* Frizzell, V.A., Jr., ed., Geology of the Baja California Peninsula, Volume

39: Los Angeles, California, Pacific Section of the Economic Paleontologists and Mineralogists, p. 219-236.

Henry, C.D., 1989, Late Cenozoic Basin and Range structure in western Mexico adjacent to the Gulf of California: Geological Society of America Bulletin, v. 101, p. 1147-1156.

Herman, S.W. and Gans, P.B., 2006, A paleomagnetic investigation of large scale vertical axis rotations in coastal Sonora: evidence for transtensional proto-Gulf deformation: Geological Society of America Abstracts with Programs, v. 38, p. 311.

Hernández-Ménez, G.L., Stock, J., Vidal-Solano, J., and Paz-Moreno, F.A., 2008, Paleomagnetic Constraints on the Extent of the Miocene Tuff of San Felipe/Tuff of Hermosillo, Sonora, Mexico, Geological Society of America Annual Meeting: Denver, CO.

Hook, S.J., Abbott, E.A., Grove, C., Kahle, A.B., and Palluconi, F.D., 1998, Multispectral thermal infrared data in geological studies, *in* Rencz, A.N., ed., Remote Sensing for the Earth Sciences, Volume 3: Manual of Remote Sensing: New York, John Wiley and Sons, p. 1-58.

Hopper, J.R., and Buck, W.R., 1996, The effect of lower crustal flow on continental extension and passive margin formation: Journal of Geophysical Research, v. 101, p. 20,175-20,194.

Huismans, R.S., and Beaumont, C., 2003, Symmetric and asymmetric lithospheric extension: Relative effects of frictional-plastic and viscous strain softening: Journal of Geophysical Research, v. 108.

Iriondo, A., 2009, Preliminary U/Pb SHRIMP Results for the Tuff of Cerro Kino, coastal Sonora, Mexico, *in* Bennett, S.E.K., ed.: Chapel Hill, p. 2.

Jones, C.H., 2002, User-driven Integrated Software Lives: "PaleoMag" Paleomagnetics Analysis on the Macintosh: Computers and Geosciences, v. 28, p. 1145-1151.

Kaus, B.J.P., and Podladchikov, Y.Y., 2006, Initiation of localized shear zones in viscoelastoplastic rocks: Journal of Geophysical Research, v. 111.

Kirschvink, J.L., 1980, The least-squares line and plane and the analysis of paleomagnetic data.: Geophys. J. R. Astron. Soc., v. 62, p. 699-718.

Kirschvink, J.L., Kopp, R.E., Raub, T.D., Baumgartner, C., T., and Holt, J.W., 2008, Rapid, Precise, and High-Sensitivity Acquisition of Paleomagnetic and Rock-Magnetic Data: Development of a Low-Noise Automatic Sample Changing System for Superconducting Rock Magnetometers: Geochemistry Geophysics Geosystems, v. 9, p. doi: 10.1029/2007GC001856.

Kusznir, N.J., and Park, R.G., 1987, The extensional strength of the continental lithosphere: its dependence on geothermal gradient, and crustal composition and thickness, *in* Coward, M.P., Dewey, J.F., and Hancock, P.L., eds., Continental Extension Tectonics, Volume Special Publication No 28, Geological Society.

Larson, R.L., Menard, H.W., and Smith, S.M., 1968, Gulf of California: a result of ocean floor spreading and transform faulting: Science, v. 161, p. 781-784.

Lavier, L.L., Buck, W.R., and Poliakov, A.N.B., 1999, Self-consistent rolling-hinge model for the evolution of large-offset low-angle normal faults: Geology, v. 27, p. 1127-1130.

Lavier, L.L., and Manatschal, G., 2006, A mechanism to thin the continental lithosphere at magma-poor margins: Nature, v. 440, p. 324-328.

Lewis, C.J., 1996, Stratigraphy and geochronology of Miocene and Pliocene volcanic rocks in the Sierra San Fermín and southern Sierra San Felipe, Baja California, Mexico: Geofisica Internacional, v. 35, p. 1-31.

Lewis, C.J., and Stock, J.M., 1998, Paleomagnetic evidence of localized vertical-axis rotation during Neogene extension of the Sierra San Fermín, northeastern Baja California, Mexico: JGR, v. 103, p. 2455-2470.

Lizarralde, D., Axen, G.J., Brown, H.E., Fletcher, J.M., González-Fernández, A., Harding, A.J., Holbrook, W.S., Kent, G.M., Paramo, P., Sutherland, F., and Umhoefer, P.J., 2007, Variation in styles of rifting in the Gulf of California: Nature, v. 448, p. 466-469.

Lonsdale, P., 1989, Geology and tectonic history of the Gulf of California, *in* Winterer, E.L., Hussong, D.M., and Decker, R.W., eds., The Eastern Pacific Ocean and Hawaii, Geology of North America, Volume N: Boulder, CO, Geological Society of America, p. 499-521.

Louden, K.E., and Chian, D., 1999, The deep structure of non-volcanic rifted continental margins: Philosophical Transactions of the Royal Society of London, v. 357, p. 767-804.

McDowell, F.W., Roldan-Quintana, J., and Amaya-Martinez, R., 1997, Interrelationship of sedimentary and volcanic deposits associated with tertiary extension in Sonora, Mexico: GSA Bulletin, v. 109, p. 1349-1360.

McGee, W.J., and Johnson, W.D., 1896, Seriland, The National Geographic Magazine, Volume 7: Washington, The National Geographic Society, p. 125-132.

McKenzie, D., 1978, Some remarks on the development of sedimentary basins: Earth and Planetary Science Letters, v. 40, p. 25-32.

Nagy, E.A., Grove, M., and Stock, J.M., 1999, Age and stratigraphic relationships of pre- and syn-rift volcanic deposits in the northern Puertecitos Volcanic Province, Baja California, Mexico: Journal of Volcanology and Geothermal Research, v. 93, p. 1-30.

Nagy, E.A., and Stock, J.M., 2000, Structural controls on the continent-ocean transition in the northern Gulf of California: Journal of Geophysical Research, v. 105, p. 16,251-16,269.

Ortlieb, L., 1991, Quaternary vertical movements along the coasts of Baja California and Sonora, *in* Dauphin, J.P., and Simoneit, B.R.T., eds., The Gulf and Peninsular Province of the Californias, Volume 47: AAPG Memoir: Tulsa, Oklahoma, The American Association of Petroleum Geologists, p. 447-480.

Oskin, M., 2002, Tectonic Evolution of The Northern Gulf of California, Mexico, Deduced from Conjugate Rifted Margins of the Upper Delfín Basin [Ph.D. thesis]: Pasadena, California Institute of Technology.

Oskin, M., Iriondo, A., and Nourse, J., 2003, Geologic Reconnaissance and Geochronology of proto-Gulf of California extension, western Sonora: Geological Society of America Abstracts with Programs, v. 35, p. 28.

Oskin, M., and Martín-Barajas, A., 2003, Continental edge tectonics of Isla Tiburón, Sonora Mexico, *in* Alcayde, M., and Caballero, A.G., eds., Geological Transects Across Cordilleran Mexico, Volume 1: Special Publication: Mexico, D.F., Universidad Nacional Autónoma de México, p. 53-70.

Oskin, M., Stock, J., and Martín-Barajas, A., 2001, Rapid localization of Pacific-North America plate motion in the Gulf of California: Geology, v. 29, p. 459-462.

Oskin, M., and Stock, J.M., 2003a, Pacific-North America plate motion and opening of the Upper Delfín basin, northern Gulf of California: Geological Society of America Bulletin, v. 115, p. 1173–1190.

Oskin, M., and Stock, J.M., 2003b, Cenozoic volcanism and tectonics of the continental margins of the Upper Delfín basin, northeastern Baja California and western Sonora, *in* Kimbrough, D.L., Johnson, S.E., Paterson, S., Martín-Barajas, A., Fletcher, J.M., and Girty, G., eds., Tectonic evolution of northwestern Mexico and the southwestern USA: Geological Society of America Special Paper 374: Boulder, Colorado, Geological Society of America, p. 421-428.

Oskin, M., and Stock, J.M., 2003c, Marine incursion synchronous with plate-boundary localization in the Gulf of California: Geology, v. 31, p. 23-26.

Page, W.R., Harris, A.G., Poole, F.G., and Repetski, J.E., 2003, Reinterpretation of the stratigraphy and structure of the Rancho Las Norias area, central Sonora, Mexico: Journal of South American Earth Sciences, v. 16, p. 523-540.

Paz-Moreno, F.A., 1992, Le volcanisme mio-plio-quaternaire de l'Etat du Sonora (nord-ouest du Mexique): évolution spatiale et chronologique; implications pétrogénétiques, Université Aix-Marseille.

Pfiffner, O.A., and Burkhard, M., 1987, Determination of paleostress axes orientations from fault, twin and earthquake data: Annales Tectonicae, v. 1.

Proffett, J.M., 1977, Cenozoic geology of the Yerington district, Nevada, and implications for the nature and origin of Basin and Range faulting: Geological Society of America Bulletin, v. 88, p. 247-266.

Ramos-Velázquez, E., Calmus, T., Valencia, V., Iriondo, A., Valencia-Moreno, M., and Bellon6, H., 2008, U-Pb and 40Ar/39Ar geochronology of the coastal Sonora batholith: New insights on Laramide continental arc magmatism: Revista Mexicana de Ciencias Geológicas, v. 25, p. 314-333.

Royer, J.-Y., Gordon, R.G., and Horner-Johnson, B.C., 2006, Motion of Nubia relative to Antarctica since 11 Ma: Implications for Nubia-Somalia, Pacific–North America, and India-Eurasia motion: Geology, v. 34, p. 501-504.

Spencer, J.E., and Normark, W.R., 1979, Tosco-Abreojos fault zone: A Neogene transform plate boundary within the Pacific margin of southern Baja California: Geology, v. 7, p. 554-557.

Stewart, J.H., 1998, Regional characteristics, tilt domains, and extensional history of the later Cenozoic Basin and Range Province, western North America, *in* Faulds, J.E., and Stewart, J.H., eds., GSA Special Paper 323: Accommodation zones and transfer zones; the regional segmentation of the Basin and Range Province, Volume 323, Geological Society of America, p. 47-74.

Stock, J., 2007, The Kinematic Puzzle of the Gulf of California Rift system: Eos Transactions American Geophysical Union, v. 88.

Stock, J., Martín-Barajas, A., Martinez-Lopez, M., and Chapman, A., 2008, Net slip across the Ballenas Transform fault measured from offset ignimbrite deposits, Fall Meet. Suppl., p. Abstract T11A-1853.

Stock, J., Paz-Moreno, F.A., Martin, K., and Lin, D., 2006, The 12.5 Ma Tuff of San Felipe: a major structural marker horizon in northwestern Mexico, Lithospheric Rupture in the Gulf of California-Salton Trough Region - NSF Margins RCL Workshop: Ensenada, Mexico.

Stock, J.M., 1989, Sequence and geochronology of Miocene rocks adjacent to the main gulf escarpment: Southern Valle Chico, Baja California Norte, Mexico: Geofisica Internacional, v. 28, p. 851-896.

Stock, J.M., and Hodges, K.V., 1989, Pre-Pliocene extension around the Gulf of California and the transfer of Baja California to the Pacific Plate: Tectonics, v. 8, p. 99-115.

Stock, J.M., Lewis, C.J., and Nagy, E.A., 1999, The Tuff of San Felipe: an extensive middle Miocene pyroclastic flow deposit in Baja California, Mexico: Journal of Volcanology and Geothermal Research, v. 93, p. 53-74.

Stock, J.M., and Molnar, P., 1988, Uncertainties and implications of the Late Cretaceous and Tertiary position of North America relative to the Farallon, Kula, and Pacific plates: Tectonics, v. 7, p. 1339-1384.

Umhoefer, P.J., and Stone, K.A., 1996, Description and kinematics of the SE Loreto basin fault array, Baja California Sur, Mexico: A positive field test of oblique- rift models: Journal of Structural Geology, v. 18, p. 595-&.

Unruh, J., Humphrey, J., and Barron, A., 2003, Transtensional model for the Sierra Nevada frontal fault system, eastern California: Geology, v. 31, p. 327-330.

Valencia-Moreno, M., Ruiz, J., Barton, M.D., Patchett, P.J., Zürcher, L., Hodkinson, D.G., and Roldán-Quintana, J., 2001, A chemical and isotopic study of the Laramide granitic belt of northwestern Mexico: Identification of the southern edge of the North American Precambrian Basement: Geological Society of America Bulletin, v. 113, p. 1409-1422.

Valencia-Moreno, M., Ruiz, J., Ochoa-Landín, L., Martínez-Serrano, R., and Vargas-Navarro, P., 2003, Geochemistry of the Coastal Sonora batholith, Northwestern Mexico: Can. J. Earth Sci., v. 40, p. 819-831.

Vidal-Solano, J., Moreno, F.A.P., Alexander Iriondo c, d., Demant, A., and Cochemé, J.-J., 2005, Middle Miocene peralkaline ignimbrites in the Hermosillo region (Sonora, Mexico): Geodynamic implications: C.R. Geoscience, v. 337, p. 1421-1430.

Vidal-Solano, J.R., Paz-Moreno, F.A., Demant, A., and Lopez-Martinez, M., 2007, Ignimbritas hiperalcalinas del Mioceno medio en Sonora Central: revaluacion de la estratigrafia y significado del volcanismo terciario: Revista Mexicana de Ciencias Geologicas, v. 24, p. 47-67.

Wallace, R.E., 1951, Geometry of shearing stress and relation to faulting: Journal of Geology, v. 59, p. 118-130.

Wegener, A., 1924, The Origin of Continents and Oceans: New York, E.P. Dutton and Company Publishers, 212 p.

Wernicke, B., and Burchfiel, B.C., 1982, Modes of extensional tectonics: Journal of Structural Geology, v. 4, p. 105-115.

Withjack, M.O., and Jamison, W.R., 1986, Deformation produced by oblique rifting: Tectonophysics, v. 126, p. 99-124.

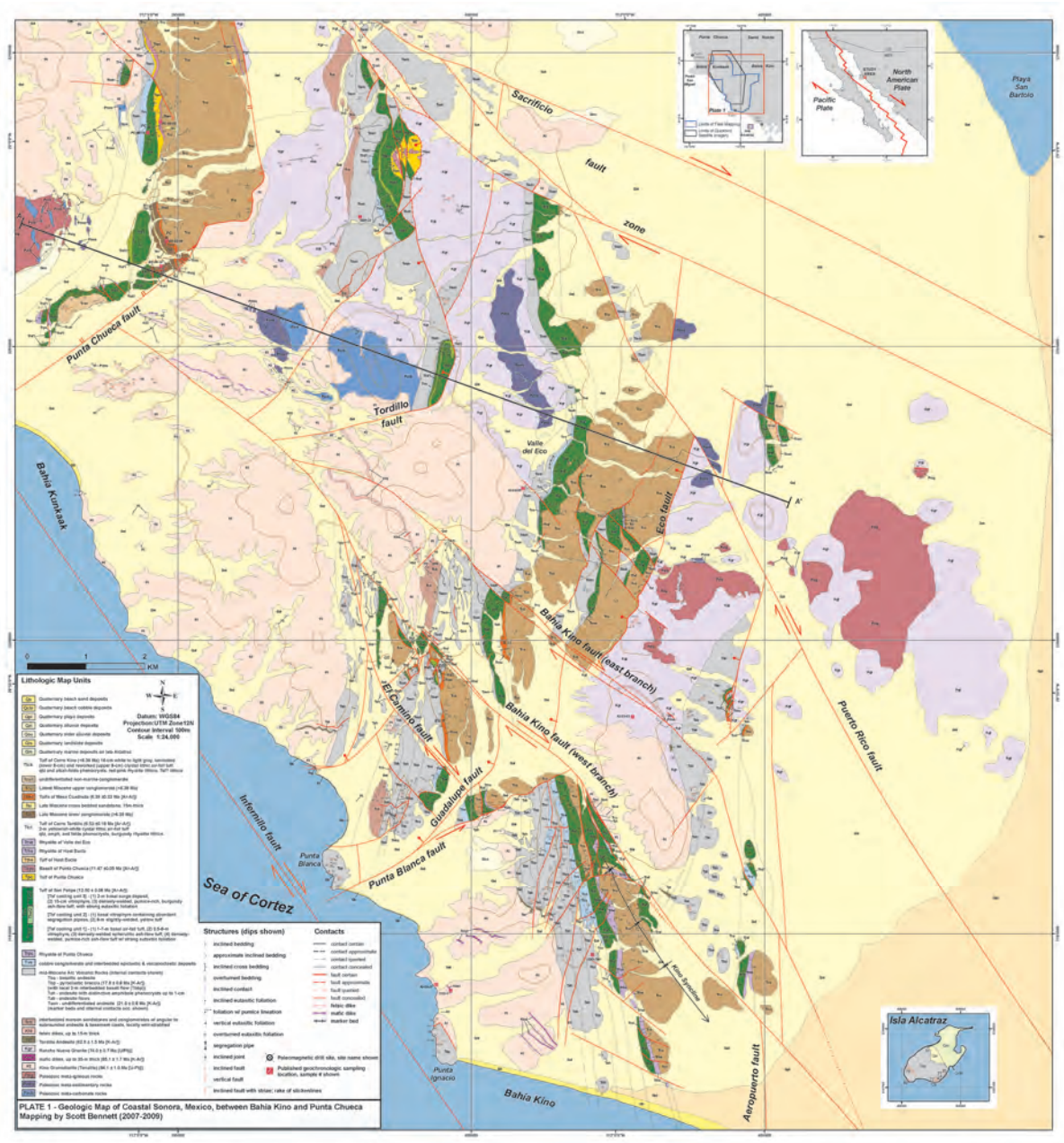

PLATE 1. Geologic map of Coastal Sonora, Mexico, between Bahia Kino and Punta Chueca. Mapping by Scott Bennett (2007-2009).

See attached full-size map (Pocket/DVD).